# UNDERSTANDING THE ROLE OF TRANSFORMING GROWTH FACTOR BETA SIGNALING IN THE UTERUS USING GENETICALLY MODIFIED MOUSE MODELS

A Dissertation

by

YANG GAO

Submitted to the Office of Graduate and Professional Studies of
Texas A&M University
in partial fulfillment of the requirements for the degree of

DOCTOR OF PHILOSOPHY

| | |
|---|---|
| Chair of Committee, | Qinglei Li |
| Committee Members, | Fuller W. Bazer |
| | Robert C. Burghardt |
| | Gregory A. Johnson |
| Head of Department, | C. Jane Welsh |

August 2017

Major Subject: Biomedical Sciences

## ABSTRACT

Transforming growth factor beta (TGFβ) superfamily signaling regulates multiple reproductive events. However, the *in vivo* role of the TGFβ signaling in uterine development and function is not well defined. Conditional knockout (cKO) of TGFβ receptor 1 (TGFBR1) in the female reproductive tract leads to remarkable smooth muscle defects. The first study of this dissertation research was to further define the role of TGFβ signaling in uterine development. We found that the myometrial defects in *Tgfbr1* cKO mice were associated with dysregulated expression of key extracellular matrix components and platelet-derived growth factors signaling during a critical time window of early postnatal uterine development. To complement the loss of function model, in the second study, we generated a uterine specific gain-of-function mouse model harboring a constitutively active TGFBR1 which leads to over-activation of TGFβ signaling. Constitutive activation of TGFBR1 caused infertility and defects in uterine morphology and function, as evidenced by abnormal myometrial structure, dramatically reduced numbers of uterine glands, and impaired uterine decidualization. These studies underscore the importance of a balanced TGFβ signaling system in establishing a uterine microenvironment conducive to normal development and function. In the third study of this dissertation research, we focused on identifying the role of TGFβ signaling in PTEN-inactivated uterine epithelial cells. Depletion of PTEN in the mouse uterus causes endometrial cancer. We found that simultaneous deletion of *Tgfbr1* and *Pten* in the mouse uterus caused severe endometrial lesions and pulmonary metastases compared

with deletion of *Pten* alone. The development of metastasis and accelerated tumor progression in the *Pten/Tgfbr1* double knockout mice was linked to increased production of pro-inflammatory chemokines, enhanced cancer cell motility evidenced by myometrial invasion and disruption, and an altered tumor microenvironment characterized by recruitment of tumor-associated macrophages. Our results suggest that TGFβ signaling synergizes with PTEN to suppress the progression of endometrial cancer.

## ACKNOWLEDGEMENTS

I would like to sincerely thank my committee chair, Dr. Qinglei Li, and my committee members, Dr. Robert C. Burghardt, Dr. Gregory A. Johnson, and Dr. Fuller W. Bazer, for their guidance and support during my Ph.D. program at Texas A&M University. Without their help, it would be impossible for me to complete my dissertation. I give my deep appreciation to my mentor Dr. Li for his efforts on my scientific training. In the past few years, he taught me how to correctly conduct my research, and more importantly, he helped me develop critical thinking skills during my study. Dr. Li is a great model both as a scientist and as a mentor. His enthusiasm and passion for science would definitely keep motivating me in the future. I am grateful for Dr. Burghardt's advice on my projects and manuscript preparation. In addition, the knowledge and skills I learned from his microscopy course strongly supported my research in the laboratory. I also appreciate the great help from Dr. Johnson and Dr. Bazer. They not only gave good suggestions on my projects, but also helped me to build up my knowledge base of reproductive biology.

I would like to extend my gratitude to all the past and current members of the Li laboratory including Xin Fang, Nan Ni, Vincent Barronette, Christian Seua, Dr. Pengfei Lin, Dr. Bo Kang, Samantha Duran, Anna Jane Davis, Dr. Shu Li, Dr. Haixia Wen, Dr. Chunjin Li, and Dr. Chao Wang for their help and assistance.

Thanks also go to my friends and colleagues and the departmental faculty and staff for making my time at Texas A&M University a great experience.

Finally, I would like to thank my family, especially my wife Yating Cheng, my mother Qingxiang Ma, my father Bencheng Gao and my sister Ming Gao for their encouragement, support, and love. I couldn't have done it without you!

## CONTRIBUTORS AND FUNDING SOURCES

### Contributors section

Part 1, faculty committee recognition

This work was supervised by a dissertation committee consisting of Dr. Qinglei Li (Chair), Dr. Gregory A. Johnson and Dr. Robert C. Burghardt of the Department of Veterinary Integrative Biosciences and Dr. Fuller W. Bazer of the Department of Animal Science.

Part 2, student/collaborator contributions

The work presented in Section 2 is reprinted with slight modification from Gao et al. "TGFBR1 Is required for mouse myometrial development" published in March 2014 with permission from Molecular Endocrinology. All work was completed by the student, under the supervision of Dr. Qinglei Li, in collaboration with Dr. Kayla J. Bayless of the Department of Molecular and Cellular Medicine, Texas A&M University. We thank Dr. Martin Matzuk for helping import the *Tgfbr1* mice. We also thank Robert Bearden and Dr. Jörg Steiner for providing the respective technical support and equipment for cell migration analyses.

The work presented in Section 3 is partially reprinted from Gao et al. "Constitutive activation of transforming growth factor beta receptor 1 in the mouse uterus impairs uterine morphology and function" published in February 2015 with permission from

Biology of Reproduction. All work was completed by the student, under the supervision of Dr. Qinglei Li, in collaboration with Samantha Duran, Dr. Robert C. Burghardt of the Department of Veterinary Integrative Biosciences, Texas A&M University; Dr. John P. Lydon of the Department of Molecular and Cellular Medicine, Baylor College of Medicine; Dr. Francesco J. DeMayo of the Department of Molecular and Cellular Medicine, Baylor College of Medicine; Dr. Kayla J. Bayless of the Department of Molecular and Cellular Medicine, Texas A&M University; and Dr. Laurent Bartholin of the Centre de Recherche en Cancérologie de Lyon. We are grateful to Dr. Barbara M. Sanborn (Colorado State University) for the generous gift of the human uterine smooth muscle cell line. We thank Drs. Stephen Safe and Louise Abbott for equipment support.

The work presented in Section 4 is reprinted with slight modification from Gao et al. "Conditional abrogation of transforming growth factor beta receptor 1 in PTEN-inactivated endometrium promotes endometrial cancer progression in mice" which is accepted by The Journal of Pathology. All work was completed by the student, under the supervision of Dr. Qinglei Li, in collaboration with Dr. Pengfei Lin of the College of Veterinary Medicine, Northwest A&F University; Dr. John P. Lydon of the Department of Molecular and Cellular Medicine. Baylor College of Medicine. We thank Dr. Kayla Bayless for critical reading of the manuscript and Dr. Robert Burghardt for helpful discussions. The authors also wish to thank Dr. Francesco DeMayo for help in importing *Pgr*-Cre mice, Dr. Yating Cheng for suggestions on ELISA analysis, and Ms. Xin Fang and Nan Ni for technical assistance.

**Funding sources**

The work in Section 2 was supported by the National Institutes of Health Grant R21HD073756 (to Q.L.) from the Eunice Kennedy Shriver National Institute of Child Health and Human Development; the Ralph E. Powe Junior Faculty Enhancement Award (to Q.L.) from Oak Ridge Associated Universities; and the New Faculty Start-up Fund (to Q.L.) from Texas A&M University. Y.G. is also partially supported by a Texas A&M College of Veterinary Medicine graduate student research award.

The work in Section 3 was supported by the National Institutes of Health grant R21HD073756 from the Eunice Kennedy Shriver National Institute of Child Health & Human Development (to Q.L.), the Ralph E. Powe Junior Faculty Enhancement Award from Oak Ridge Associated Universities (to Q.L.), the New Faculty Start-up Fund from Texas A&M University (to Q.L.), INSERM ‘‘Avenir Program" (to L.B.), ARC 3891 (to L.B.), INCA PLBIO (to L.B.), and Ligue contre le cancer (to L.B.).

The work in Section 4 was supported in part by the New Faculty Start-up Fund from Texas A&M University and the National Institutes of Health grant R21HD073756 from the Eunice Kennedy Shriver National Institute of Child Health & Human Development (to Q.L.).

## TABLE OF CONTENTS

Page

## LIST OF FIGURES

Page

## LIST OF TABLES

Page

# 1. INTRODUCTION AND LITERATURE REVIEW

## 1.1 Transforming growth factor beta (TGFβ) superfamily signaling

The discovery of TGFβ dates back to the 1970s to 1980s [1, 2]. In 1978, de Larco and Todaro found that murine sarcoma virus-transformed mouse fibroblasts produced a polypeptide growth factor, sarcoma growth factor (SGF), that promoted cell growth in soft agar [3]. In 1981, SGF was found to be a mixture of at least two distinct substances, including TGFα and TGFβ [4, 5]. Subsequently, TGFβ1 was purified from human platelets [6] and its cDNA cloned [7].

Shortly after the discovery of TGFβ1, other proteins were discovered that shared sequence homology with TGFβ1, such as inhibin, Müllerian inhibiting substance/anti-Müllerian hormone (MIS/AMH), and bone morphogenetic proteins (BMPs) [8-13]. Currently, there are more than 40 proteins functioning as ligands for TGFβ superfamily signaling, including TGFβs, BMPs, growth differentiation factors (GDFs), activins, inhibins, AMH, and the most distantly related glial cell-derived neurotrophic factors (GDNFs) [14, 15]. This introduction will mainly focus on TGFβ signaling.

### 1.1.1 TGFβ isoforms synthesis and activation

TGFβ ligands (TGFβ1, TGFβ2, and TGFβ3) are synthesized as pre-pro-peptides containing an N-terminal signal peptide, a latency-associated peptide (LAP), and a C-terminal region [16-18]. The signal peptide is necessary for translocation to the cell

membrane and can be cleaved by a signal peptidase, yielding a pro-peptide of TGFβ [16, 19]. LAP is cleaved from the pro-TGFβ by furin convertase, but still noncovalently interacts with the disulfide-linked TGFβ homodimers to form the small latent complex (SLC) [20, 21]. A latent TGFβ-binding protein (LTBP) binds to the SLC to form a large latent complex (LLC), which will be secreted into the extracellular matrix compartment [17, 20]. Several substances are responsible for the release or exposure of the biologically active TGFβ. The substances include plasmin, matrix metalloproteinase 2 (MMP2), MMP9, thrombospondin 1 (TSP1), reactive oxygen species (ROS), integrin αvβ6, and integrin αvβ8. In addition, physical conditions such as extreme pH, temperature, and radiation also influence the activation of TGFβ by promoting the release of mature TGFβ [17, 22-35].

### 1.1.2 TGFβ receptors

TGFβ superfamily ligands, except GDNFs that utilize a tyrosine kinase receptor, activate the intracellular signaling cascades via the transmembrane serine-threonine kinases receptors [36-38]. Based on their structures and functions, TGFβ superfamily receptors are classified into three types [9, 39]. Type I and type II receptors, the major receptors for TGFβ superfamily members [40], are single-transmembrane proteins containing an extracellular domain, a transmembrane domain, and a cytoplasmic serine-threonine kinase domain [41]. The Type III receptor (or betaglycan) is a membrane-anchored proteoglycan that facilitates the binding of ligands to the type II receptors [40, 42, 43].

There are seven type I receptors in mammals, namely activin receptor-like kinase 1 (ALK1), ALK2, ALK3, ALK5, ALK6, and ALK7 [14, 44]. The alternative names for the type I receptors are listed in Table 1. Type I receptors contain a highly conserved region (i.e., GS domain), which is characterized by the presence of a SGSGS sequence [45]. Phosphorylation of the GS domain by type II receptors induces the intra-cellular responses, while GS domain mutations may lead to constitutive activation of type I receptors [45-51]. Among the seven type I receptors, TGFBR1 is the major receptor that propagates the signal of TGFβ ligands, although ACVRL1 and ACVR1 can also be activated by TGFβ in mouse embryonic endothelial cells and human endothelial cells, respectively [45, 52, 53].

**Table 1.** Two nomenclature systems for the TGFβ type I receptors

| Activin receptor-like kinases nomenclature system | Alternative nomenclature system |
|---|---|
| Activin receptor-like kinase 1 (ALK1) | Activin A receptor-like type 1 (ACVRL1) |
| Activin receptor-like kinase 2 (ALK2) | Activin A receptor type 1 (ACVR1) |
| Activin receptor-like kinase 3 (ALK3) | BMP receptor 1A (BMPR1A) |
| Activin receptor-like kinase 4 (ALK4) | Activin A receptor type 1B (ACVR1B) |
| Activin receptor-like kinase 5 (ALK5) | TGFβ receptor 1 (TGFBR1) |
| Activin receptor-like kinase 6 (ALK6) | BMP receptor 1B (BMPR1B) |
| Activin receptor-like kinase 7 (ALK7) | Activin A receptor type 1C (ACVR1C) |

Five type II receptors have been identified in mammalian species, including ACVR2, ACVR2B, AMH receptor 2 (AMHR2), BMPR2, and TGFBR2 [14, 44]. Type II receptors are constitutively active. Upon ligand binding, they phosphorylate and activate

type I receptors [45, 54, 55]. Among the five type II receptors, TGFBR2 mediates TGFβ signaling [45]. It has been suggested that TGFβ1 and TGFβ3 bind to TGFBR2 with a high affinity in the absence of TGFBR1, but TGFβ2 only binds to TGFBR2 when TGFBR1 is present in human fibroblast cells [56, 57].

Type III receptor TGFBR3 i.e., betaglycan, is a co-receptor which presents the TGFβ ligands to TGFBR2 [58]. It has a large N-terminal extracellular domain for glycosaminoglycan attachment and TGFβ binding, a single transmembrane domain, and a small cytoplasmic domain interacting with TGFBR2 to enhance the TGFβ signaling [42, 43, 59, 60]. TGFBR3 not only increases the responsiveness of TGFBR2 to TGFβ2 [42, 43, 61], but also that of ACVR2 to inhibin [43, 62]. A membrane glycoprotein endoglin (CD105), which shares high homology (63%) to the TGFBR3 in the transmembrane and cytoplasmic domain, has also been identified as a co-receptor for TGFβ, particularly, TGFβ1 and TGFβ3 [40, 63].

### 1.1.3 SMAD proteins

Sma and Mad (mother against decapentaplegic)-related proteins (SMADs) are the intracellular transducers of canonical TGFβ superfamily signaling [64, 65]. Mammalian SMAD proteins (i.e., SMAD1, 2, 3, 4, 5, 6, 7, and 9) can be classified into receptor-regulated SMADs (R-SMADs; SMAD1/2/3/5/9), common SMAD (Co-SMAD; SMAD4), and inhibitory SMADs (I-SMADs; SMAD6/7). R-SMADs and co-SMAD comprise two conserved domains [i.e., the N-terminal Mad Homology 1 (MH1) domain

and the C-terminal MH2 domain] connected by a variable linker region [66]. The MH1 domain binds to the SMAD-binding element (SBE) and it is implicated in gene regulation [67]. The MH2 domain mediates protein-protein interactions and is involved in the SMAD-receptor interaction [68], the binding of R-SMAD to the SMAD anchor for receptor activation (SARA) [69], the oligomerization of R-SMADs and co-SMAD [70, 71], and the association of SMADs with transcriptional coactivators [72]. In addition, R-SMADs have a Ser-Ser-X-Ser (SSXS) motif which can be phosphorylated by type I receptors [73-75]. Co-SMAD does not possess the SSXS motif and, therefore, does not bind to type I receptors [76]. In contrast to R-SMADs and co-SMAD, I-SMADs have a conserved MH2 domain, but divergent MH1 domain and linker region [77]. In general, SMADs 1/5/9 transduce BMP signaling while SMADs 2/3 mediate TGFβ/activin signaling [64, 65]. Although both I-SMADs inhibit BMP signaling, SMAD7 can also target TGFβ signaling [78, 79].

### 1.1.4 Canonical and non-canonical TGFβ superfamily signaling

The canonical TGFβ superfamily signaling is induced when ligand-receptor complexes form [14, 40, 44]. Within the complex, the Type II receptor phosphorylates and activates the type I receptor, which in turn phosphorylates the R-SMADs. R-SMADs bind to SMAD4, enter the nucleus, and regulate the expression of down-stream target genes. Figure 1 illustrates the canonical, or SMAD-dependent, TGFβ superfamily signaling pathways.

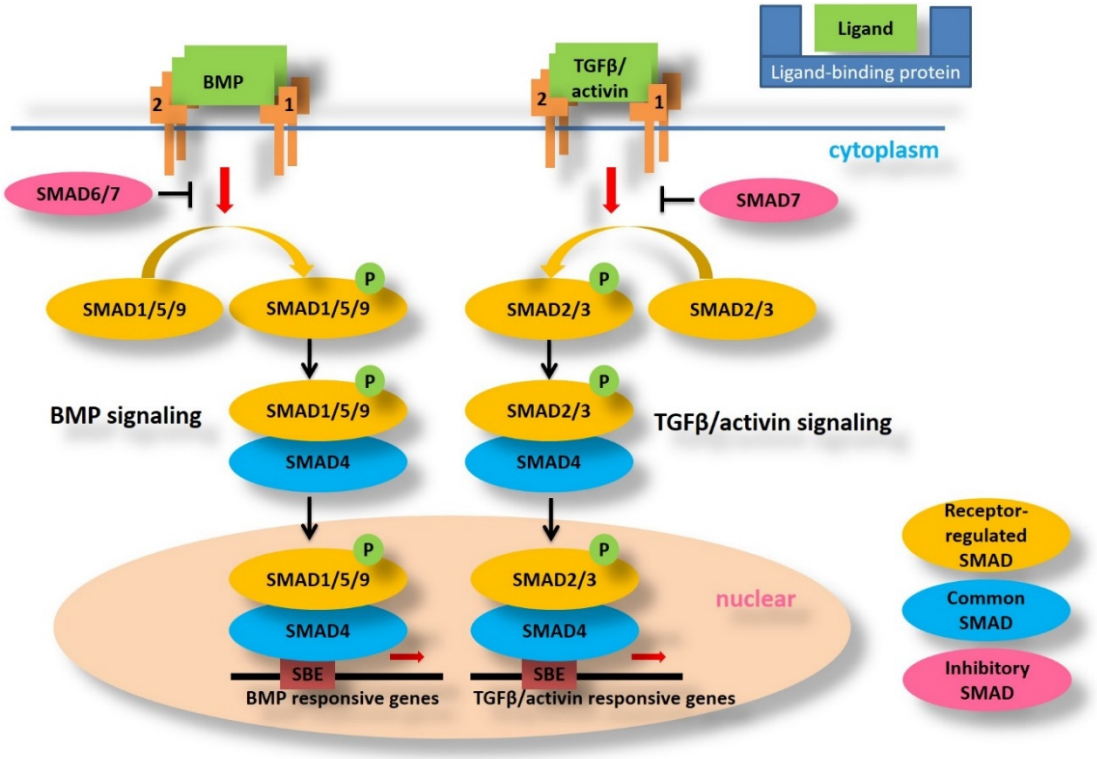


**Figure 1.** Canonical TGFβ superfamily signaling pathway. The canonical TGFβ superfamily signaling is induced by ligands binding to their receptor complex. The activated receptor complex phosphorylates receptor-regulated SMADs (i.e., SMAD2/3 and SMAD1/5/9) which then bind to the common SMAD (i.e., SMAD4) and translocate into the nucleus to regulate the expression of downstream targets. SMADs 2/3 and SMADs 1/5/9 transduce TGFβ/activin and BMP signaling, respectively. TGFβ superfamily signaling pathways are negatively regulated by the ligand-binding proteins (e.g. follistatin, gremlin and noggin) and inhibitory SMADs (i.e., SMAD6 and SMAD7).

The canonical TGFβ superfamily signaling has been shown to cross-talk with a variety of signaling pathways including, but not limited to, mitogen-activated protein kinase (MAPK), phosphatidylinositol-3 kinase (PI3K)/AKT, WNT, Hedgehog, Notch, Hippo, nuclear factor κB (NF-κB), Janus kinase/signal transducers and activators of transcription (JAK/STAT), interleukin (IL)/interferon gamma (IFNγ)/tumor necrosis factor alpha (TNFα) cytokines, and microRNA (miRNA) machinery (reviewed in [80-

83]). The interaction between TGFβ superfamily signaling and other signaling pathways may lead to either synergistic or antagonistic effects on signaling outcome.

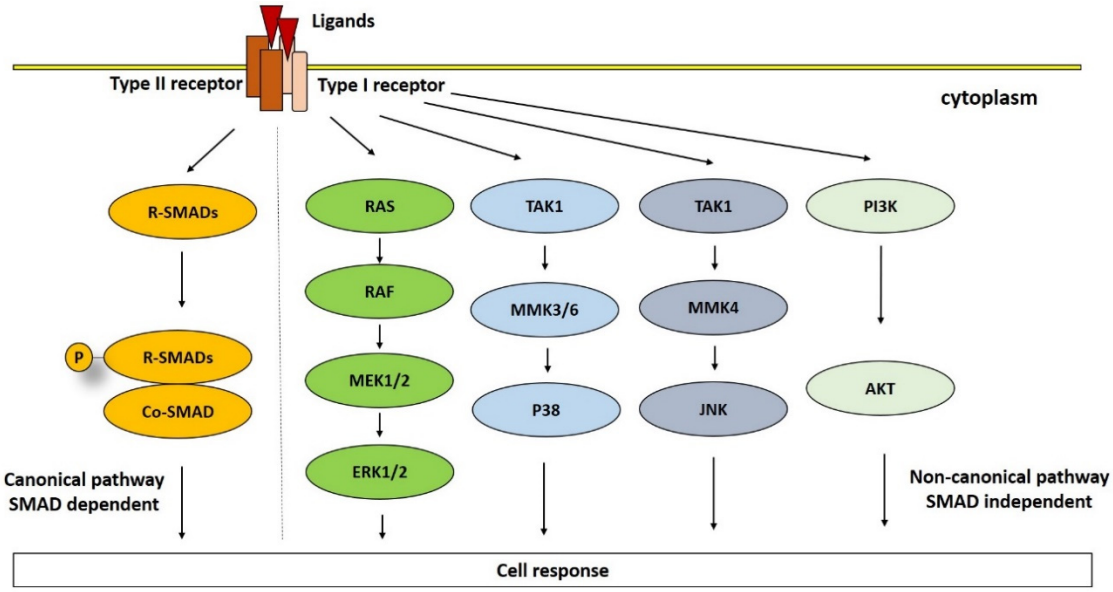


**Figure 2.** Non-canonical TGFβ superfamily signaling pathways. The canonical pathway is SMAD-dependent (Left). The non-canonical pathway is SMAD-independent (Right), such as RAS-RAF-MERK1/2-ERK1/2, TAK1-MMK3/6-P38, TAK1-MMK4-JNK and PI3K-AKT pathways.

The non-canonical TGFβ superfamily signaling pathways are SMAD independent, such as ERK, P38, JNK and PI3K/AKT pathways (Figure 2). ERK, P38 and JNK belong to the MAPK family. For ERK signaling, extracellular mitogens bind to membrane receptor and serially activate the intracellular kinase cascades of GTPase RAS, RAF, MEK1/2, and then ERK1/2 [84-86]. TGFβ can induce a rapid activation of RAS in rat intestinal epithelial cells and mink lung epithelial cells [87]. Activation of ERK1/2 by TGFβ can occur in various cell types [88-90]. Activation of transforming growth factor

beta-activated kinase 1 (TAK1) by TGFβ and BMP [91] leads to the activation of MKK3/6-P38 and MKK4-JNK signaling pathways [92, 93]. The MAPK signaling cascades are key regulators of TGFβ induced epithelial to mesenchymal transition (EMT) [94-96]. PI3K/AKT signaling is known to regulate cell proliferation and survival [97, 98]. TGFβ activates PI3K/AKT signaling via non-canonical signaling [99-101], and PI3K inhibitor LY294002 prevents TGFβ induced AKT activation and cell migration [101].

### 1.2 TGFβ superfamily signaling in the uterus

The uterus is a key reproductive organ that supports pregnancy. The endometrial layer of the uterus consists of luminal and glandular epithelia and surrounding endometrial stroma and plays an important role in development of the conceptus (embryo and its extra-embryonic membranes). Under the influence of steroid hormones and growth factors, the endometrium undergoes cyclic remodeling during the estrous cycle in mice or menstrual cycle in humans [102, 103]. The normal functional luminal epithelium is critical for attachment and implantation of blastocysts [104]. Secretions from the uterine epithelium, such as leukemia inhibitory factor (LIF) [105] and mucin 1 (MUC1) [106], play essential roles in conceptus development during pregnancy. Meanwhile, endometrial glands provide an important source of nutrients and growth factors for establishing a successful pregnancy [107]. Endometrial stromal cells produce growth factors and undergo decidualization to support implantation and conceptus development in some species including primates and rodents [108]. The myometrium is composed

primarily of smooth muscle cells, which contain contractile machinery that is tightly regulated during pregnancy and parturition by many factors such as hormones [109, 110], ion channels [111-114], nitric oxide [115-118], and microRNAs [119].

### 1.2.1 Uterine development

The uterus develops from the Müllerian duct during embryogenesis and the developmental events continue after birth. In mice, Müllerian ducts form via invagination of the coelomic epithelium around embryonic Day 11.75 [107, 120]. At birth, the uteri of mice consist of a simple epithelium surrounded by undifferentiated mesenchyme [107, 121]. Between birth and postnatal day 3 (PD3), smooth muscle cells differentiate from the mesenchyme and start to form the inner circular myometrial layer, which is evident by PD5 [121, 122]. By PD10, longitudinal smooth muscle layers form bundle-like structures. The uterus acquires its basic myometrial structure by PD15 [121]. Myometrial development is regulated/influenced by hormonal, cellular, and molecular signals [123-128]. Estrogen seems to play a role in regulating the development of the circular myometrium [123]. Tamoxifen-treated neonatal mice have a disorganized circular myometrium with reduced laminin expression and they develop a uterine pathology reminiscent of adenomyosis, with the presence of uterine glands within the myometrium [123]. However, mice treated with estradiol develop intact but hypertrophied muscle layers [123]. Additionally, the WNT/beta-catenin signaling pathway regulates mouse uterine development [124-127]. *Wnt-7a* mutant female mice develop abnormal oviducts and uteri, and smooth muscle defects are prominent in their

uteri [124, 127]. Forkhead box L2 (*Foxl2*) also acts through WNT signaling to regulate uterine maturation and mice with conditional deletion of *Foxl2* in the uterus develop a hypertrophic, disorganized inner myometrial layer [128]. However, key signaling pathways that govern myometrial development remain to be defined.

Accompanying myometrial formation is adenogenesis, a process whereby endometrial glands develop [129-131]. Adenogenesis occurs via invagination of uterine luminal epithelium after PD5 in mice [131]. Uterine glands are essential for fertility and pregnancy in several species [132]. Despite the well-established role of uterine glands in reproduction and the recent progress in identifying adenogenesis-associated genes such as forkhead box A2 (*Foxa2*), *Wnt4*, *Wnt5a*, *Wnt7a*, and cadherin 1 (*Cdh1*) [124, 127, 133-137], mechanisms underlying the development of uterine glands are not well defined. Of note, the proliferation of uterine epithelial cells is critical for uterine development and function. Abnormal proliferation of uterine epithelial cells results in endometrial hyperplasia or cancer.

### 1.2.2 The expression and function of TGFβ superfamily members in the uterus

TGFβ superfamily members are key regulators of female reproductive events, such as follicular development, ovulation, oocyte-cumulus cell communications, implantation and development of the blastocyst/conceptus, uterine decidualization, and placentation [138-151]. TGFβ receptors, and SMADs, are signaling components, including TGFβ ligands, expressed in the myometrial cells of mice and humans and regulate DNA

synthesis in human myometrial cells [152-154]. In the rat uterus, myometrial expression of TGFβ1 and TGFβ3 is increased during mid-gestation, with TGFβ3 strongly localized to the circular myometrial layer during late pregnancy [155]. In human endometria, TGFβs, TGFBR2 and SMAD2/3 mRNAs and proteins are express in both stromal cells and epithelia [156, 157]. In the endometrium of prepubertal mice, expression of TGFβ ligands is increased by diethylstilbestrol [158]. *Smad2* and *Smad4* mRNAs are predominately localized in mouse uterine epithelial cells during the estrous cycle and pre-implantation period, but in decidual cells after blastocyst implantation [159]. The mRNA transcripts of BMP ligands and receptors are expressed in rat and mouse uteri [160, 161]. BMP2 and BMP4 proteins are localized in the mouse endometrium and myometrium with the highest expression in epithelial cells [160, 162]. Results of tissue microarrays demonstrate the dynamic expression of BMP ligands, receptor, and SMADs in human endometrium [163]. Phospho-SMADs 1/5/9 (pSMADs 1/5/9) are detected in the endometrium and myometrium of mice [162]. In addition, other TGFβ superfamily members such as activin, inhibin, and myostatin are also expressed in human and murine uteri [164-169].

The expression of TGFβ superfamily components in the uterus indicates that TGFβ superfamily signaling may play a role in uterine development and function. However, the embryonically lethal phenotype of most TGFβ superfamily members prevents understanding of their *in vivo* functions in the uterus (reviewed in [14, 170]). The application of the Cre-LoxP system to generate conditional knockout (cKO) mice

overcomes this difficulty (Table 2). Two Cre mouse models, anti-Mullerian hormone receptor type 2 (*Amhr2*)-Cre and progesterone receptor (*Pgr*)-Cre are commonly used to study gene function in the uterus. *Amhr2*-Cre is expressed in uterine stromal cells and myometrial cells [171]. *Pgr*-Cre deletes genes in uterine epithelia, stromal cells, and myometrial cells [172].

**Table 2.** Uterine defects in mouse models with conditional deletion of TGFβ superfamily members

| Mouse models | Fertility and defects in uterine development and function |
|---|---|
| Ligands | |
| *Bmp2; Pgr*-Cre | Infertility; failure in formation of implantation sites due to impaired decidualization [173] |
| *Nodal; Pgr*-Cre | Subfertility; placental defects due to malformation of the maternal decidua basalis [174] |
| Receptors | |
| *Bmpr2; Pgr*-Cre | Infertility; multiple defects during decidualization and placentation including impaired decidual cell proliferation and differentiation, attenuated trophoblast invasion, compromised vascularization and spiral artery remodeling, as well as depletion of uNK cells [147] |
| *Acvr1; Pgr*-Cre | Infertility; delayed implantation and defective stromal cell decidualization [175] |
| *Bmpr1a; Pgr*-Cre | Infertility; nonreceptive luminal uterine epithelium with increased microvilli density and cell polarity, defective decidualization [176] |
| *Acvr1b; Pgr*-Cre | Subfertility; similar phenotype to *Nodal, Pgr*-Cre [177] |
| *Tgfbr1; Pgr*-Cre | Subfertility; delayed implantation and defects in lumen closure, uNK cell differentiation, spiral artery remodeling, and placentation [178] |
| *Tgfbr1; Amhr2*-Cre | Infertility; disrupted uterine smooth muscle development; endometrial hyperplasia in aged mice [179, 180] |
| *Bmpr1b* | Infertility; endometrial developmental defects including thinner stromal layer and underdeveloped or absent endometrial glands [181] |
| SMADs | |
| *SMAD1/5/4; Amhr2*-Cre | Infertility; disorganized myometrium and hyperplastic epithelium; defective implantation and decidualization [182] |

Conditional deletion of *Tgfbr1* by *Amhr2*-Cre showed that TGFβ signaling is essential for maintaining the integrity of the female reproductive tract [179]. The *Tgfbr1 Amhr2*-Cre cKO mice are infertile and develop bilateral oviductal diverticula, leading to infertility. Of note, smooth muscle defects are evident in the reproductive tract, including the oviduct and uterus [179]. These mutant mice also have enhanced uterine epithelial cell proliferation, which culminates in endometrial hyperplasia, presumably due to altered paracrine growth factor signaling [180]. Interestingly, conditional deletion of *Smad1/5/4* using *Amhr2*-Cre leads to the formation of oviductal diverticula as well as disorganized myometrium and hyperplastic uterine epithelia [182].

Under the regulation of estrogen and progesterone, endometrial stromal cells differentiate into decidual cells to prepare for implantation of the blastocyst and development of the conceptus [183]. Decidualization in the human occurs in the late secretory phase of menstrual cycle, while in the mouse, decidualization is induced by the implanting blastocysts and can be artificially induced by mechanical stimulation [183]. Placentation, the formation of a placenta, is another critical physiological process that is indispensable for conceptus development; malfunction of the placenta results in fetal growth restriction and fetal death [184, 185]. TGFβ superfamily members including TGFβ, BMP, activin and inhibin are expressed in the uterus during the peri-implantation period [186-190]. Administration of anti-TGFβ1 antibody into the murine uterine lumen reduces the number of implanted blastocysts [191]. Conditional knockout of *Tgfbr1* with *Pgr*-Cre results in delayed implantation of blastocysts, shallow trophoblast invasion, and

uterine lumen closure defects [178]. The different phenotypes of *Tgfbr1 Amhr2*-Cre and *Tgfbr1 Pgr*-Cre cKO mice suggest that the role of TGFβ receptor signaling in the uterus is time and cell type dependent. In humans, TGFβ signaling regulates decidualization of the endometrial stromal cells and trophoblast differentiation and invasion [192-194].

BMP signaling is required for implantation, decidualization, and placentation as demonstrated using several cKO mouse models. *Bmp2 Pgr*-Cre cKO females show impaired decidualization, which is linked to dysregulated WNT signaling, PGR, and prostaglandin synthase 2 (*Ptgs2*) [173]. BMP2 also regulates human endometrial stromal cell decidualization though WNT signaling [195]. Conditional inactivation of *Bmpr2* using *Pgr*-Cre causes defects in decidual cell proliferation, decidual vascularization, trophoblast differentiation and invasion, and uterine natural killer (uNK) cell recruitment [147]. These defects result in severe hemorrhage and intrauterine growth retardation, leading to pregnancy loss during mid-gestation [147]. ACVR1 mediates signaling induced by BMP, activin, and TGFβ [53, 196, 197]. Conditional ablation of *Acvr1* using *Pgr*-Cre suppresses the expression of CCAAT/enhancer-binding protein β (*Cebpb*), a critical regulator of PGR, through SMAD1/5. The *Acvr1 Pgr*-Cre cKO mice show delayed implantation of blastocysts, impaired stromal cell decidualization, and sterility [175]. Conditional deletion of *Bmpr1a* using *Pgr*-Cre also results in infertility. The uterine luminal epithelium of *Bmpr1a Pgr*-Cre cKO mice has increased microvilli density, estrogen response, and cell proliferation, and maintains the polarity of apical epithelial cells during implantation [176]. Moreover, deletion of *Bmpr1a* in the uterus

reduces the expression of Kruppel-like factor 15 (*Klf15*), a transcription factor that inhibits epithelial cell proliferation during implantation through SMAD signaling [176, 198]. In addition to the aforementioned myometrial and epithelial cell defects, *Smads1/5/4 Amhr2*-Cre cKO mice also have implantation failure, unclosed uterine lumen, and defective decidualization [182].

Nodal signaling components expressed in the human endometrium are involved in tissue remodeling during the menstrual cycle, decidualization, and placentation [199-201]. In the murine uterus, Nodal expression is induced by blastocyst implantation and linked to decidualization and placentation [201]. Conditional deletion of *Nodal* using *Pgr*-Cre causes subfertility due to post-implantation placentation abnormalities and intrauterine growth restriction. Loss of *Nodal* in the uterus reduces proliferation and increases apoptosis in cells of the maternal decidua basalis and compromises placentation [174]. Nodal signals through ACVR1B and ACVR1C [202]. Conditional inactivation of *Acvr1b* using *Pgr*-Cre phenocopies the defects of Nodal *Pgr*-Cre cKO mice [177]. *Acvr1b Pgr*-Cre cKO mice display placental defects including expansion of trophoblast giant cells and reductions in spongiotrophoblast and labyrinth [177].

Activins and inhibins are expressed in human endometrium and placenta and may regulate decidualization and placentation [203, 204]. The aforementioned uterine defects [175, 177] (also see Table 2) demonstrated by conditional ablation of the type I receptors for activin, *Acvr1* and *Acvr1b*, suggest a role of activin signaling in uterine functions.

### 1.2.3 TGFβ superfamily and uterine diseases

TGFβ superfamily signaling has been explored in many common uterine diseases such as uterine fibroids, adenomyosis, and endometrial cancer (reviewed in [151, 170, 205, 206]). Uterine fibroids, also known as leiomyomas, emerging from the myometrium, are the most common noncancerous tumors in the uterus. It is estimated that 5 to 70% women will have this disease during their lifetime and 15 to 30% of them may develop severe symptoms such as uterine bleeding, pelvic pain and miscarriage [180, 207, 208]. Expression of TGFβ ligands and receptors, activin A, and myostatin are higher in human leiomyoma versus myometrium during the secretory phase of the menstrual cycle [209, 210]. The concentrations of TGFβ in serum are higher in women of childbearing age with uterine fibroids than healthy subjects [211]. TGFβ and activin signaling promote leiomyoma development via regulation of cell growth and uterine fibrinogenesis [212, 213]. Treatment with TGFβ3 and activin A up-regulates extracellular matrix genes such as collagen 1A1, fibronectin 1 and versican in myometrial and/or leiomyoma cells [212-215]. Therefore, several drugs have been developed to target the enhanced TGFβ signaling in uterine fibroids, including gonadotropin-releasing hormone-analogs, tibolone and asoprisnil [216, 217].

Adenomyosis is defined by the presence of endometrial glands and stroma within the myometrium and may occur in 8 to 27% females [218, 219]. It has a negative effect on female fertility and may induce malignant conditions such as endometrial cancer [218-220]. The etiology of adenomyosis is not clear. Ectopic endometrium from women with

adenomyosis has increased levels of TGFβ1 and pSMAD3 compared to control endometrium [221]. Consistently, tamoxifen induced adenomyosis in mice is associated with up-regulation of expression of TGFβ1 and pSMAD3 in the cytoplasm of ectopic epithelium, coinciding with epithelial–mesenchymal transition and fibroblast-to-myofibroblast transdifferentiation [221]. Conditional deletion of *Tgfbr1* using *Amhr2*-Cre in uterine mesenchymal cells also causes adenomyosis [179]. In addition, expression of myostatin, activin A, follistatin, *ACVR2*, and *ACVR2B* mRNAs is greater in the adenomyotic nodule than in control endometrium, indicating that activin signaling may play a role in adenomyosis [222].

As the most common gynecological cancer, endometrial cancer ranks fourth in female cancers within the USA [223]. Approximately 61,380 new cases and 10,920 deaths from uterine corpus cancers are projected to occur in 2017 in the United States, 92% of which are endometrial cancers [223]. Mutations affecting TGFβ signaling components including TGFβ receptors and SMADs and alterations in TGFβ signaling activity are reflected in changes in gene expression and/or phosphorylation of key signal transducers that may play a role in the pathoetiology of human endometrial cancer [205, 206]. TGFBR1 has a 5.6% mutation and alteration rate in human endometrial cancer [206, 224-226]. Cancerous human endometrium has markedly lower levels of TGFBR1 protein expression [227, 228]. TGFBR2 is mutated/altered in 6.5% endometrial tumors [206, 224-226]. The Cancer Genome Atlas (TCGA) studies suggested that the percentages of altered SMAD proteins are 13% for SMAD2, 7% for SMAD3, and 10%

for SMAD4 [206, 224-226]. Decreased expression of *SMAD2* and *SMAD4* mRNAs in invasive endometrial cancers versus non-infiltrating cancers were reported [229]. Of note, altered subcellular (i.e., cytoplasmic vs. nuclear) distribution of SMAD2 and SMAD4 may also play a role in endometrial cancer progression [229]. Moreover, immunoreactive signals of pSMAD2 are weak to undetectable in endometrial cancer samples compared with normal endometrium [228]. In addition, SMAD7, the inhibitory SMAD that serves as a negative modulator of TGFβ signaling, is altered in 10% of endometrial cancers, with mRNA up-regulation being the greatest change [206, 224-226]. High SMAD7 expression also correlates with a shorter time to the recurrence of endometrial cancer [230].

### 1.3 Aims and hypothesis

The overall goal of this study is to understand the contributions of TGFβ signaling to maintain normal development and function of the uterus. Based on previous studies and literature, **we hypothesize that TGFβ signaling is required for uterine development and function. Dysregulated TGFβ signaling will cause abnormal uterine cell proliferation and differentiation, leading to developmental defects in the uterus and reproductive failure.** This hypothesis will be tested by addressing the following specific aims.

### 1.3.1 Specific aim 1: define the role of TGFβ signaling in uterine development

We hypothesize that TGFβ signaling plays a key role in regulating myometrial development, which is indispensable for a successful pregnancy. The role of TGFβ signaling in myometrial development will be examined using mice with conditional deletion of *Tgfbr1* by *Amhr2*-Cre.

### 1.3.2 Specific aim 2: identify the effect of dysregulation of TGFβ signaling on uterine development and function

We hypothesize that precisely controlled TGFβ signaling is conducive to uterine development and function, and that dysregulation of TGFβ signaling will lead to uterine defects resulting from altered proliferation/differentiation of uterine cells. We will use mice harboring constitutively active TGFBR1 to examine the consequences of enhanced TGFβ signaling in uterine development and function.

### 1.3.3 Specific aim 3: identify the role of TGFβ signaling in PTEN-inactivated uterine epithelial cells

We hypothesize that TGFβ signaling inhibits the migration/invasion of cancerous epithelial cells in PTEN-inactivated uteri. We will generate mice with conditional deletion of TGFBR1 in the PETN null uterus to determine the interactions between TGFβ signaling and PTEN/AKT signaling in cancerous epithelial cells.

### 1.3.4 Significance and rationale

In the United States, approximately 6% (1.5 million) of married women aged 15 to 44 were infertile between 2006 and 2010 [231]. Furthermore, about 12% (6.7 million) of all women aged 15 to 44 have impaired fecundity, that is, difficulty in either getting pregnant or carrying a pregnancy to give live birth [231]. Among this dramatic number of reproductive-aged women facing pregnancy loss and infertility, many of them are associated with uterine dysfunction and diseases. Therefore, understanding the underlying regulation and mechanisms of uterine development, function and diseases are of particular importance.

Despite the evidence for expression of TGFβ signaling components in the uterus and the reported involvement of TGFβ signaling in uterine functions (reviewed in [151, 170]), the *in vivo* role of TGFβ signaling in the uterus remains elusive, partially because of the redundancy of the ligands [232, 233] and the lack of suitable animal models. Deletion of TGFβ ligands, TGFBR1, or TGFBR2 results in embryonic lethality or death in pups shortly after birth, preventing functional studies of TGFβ signaling in the mouse uterus during the postnatal period [234-239].

TGFβ signaling is required for the integrity of the female reproductive tract [179]. The tissue/cell specific targeting approach for studying TGFβ signaling has been validated as an effective means to define gene function in the reproductive system [145, 147, 179,

240, 241]. Genetic manipulation of *Tgfbr1* expression using the Cre-Lox method overcomes the issues of ligand redundancy and embryonic lethality due to global inactivation of individual TGFβ genes. The proposed study is expected to provide new mechanistic insights into the role of TGFβ signaling in uterine development, function, and diseases. These studies will have a potential impact on the development of new diagnostic and therapeutic strategies for mitigating fertility defects and uterine diseases associated with dysregulated TGFβ signaling.

## 2. TGFBR1 IS REQUIRED FOR MOUSE MYOMETRIAL DEVELOPMENT*

### 2.1 Introduction

The uterus serves as an "incubator" of a new life in mammals [242]. It develops from the Müllerian duct, a tube formed via invagination of the coelomic epithelium during embryogenesis [107, 120]. Myometrium is composed primarily of smooth muscle cells or myocytes, which contain contractile machinery that is tightly regulated during pregnancy and parturition. The role of the myometrium in pregnancy-associated events has been well established. During pregnancy, the myometrial cells transform from a quiescent to a contractile phenotype. Myometrial contractility is regulated/influenced by hormonal, cellular, and molecular signals [109-112, 115, 116, 119, 243]. Structural and functional abnormalities of myometrium may lead to reproductive disorders, resulting in neonatal mortality and morbidity.

In mice, myometrial development occurs after birth, and the uterus acquires all basic structures and configuration by postnatal day 15 (P15) [121, 244]. Myometrial maturation continues into adulthood. Notably, mechanisms that control myometrial development are not well understood. Estrogen seems to play a role in regulating the development of circular myometrium [123]. Tamoxifen-treated neonatal mice

---

* Reprinted in slight modified form with permission from "TGFBR1 is required for mouse myometrial development" by Gao Y, Bayless KJ, Li Q. Mol Endocrinol 2014; 28:380–394.

demonstrate disorganized circular myometrium with reduced laminin expression and develop a uterine pathology reminiscent of adenomyosis, which is defined as the presence of endometrium and uterine glands within myometrium [123]. However, mice treated with estradiol develop intact but hypertrophied muscle layers [123]. Additionally, wingless/integrase-1 (WNT)/β catenin signaling pathway is known to regulate mouse uterine development [124-127]. *Wnt-7a* mutant female mice develop abnormal oviduct and uterus, and smooth muscle defects were observed in the uterus [124, 127]. Despite this knowledge, mechanisms that control the development of morphologically and functionally normal myometrium remain to be elucidated.

Transforming growth factor β (TGFβ) superfamily signaling regulates essential cellular functions and developmental processes [9]. In an earlier study, we generated a conditional knockout (cKO) of the TGFβ type 1 receptor (*Tgfbr1*) using Cre recombinase driven by anti-Müllerian hormone receptor type 2 (*Amhr2*), which is expressed in the mesenchymal cells of the oviduct and uterus [179]. The *Tgfbr1* cKO females are infertile and develop smooth muscle defects in the reproductive tract. Disorganized myometrium is a striking phenotype of the uterus [179]. However, the timing of myometrial defects during postnatal uterine development and the underlying mechanisms are not clear.

TGFβ ligands are regulators of smooth muscle cell differentiation *in vitro* [245, 246]. However, little is known about the role of TGFβ signaling in uterine smooth muscle cell

differentiation *in vivo*. Since uterine smooth muscle cell differentiation is a critical step of myometrial development, it is essential to define smooth muscle differentiation in the *Tgfbr1* cKO model. Notably, postnatal uterine development involves extensive remodeling of extracellular matrix (ECM) [247], which regulates cellular behavior/properties such as proliferation, differentiation, and migration [248, 249]. TGFβ signaling regulates ECM production [250, 251]. Of note, basement membranes enclosing smooth muscle cells play key roles in regulating the phenotype and function of these cells [252, 253]. It has been shown that basement membranes surrounding mouse uterine smooth muscle cells contain collagen IV [254].

Therefore, in this study, we tested whether differentiation of uterine smooth muscle cells and production of key proteins associated with basement membrane were altered in *Tgfbr1* cKO uteri during postnatal uterine development. Our studies focused on a critical time window of postnatal uterine development (i.e., postnatal days 0-15), during which uterus acquires essential configuration. We herein identified an important role of TGFBR1 in regulating myometrial configuration and basement membrane component synthesis during postnatal uterine development, and provided further mechanistic insights into the myometrial defects in *Tgfbr1* conditionally ablated uterus.

## 2.2 Materials and methods

### 2.2.1 Ethics statement

Procedures of mouse manipulation were approved by the Institutional Animal Care and Use Committee (IACUC) at Texas A&M University. Mice were maintained on a C57BL/6/129S6/SvEv genetic background and housed in standard cages under a 12 h light/12 h dark cycle with access to food and water ad libitum. All necessary procedures were taken to minimize the discomfort, distress, and pain of the mice during experiment.

### 2.2.2 Construction of *Tgfbr1* conditional knockout mice

Generation of *Tgfbr1* cKO mice using a *Cre-loxP* strategy was described previously [179]. The *Amhr2*$^{cre}$ allele was kindly provided by Dr. Richard Behringer [171]. A bacterial *lacZ* gene was inserted into the *Tgfbr1* gene to generate a loss-of-function (i.e., a *Tgfbr1* null allele). In the *Tgfbr1* conditional allele, the exon 3 of *Tgfbr1* gene was flanked by two *loxP* sites as described [238]. Genotyping was performed using tail DNAs and polymerase chain reaction (PCR) [179].

### 2.2.3 Sample collection and processing

Uterine samples from control and *Tgfbr1* cKO mice were collected at postnatal day 0 (Birth; P0), P3, P5, P10, and P15. Adult uterine samples were collected from 3 month old control and *Tgfbr1* cKO mice. The samples were processed for histological analysis, RNA isolation, X-gal staining, and immunofluorescence. For periodic acid-Schiff (PAS)-hematoxylin staining and immunofluorescence, uterine samples were fixed in

10% neutral buffered formalin (NBF) (Sigma) immediately after collection. Samples were then washed with 70% ethanol before being processed for paraffin embedding. For RNA preparation, samples were homogenized in RNA lysis tissue (RLT) buffer (Qiagen) and stored at -80°C until isolation. Sample processing for X-gal staining was described below.

### 2.2.4 Histological assays

All samples were processed and embedded using the Histology Laboratory of Veterinary Integrative Biosciences at Texas A&M University. Uterine tissues were serially sectioned at 5 μm and processed for PAS-hematoxylin staining [145].

### 2.2.5 RNA isolation, reverse transcription, and quantitative real-time PCR

Total RNA was isolated from uterine samples using RNeasy Mini Kit (Qiagen) according to manufacturer's instructions. On-column DNase (Qiagen) digestion was incorporated into RNA isolation procedure to remove potential genomic DNA contamination. RNA concentration and the ratio of the absorbance at 260 nm and 280 nm were measured using a NanoDrop Spectrophotometer ND 1000 (NanoDrop Technologies). Reverse transcription (RT) was carried out using 200 ng total RNA and superscript III (Invitrogen) reverse transcriptase to synthesize the first DNA strand. Quantitative real-time PCR (qPCR) was performed using a CFX384/CFX Connect Real-time PCR Detection System (Bio-Rad). The PCR program consisted of 95°C for 30s, 40 cycles of 95°C for 5 s, and 60°C for 30s. All assays were performed in duplicate using

iTaq Universal SYBR Green Supermix (Bio-Rad) and gene specific primers (Table 3). Specificity of the amplification was verified by dissociation curve and gel electrophoretic analyses. Ribosomal protein L19 (*Rpl19*) was used as an internal control. Relative levels of gene expression were calculated using ΔΔCT method [255].

**Table 3.** Primers for quantitative real-time PCR

| **Name** | **Sequence (5′-3′)** | | **Reference** |
|---|---|---|---|
| *Col4a1* | Forward | CTGGCACAAAAGGGACGAG | PrimerBank ID |
| | Reverse | ACGTGGCCGAGAATTTCACC | 33859528a1 |
| *Col4a2* | Forward | GACCGAGTGCGGTTCAAAG | PrimerBank ID |
| | Reverse | CGCAGGGCACATCCAACTT | 556299a1 |
| *Col4a3* | Forward | CAAAGGCATCAGGGGAATAACT | PrimerBank ID |
| | Reverse | ACCCTTAGATCCGTTGCATCC | 145699100c1 |
| *Col4a4* | Forward | ATGAGGTGCTTTTTCAGATGGAC | PrimerBank ID |
| | Reverse | GGGGCCGCCATACTTCTTG | 34328045a1 |
| *Col4a5* | Forward | AGGCGAAATGGGTATGATGGG | PrimerBank ID |
| | Reverse | CTCCCTTACCGCCCTTTTCTC | 26348681a1 |
| *Col4a6* | Forward | ATCGGATACTCCTTCCTCATGC | PrimerBank ID |
| | Reverse | CCAGGGGAGACTAGGGACTG | 13435918a1 |
| *Fn1* | Forward | GATGTCCGAACAGCTATTTACCA | PrimerBank ID |
| | Reverse | CCTTGCGACTTCAGCCACT | 29835174a1 |
| *Lama1* | Forward | CGGGTCTGTGACGGTAACAGT | [256] |
| | Reverse | GCCATCGATTGCGTGTGAT | |
| *Lama2* | Forward | GGAAAAAGGACCCGAGATGTACT | [256] |
| | Reverse | TGAGGGTTCCTCACAGGCTG | |
| *Lama3* | Forward | TCTTGTAGGGTCTGCCCCTG | [256] |
| | Reverse | AGCTCCACCATCCACAGCAC | |
| *Lama4* | Forward | CAGCTGGACGACTACAACGC | [256] |
| | Reverse | ATGGTCGAGGGCCTGGTTA | |
| *Lama5* | Forward | CGGATGGGACCTGTGAAGA | [256] |
| | Reverse | GCTCTCCTGTGAAGTTCGGC | |
| *Lamb1* | Forward | CCACTGGCGACCTTCTCATC | [256] |
| | Reverse | CTGGTTTGTGCAGTCCACATG | |
| *Lamb2* | Forward | GAACTTCGCTTGGGCCTACTT | PrimerBank ID |
| | Reverse | GGTGGCTGGATAGCAGCTT | 31982223a1 |

**Table 3.** Continued.

| Name | | Sequence (5′-3′) | Reference |
|---|---|---|---|
| *Lamb3* | Forward | GGCTGCCTCGAAATTACAACA | PrimerBank ID |
| | Reverse | ACCCTCCATGTCTTGCCAAAG | 6678660a1 |
| *Lamc1* | Forward | AAGTCCTGTCACCTGTGCGAC | [256] |
| | Reverse | CATAGTCTGGCTTTGCCACCA | |
| *Lamc2* | Forward | CAGACACGGGAGATTGCTACT | PrimerBank ID |
| | Reverse | CCACGTTCCCCAAAGGGAT | 19115956a1 |
| *Lamc3* | Forward | CGGAGCCCTGCATCACAAA | PrimerBank ID |
| | Reverse | AGCAAGGTCGTCCTCAAAGC | 6453719a1 |
| *Tagln* | Forward | CGATGGAAACTACCGTGGAGA | [257] |
| | Reverse | TGAAGGCCAATGACGTGCT | |
| *Acta2* | Forward | GTCCCAGACATCAGGGAGTAA | PrimerBank ID |
| | Reverse | TCGGATACTTCAGCGTCAGGA | 6671507a1 |
| *Actg2* | Forward | CCGCCCTAGACATCAGGGT | PrimerBank ID |
| | Reverse | TCTTCTGGTGCTACTCGAAGC | 6752952a1 |
| *Cnn1* | Forward | GGTGAAACCCCACGACATCTT | [257] |
| | Reverse | TTTGTCTTGGCCATGCTGG | |
| *Myh11* | Forward | CATCCTGACCCCACGTATCAA | [257] |
| | Reverse | ATCGGAAAAGGCGCTCATAGG | |
| *Des* | Forward | TACACCTGCGAGATTGATGCC | [257] |
| | Reverse | GCGCAATGTTGTCCTGATAGC | |
| *Smtn* | Forward | TCACTACCTTCAGCCATGCCT | [257] |
| | Reverse | GCCATTAGCTGCTTCCACTGT | |
| *Myocd* | Forward | CCAACACCTTGCCCAGTTATC | [179] |
| | Reverse | GGAGCTTGTGCTGCCAAAG | |
| *Tgfb1* | Forward | CTCCCGTGGCTTCTAGTGC | PrimerBank ID |
| | Reverse | GCCTTAGTTTGGACAGGATCTG | 6755775a1 |
| *Tgfb2* | Forward | TCGACATGGATCAGTTTATGCG | PrimerBank ID |
| | Reverse | CCCTGGTACTGTTGTAGATGGA | 6678317a1 |
| *Tgfb3* | Forward | CAGGCCAGGGTAGTCAGAG | [258] |
| | Reverse | ATTTCCAGCCTAGATCCTGCC | |
| *Pdgfa* | Forward | GAGGAAGCCGAGATACCCC | PrimerBank ID |
| | Reverse | TGCTGTGGATCTGACTTCGAG | 6715566a1 |
| *Pdgfb* | Forward | AAGTGTGAGACAATAGTGACCCC | PrimerBank ID |
| | Reverse | CATGGGTGTGCTTAAACTTTCG | 6755010a1 |
| *Pdgfc* | Forward | GCCAAAGAACGGGGACTCG | PrimerBank ID |
| | Reverse | AGTGACAACTCTCTCATGCCG | 10242385a1 |
| *Pdgfd* | Forward | TACAGTTGCACTCCCAGGAAT | PrimerBank ID |
| | Reverse | CTTCCAGTTGACAGTTCCGCA | 27229137a1 |
| *Rpl19* | Forward | ATGAGTATGCTCAGGCTACAGA | PrimerBank ID |
| | Reverse | GCATTGGCGATTTCATTGGTC | 6677773a1 |

### 2.2.6 X-gal staining

X-gal staining was conducted as described previously [179]. Briefly, mouse uterine samples were fixed in fixation buffer (2% paraformaldehyde, 0.2% glutaraldehyde, and 0.1 M phosphate pH 7.4) and then rinsed with rinse buffer (0.01% sodium deoxycholate, 0.02% NP-40, 2 mM $MgCl_2$, and 0.1 M phosphate pH 7.4). The samples were stained for 16 h at room temperature in staining buffer (5 mM potassium ferricyanide, 5 mM potassium ferrocyanide, and 1 mg/ml X-gal dissolved in rinse buffer). After staining, the samples were washed with PBS, fixed in 10% NBF, and further processed for paraffin embedding and sectioning. At the final step, the sections were deparaffinized, rehydrated, and counterstained with fast red (Vector lab).

### 2.2.7 Immunofluorescence, immunohistochemistry, and immunocytochemistry

Paraffin-embedded samples were cut into serial sections (5 μm), which were subsequently deparaffinized in xylene and rehydrated in graded alcohol. The sections were boiled in 10 mM citrate buffer (pH 6.0) for 20 min to expose the antigens. After antigen retrieval, sections were briefly washed with Tris-buffered saline (TBS) and blocked with 3% bovine serum albumin (BSA) for 1h at room temperature. Primary antibodies (Table 4) were then added and incubated at 4°C overnight. After primary antibody incubation, the sections were washed and incubated with Alexa Fluor 488 or 594 conjugated anti-rabbit/rat/mouse IgG (Invitrogen). The sections were thoroughly washed before being mounted with ProLong Gold Antifade Reagent with DAPI (Invitrogen). Omission of primary antibodies and replacement of primary antibodies by

normal IgGs were used as negative controls. The immunoreactive signals were examined and images were captured using IX47 fluorescence microscope with a digital camera (Olympus). For immunohistochemistry, an ABC method was used following primary antibody incubation as described [179]. The signals were developed and visualized using a DAB substrate kit (Vector Labs). Then immunostained sections were counterstained with hematoxylin, and mounted with Permount (Fisher).

**Table 4.** Primary antibodies for immunofluorescence

| Name | Manufacturer | Catalog no. | Host | Dilution |
|---|---|---|---|---|
| ACTA2 | Abcam | ab5694 | Rabbit | 1:1000 |
| ACTA2 | Abcam | ab76549 | Mouse | 1:1600 |
| CNN1 | Millipore | 04-589 | Rabbit | 1:500 |
| Vimentin | Cell Signaling | 5741 | Rabbit | 1:200 |
| Collagen IV | Abcam | ab19808 | Rabbit | 1:200 |
| Laminin | Abcam | ab11575 | Rabbit | 1:200 |
| FN1 | Abcam | ab23750 | Rabbit | 1:400 |
| CD31 | Abcam | ab28364 | Rabbit | 1:200 |
| ACTG2 | Abcam | ab155308 | Rabbit | 1:1000 |
| TAGLN | Abcam | ab14106 | Rabbit | 1:1500 |
| KRT8 | DSHB* | TROMA-I | Rat | 1:100 |
| FOXA2 | Abcam | ab108422 | Rabbit | 1:250 |
| PR | Thermo Scientific | RB-9017 | Rabbit | 1:500 |
| PDGFRA | Cell Signaling | 3174 | Rabbit | 1:200 |
| PDGFRB | Cell Signaling | 3169 | Rabbit | 1:200 |

**Note:** * Developmental Studies Hybridoma Bank

Immunocytochemistry was performed using a standard protocol. Briefly, the cells were fixed with 4% paraformaldehyde in PBS for 15 min at room temperature and then permeabilized with 0.1% Triton X-100 for 15 min. The cells were then washed with PBS, blocked with 10% normal goat serum, and incubated with rabbit anti-calponin 1

antibody (Millipore) overnight. After washing, the cells were incubated with Alexa Fluor 594 conjugated anti-rabbit IgG (Invitrogen) for 1 h. The filamentous actin (F-actin) was stained with phalloidin conjugated to Alexa-488 (Invitrogen). The nucleus was labeled with DAPI using ProLong Gold Antifade Reagent (Invitrogen).

### 2.2.8 Western blot

Western blot was performed as described [145]. Briefly, protein lysates (25 μg) were resolved on 10% Tris gel (Bio-Rad) and electro-blotted to the PVDF membranes (Bio-Rad). The membrane was incubated with rabbit anti-platelet-derived growth factor (PDGF) AA antibody (1:500; Millipore) and rabbit anti-GAPDH (1:1000; Cell Signaling) in 5% BSA. The secondary antibody was horseradish peroxidase (HRP)-conjugated donkey anti-rabbit (1:10,000 in 5% milk; Jackson ImmunoResearch). SuperSignal West Dura Chemiluminescent Substrate (Pierce) was used to detect the signals according to the manufacturer's instruction. Signals were developed using Kodak Image Station 4000 mm PRO (Kodak). The band intensity for PDGFAA and GAPDH was quantified using ImageJ software (NIH, 1.47v) and expressed as a ratio of the intensity of PDGFAA to that of GAPDH to normalize the variation in sample loading.

### 2.2.9 Mouse uterine smooth muscle cell isolation and culture

Uterine smooth muscle cell isolation was performed according to previously published protocols with slight modifications [119, 259]. Uteri from 2-3 month old adult virgin mice were collected and kept in Hank's Buffered Salt Solution (HBSS) (Buffer A; pH

7.4) containing penicillin and streptomycin (Gibco; 100 U/ml) and amphotericin B (Sigma; 2.5 μg/ml). The uterine horns were washed with buffer A without calcium and magnesium (Buffer B) and cut into 2-3 mm pieces and subject to enzymatic digestion at 37 °C with agitation using buffer B containing 1 mg/mL collagenase type II (Sigma), 0.15 mg/mL DNase I (Roche), 1 mg/mL BSA (Sigma), 0.1 mg/mL soybean trypsin inhibitor (Sigma), and 10% FBS (Gibco). After 30 min incubation, the digestion mixture was triturated for 3 min. Equal volume of buffer C (buffer B plus 10% FBS) was added to the digestion mixture before passing through a cell strainer. The first digestion mixture was discarded to minimize cell debris and damaged cells. The remaining tissues were subject to the above incubation-aspiration procedure for five times. The cell suspension from each digestion was kept on ice and combined after the digestion procedure was completed. The combined mixture was centrifuged at 200 × g for 15 min, and the cell pellet was collected and resuspended in phenol red-free Dulbecco's modified Eagle's Medium (DMEM; Thermo Scientific) containing 10% FBS, 100 U/mL penicillin/streptomycin, 2.5 μg/mL amphotericin B (Sigma), and 25 mM Hepes (Gibco). The cells were allowed to an additional attachment step to improve the purity of uterine smooth muscle cells as described [119, 259]. Cells were cultured at 37 °C with 5% $CO_2$.

### 2.2.10 Mouse uterine stromal cell isolation and culture

Isolation and culture of uterine stromal cells were carried out based on a protocol described elsewhere with slight modifications [260, 261]. In brief, uterine horns of adult virgin mice were cleaned of fat, opened longitudinally, cut into 3-5 mm pieces, and

washed with HBSS without calcium and magnesium containing 100 U/ml penicillin/streptomycin (Gibco). The tissues were then incubated in HBSS without calcium and magnesium that contained 0.5% trypsin (AMRESCO; 100 U/ml) for 1 h at 4 °C, followed by two further incubations for 1 h at room temperature and 10 min at 37 °C. The supernatant was discarded and the tissues were washed with HBSS before further digestion using 0.05% collagenase (Sigma) for 45 min at 37 °C. To disperse the stromal cells, the digestion mixture was vortexed until the supernatant was turbid. The mixture was then passed through a 70-μm cell strainer (BD). Cells were collected by centrifugation at 400 × g for 10 min and cultured in DMEM-F12 (Lonza) supplemented with 10% FBS and 100 U/mL penicillin/streptomycin. The cells were then seeded in culture dishes and incubated at 37 °C with 5% $CO_2$. After 90 min incubation, cells were washed with HBSS without calcium and magnesium and cultured in DMEM-F12 supplemented with 10% FBS and 100 U/mL penicillin/streptomycin.

### 2.2.11 Cell migration assay

Cell migration analysis was performed using a Boyden chamber assay with slight modifications [262]. Selection of the dosage of PDGFAA (20 ng/mL) and PDGFBB (20 ng/mL) was based on a preliminary dose-response experiment. Briefly, uterine stromal cells were trypsinized and re-suspended in serum-free DMEM medium. DMEM with or without PDGFAA/PDGFBB was loaded onto the lower well of a 48-well chemotaxis chamber (Neuro Probes, Inc). The chamber was fitted with a polycarbonate membrane (8-μm pore size) that was coated with 30 μg/mL of collagen I (R&D). Fifty μl of uterine

stromal cells (~$5\times10^4$ cells) was added to the upper assay chamber and incubated for 5 h at 37°C with 5% $CO_2$. The membrane was then immersed in 3% glutaraldehyde solution (Sigma) for 20 min before being stained with 0.1% Amido Black (Sigma) for 20 min. After staining, the cells that adhered to the top layer of the membrane were removed using a cotton swab. The membrane was then mounted on a glass slide, imaged, and analyzed by densitometry using Quantity One software (Bio-Rad). The mean value of the control mice without PDGFs was set to 100% and the results were expressed as the percentage of the control for PDGF treatment.

#### 2.2.12 Statistical analyses

A one-way analysis of variance (ANOVA) was conducted to determine the difference among groups. When a significant difference was detected by ANOVA, the difference between means was further defined by a post-hoc Dunnett test. Comparison of means between two groups was assessed using student *t*-test. Data represent mean ± standard error of the mean (SEM). Statistical significance was defined at $P < 0.05$. All statistical analyses were performed using SPSS software (Statistical Package for the Social Sciences; Version 21).

### 2.3 Results

#### 2.3.1 TGFBR1 is required for normal myometrial development

Our previous studies demonstrated that TGFBR1 is essential for female reproductive tract integrity and function [179]. Conditional knockout of *Tgfbr1* in the female

reproductive tract using *Amhr2*-Cre leads to prominent smooth muscle defects in the oviduct and uterus with full penetrance [179]. To define a time line of the myometrial defects during postnatal uterine development, we first performed PAS staining to compare myometrial development in *Tgfbr1* cKO and control mice at P0, P3, P5, P10, and P15 (Appendix A-1). At P3, three layers of the uterus (i.e., inner, middle and outer layers) were evident by PAS-hematoxylin staining in the controls (Appendix A-1C) [121]. Highly organized smooth muscle layers were formed developmentally in the controls (Appendix A-1A, C, E, G, and I), but not in the *Tgfbr1* cKO mice (Appendix A-1B, D, F, H, and J).

To better visualize the myometrial compartment and monitor its development, we performed immunofluorescence using an antibody directed against calponin 1 (CNN1) (Figure 3). At birth (P0), the CNN1 signal intensity was low in the uteri of control and *Tgfbr1* cKO mice (Figure 3A and B). At P3, the prospective circular myometrial layer in the control mice was clearly identified using the anti-CNN1 antibody (Figure 3C). In contrast, CNN1-positive cells were dispersed and an intact circular myometrial layer was not found in the *Tgfbr1* cKO mice (Figure 3D). At P5, a pronounced disruption of the circular myometrial layer was evident in the *Tgfbr1* cKO mice compared to control mice (Figure 3E and F). Further development of the longitudinal myometrium characterized by smooth muscle bundles was visualized at P10 and P15 in the wild type uterus (Figure 3G and I), which is in contrast to the age-matched *Tgfbr1* cKO mice whose longitudinal layers were thinner and not well organized into bundles in certain regions at these time

points (Figure 3H and J). Immunofluorescence using additional smooth muscle markers including smooth muscle alpha actin (ACTA2), smooth muscle gamma actin (ACTG2), and transgelin (TAGLN) confirmed these findings (data not shown). These data indicate that TGFBR1 is indispensable for proper myometrial development in mice.

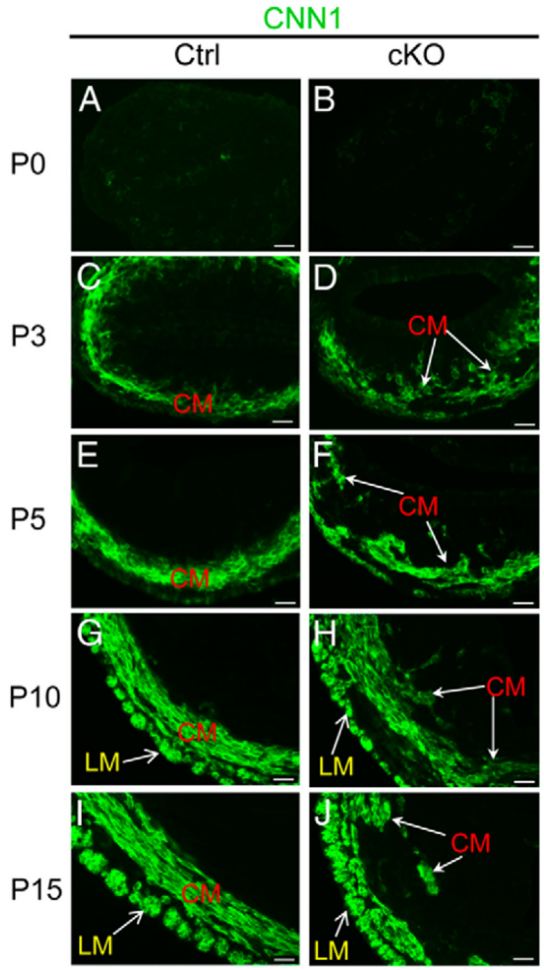


**Figure 3.** Myometrial defects in Tgfbr1 cKO mice during early uterine development. Localization of CNN1 (Green) at P0 (A and B), P3 (C and D), P5 (E and F), P10 (G and H), and P15 (I and J) in control and *Tgfbr1* cKO mice. Representative images are shown for each time point ($n = 3$). Note that at birth (P0), the CNN1 signal intensity was low in the uteri of control and *Tgfbr1* cKO mice. CNN1-positive cells emerged at P3, and defects in uterine smooth muscle cell formation occurred as early as P3 examined. CM, circular smooth muscle layer; LM, longitudinal smooth muscle layer. Scale bar = 20 μm.

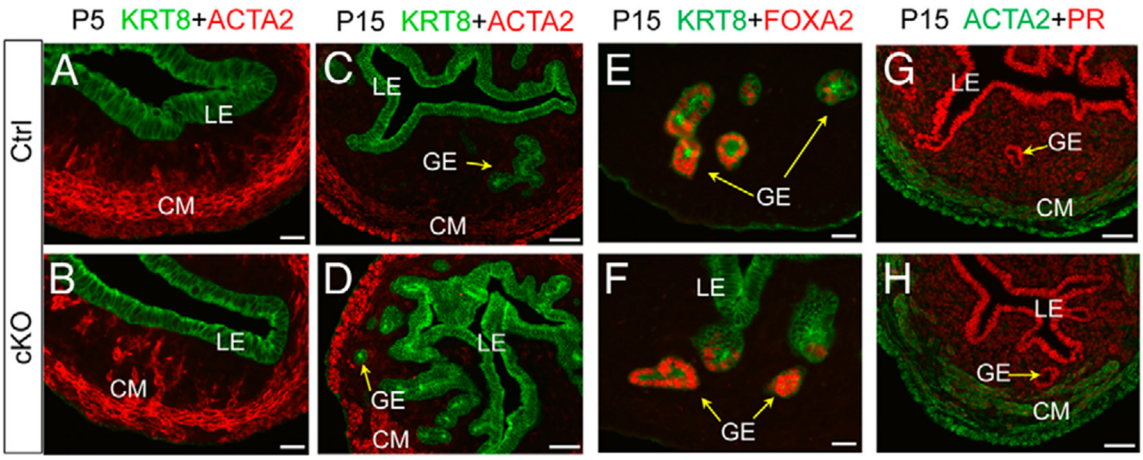


**Figure 4.** Adenogenesis in *Tgfbr1* cKO mice. (A-D) Localization of KRT8 (Green) and ACTA2 (Red) in the uteri of control and *Tgfbr1* cKO mice at P5 (A and B) and P15 (C and D). Note that KRT8 was restricted to uterine luminal epithelium and surface epithelium before uterine gland formation at P5, and the presence of KRT8-positive uterine glands in the disrupted myometrial layers of *Tgfbr1* cKO mice at P15. (E and F) Localization of FOXA2 (Red) and KRT8 (Green) in the uteri of control and *Tgfbr1* cKO mice at P15. (G and H) Localization of PR (Red) and ACTA2 (Green) in the uteri of control and *Tgfbr1* cKO mice at P15. Representative images are shown for each group (*n* = 3). LE, luminal epithelium; GE, glandular epithelium; CM, circular smooth muscle layer. Scale bar = 20 μm (A, B, E, and F) and 50 μm (C, D, G, and H).

### 2.3.2 Uterine glands develop in the *Tgfbr1 Amhr2*-Cre conditional knockout mice

In contrast to the marked disruption of myometrial development in the *Tgfbr1* cKO mice, development of uterine glands seemed to be initiated and progressed similarly as control mice during early postnatal development (Figure 4). Immunofluorescence analysis of cytokeratin 8 (KRT8), an epithelial marker, revealed that KRT8 was restricted to uterine luminal epithelium and surface epithelium in both control and *Tgfbr1* cKO mice at P5 before uterine gland formation (Figure 4A and B). At P15, uterine adenogenesis occurred in both control and *Tgfbr1* cKO mice (Figure 4C and D). FOXA2, a regulator of uterine adenogenesis, was expressed in the glandular epithelium

of both *Tgfbr1* cKO and controls (Figure 4E and F). Because progesterone signaling is a key determinant of uterine adenogenesis [263], we examined progesterone receptor (PR) expression and found that the distribution pattern of PR was comparable between control and *Tgfbr1* cKO uteri during early uterine development (Figure 4G and H), which is in agreement with uterine gland formation in these mice during the early developmental period. However, in contrast to controls where no uterine glands within the myometrium (Figure 4C). KRT8-positive uterine glands were detected within the myometrial lesions in *Tgfbr1* cKO mice (Figure 4D). Thus, despite the fact that adenogenesis was normally initiated in the *Tgfbr1* cKO uteri, further development of uterine glands seemed to be hampered, at least partially due to the incorrect spatial distribution predisposed by the failure of myometrial formation. Collectively, these findings lend support to a cellular basis for the adenomyosis observed in adult *Tgfbr1* cKO uteri, where morphologically normal/abnormal uterine glands were intermingled within the myometrium (Appendix A-2).

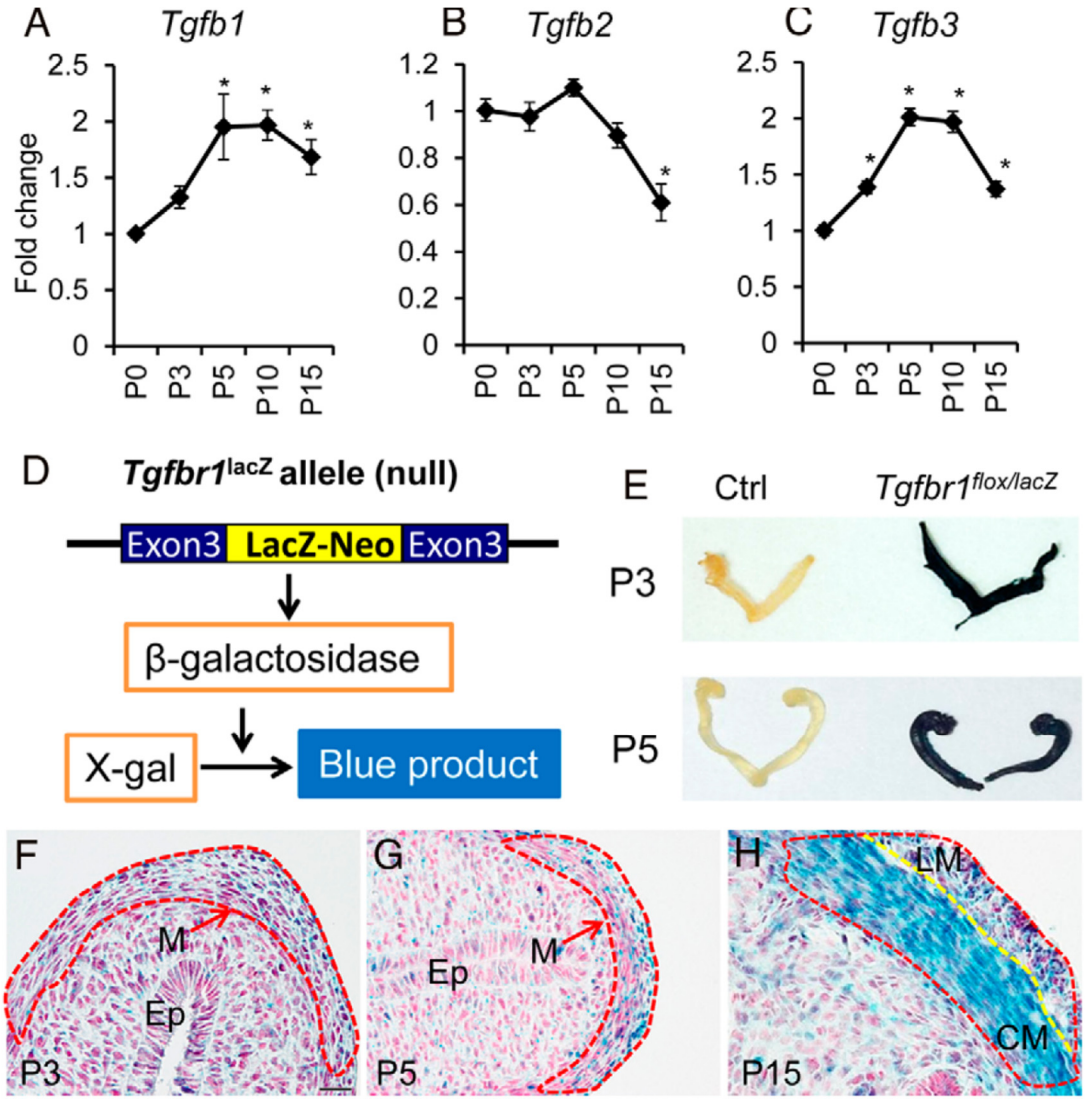


**Figure 5.** TGFβ isoforms and TGFBR1 are expressed in the mouse uterus during its early development. (A-C) Transcript levels of *Tgfb1* (A), *Tgfb2* (B), and *Tgfb3* (C) during postnatal uterine development at P0 ($n = 5$), P3 ($n = 4$), P5 ($n = 3$), P10 ($n = 4$), and P15 ($n = 4$). Data are mean ± SEM. *$P < 0.05$ vs. P0. (D) Schematic representation of *Tgfbr1*$^{lacZ}$ allele and X-gal staining. (E) Gross anatomy of uteri of control (Ctrl) and *Tgfbr1*$^{flox/lacZ}$ mice after X-gal staining. Note the dark blue staining in the *Tgfbr1*$^{flox/lacZ}$ uterus and no discernible staining in uteri of control mice. (F-H) X-gal staining of uterine sections from P3 (F), P5 (G), and P15 (H) mice harboring a *Tgfbr1*$^{lacZ}$ allele. $n$ = 3-5 for each time point. Dotted red lines outline the myometrium. The dotted yellow line marks the boundary between circular and longitudinal smooth muscle layers. Note that the signals for X-gal staining were increased with the progression of uterine smooth muscle cell differentiation. Ep, epithelium; M, myometrium; LM, longitudinal smooth muscle; CM, circular smooth muscle. Scale bar (20 μm) is representatively shown in (F). Sections in panels F-H were counterstained with nuclear fast red.

### 2.3.3 TGFβ ligand/receptor components are expressed during postnatal uterine development

To examine the potential involvement of TGFβ isoforms (*TGFB1-3*)/receptor signaling, we analyzed their expression during postnatal uterine development. *Tgfb1* and *Tgfb3* transcript levels increased after birth and reached a plateau at P5 (Figure 5A and C). In contrast, expression of *Tgfb2* mRNA did not increase, but remained constant from P0 to P5 and declined at P15 (Figure 5B). To determine the localization of TGFBR1, the type 1 receptor for TGFB1-3, in the mouse uterus during early myometrial development, we performed X-gal staining of uterine samples containing a *Tgfbr1* LacZ allele (i.e., $Tgfbr1^{lacZ}$) in which expression of β-galactosidase is driven by the *Tgfbr1* promoter (Figure 5D-H). While control uterine horns showed no discernible staining, the uteri from $Tgfbr1^{flox/lacZ}$ mice had strong blue staining (Figure 5E). Histological analysis further revealed that the X-gal staining was more strongly localized to the myometrial cells, with increasing staining intensity from P3 to P15 in this compartment (Figure 5F-H). Taken together, these results provide evidence that TGFβ signaling may regulate myometrial development through paracrine and/or autocrine actions.

### 2.3.4 Uterine smooth muscle cells express lineage markers in *Tgfbr1* cKO mice

*In vitro* studies suggest that TGFβ signaling regulates smooth muscle gene expression [264-266]. However, it is not clear whether TGFβ signaling is required for uterine smooth muscle cell differentiation *in vivo*. Therefore, we sought to determine whether deletion of *Tgfbr1* in uterine mesenchymal cells affects differentiation of smooth muscle

cells during early uterine development. As a first step, we analyzed the expression of a variety of well-established smooth muscle marker genes including *Acta2*, *Actg2, Cnn1*, *Tagln*, desmin (*Des*), smoothelin (*Smtn*), and smooth-muscle myosin heavy chain (*Myh11*), as well as a critical regulator of smooth muscle gene expression, myocardin (*Myocd*) [267] during postnatal development in wild type mice using qPCR (Figure 6). Consistent with the initiation and progression of smooth muscle cell differentiation during postnatal uterine development, mRNA levels for all the examined smooth muscle marker genes were increased and reached the highest levels at P10 or P15 (Figure 6A-G). Interestingly, the transcript abundance for *Myocd* was increased about 2-fold and reached a plateau at P3 (Figure 6H).

Next, we examined whether conditional deletion of *Tgfbr1* altered the expression of the aforementioned smooth muscle genes. In line with the protein expression of CNN1 (Figure 3), the transcript levels of *Cnn1* were not distinguishable between control and *Tgfbr1* cKO uteri at P5 (Figure 6I). Except for a decline in *Tagln* transcript levels, the abundance of *Acta2*, *Des*, *Smtn*, *Myh11*, *Actg2*, and *Myocd* mRNAs remained comparable between *Tgfbr1* cKO and control mice (Figure 6I). Similar changes in the expression of examined genes were also found at P10 when expression of the majority of the smooth muscle markers reached the highest abundance (data not shown). These results suggest that myometrial defects in *Tgfbr1* cKO mice may not directly arise from an intrinsic deficiency in uterine smooth muscle cell differentiation.

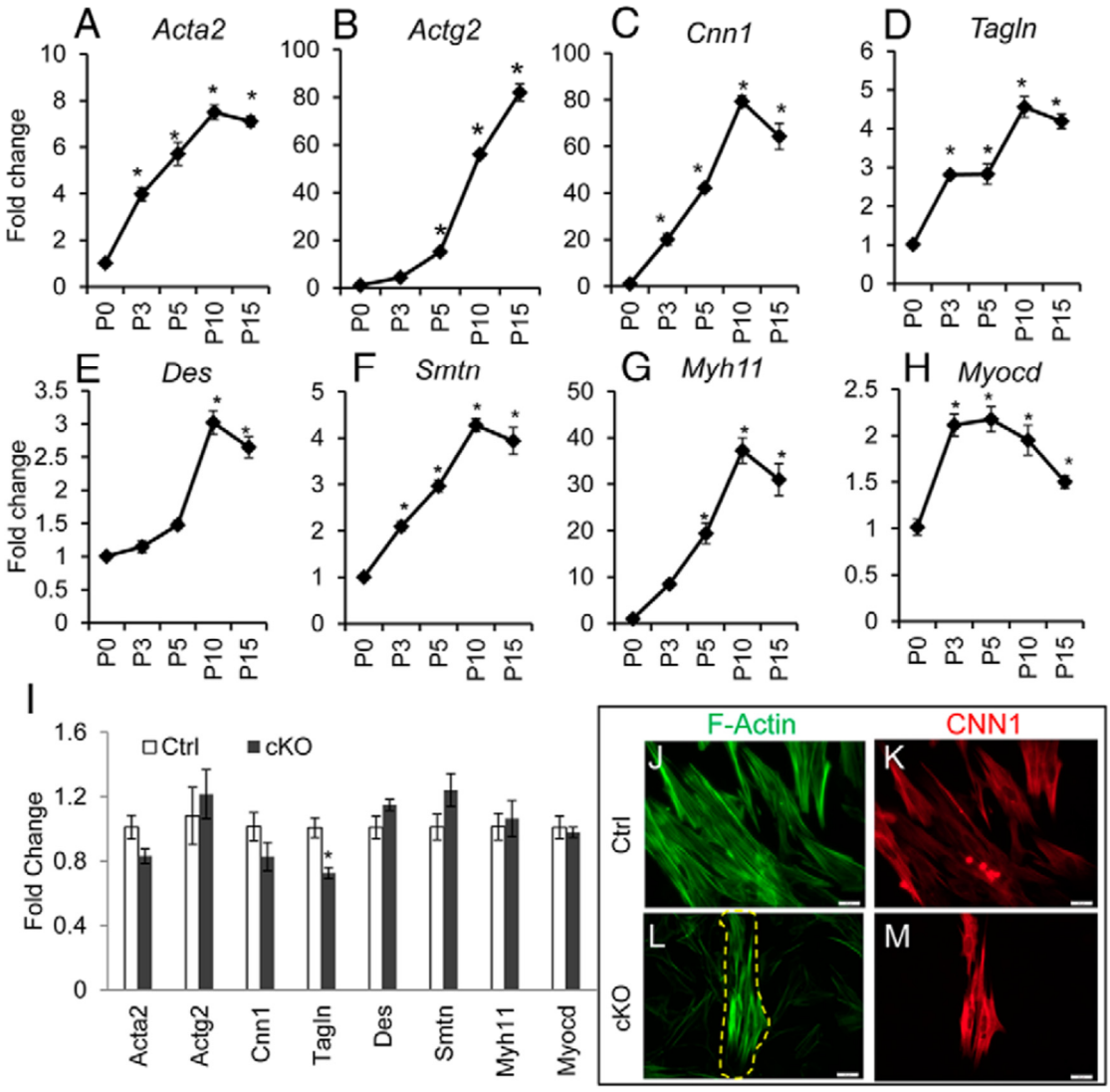


**Figure 6.** Developmental dynamics of mRNA abundance for smooth muscle markers/regulator during postnatal uterine development and the effect of conditional ablation of *Tgfbr1* on expression of smooth muscle genes and F-actin cytoskeleton of uterine smooth muscle cells. Transcript levels of *Acta2* (A), *Actg2* (B), *Cnn1* (C), *Tagln* (D), *Des* (E), *Smtn* (F), *Myh11* (G), and *Myocd* (H) in the wild type uterus during postnatal uterine development at P0 ($n = 5$), P3 ($n = 4$), P5 ($n = 3$), P10 ($n = 4$), and P15 ($n = 4$). (I) Relative levels of expression of mRNAs for smooth muscle genes/regulator in the uteri of control ($n = 5$) and *Tgfbr1* cKO mice ($n = 5$) at P5. Note that mRNA levels for smooth muscle marker genes reached the highest levels at P10 or P15, and no significant difference was detected between control and *Tgfbr1* cKO mice except for *Tagln*, which showed about 30% reduction. Data are mean ± SEM. *$P < 0.05$ vs. P0 (A-H) or corresponding controls (I). (J-M) F-actin (Green) and CNN1 staining (Red) of control (J and K) and *Tgfbr1* cKO (L and M) smooth muscle cells. The dotted yellow line marks smooth muscle cells. Scale bar = 20 μm.

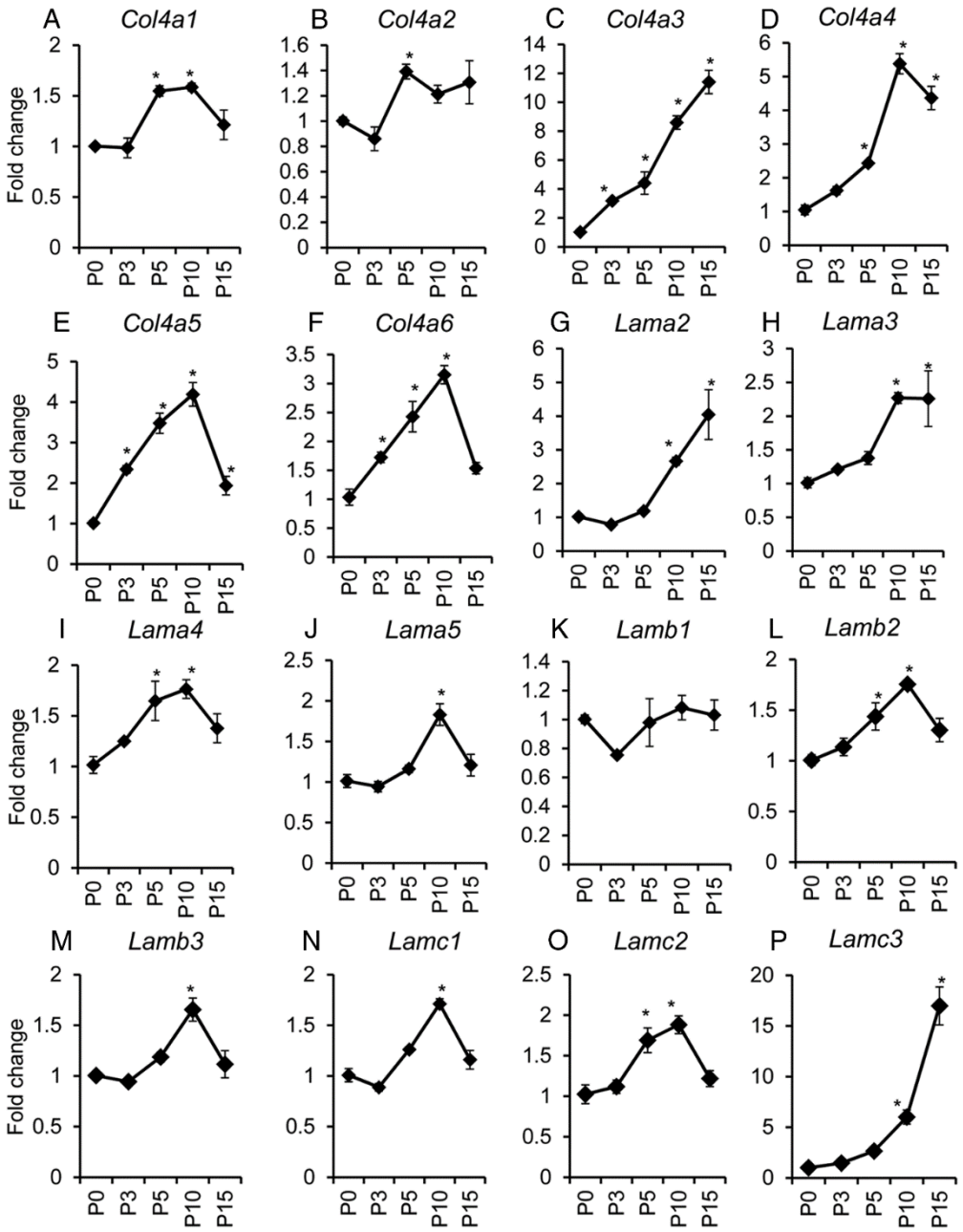


**Figure 7.** Temporal changes in abundances of collagen IV and laminin mRNAs during early postnatal uterine development. Transcript levels of *Col4a1* (A), *Col4a2* (B), *Col4a3* (C), *Col4a4* (D), *Col4a5* (E), *Col4a6* (F), *Lama2* (G), *Lama3* (H), *Lama4* (I), *Lama5* (J), *Lamb1* (K), *Lamb2* (L), *Lamb3* (M), *Lamc1* (N), *Lamc2* (O), and *Lamc3* (P) in wild type uteri during postnatal development at P0 ($n = 5$), P3 ($n = 4$), P5 ($n = 3$), P10 ($n = 4$), and P15 ($n = 4$). Note that collagen IV genes were developmentally regulated and expression plateaued at P5 (*Col4a1* and *Col4a2*), P10 (*Col4a4, Col4a5*, and *Col4a6*), or P15 (*Col4a3*), while expression of mRNAs for the majority of laminin genes peaked at P10 and P15. Data are mean ± SEM. *$P < 0.05$ vs. P0.

To further characterize the cellular properties of the uterine smooth muscle cells *in vitro*, we isolated and cultured mouse uterine myocytes. We were able to enrich uterine smooth muscle cells from wild type control mice (Figure 6J and K). In the controls, F-actin was clearly stained and distributed in an organized pattern (Figure 6J), and the identity of smooth muscle cells was confirmed using immunofluorescence staining of CNN1 (Figure 6K), as well as ACTA2 (data not shown). However, the same smooth muscle cell isolation protocol did not efficiently enrich for myocytes from *Tgfbr1* cKO mice (Figure 6L and M), potentially due to the disruption of the myometrium within the uterus (i.e., myometrial cells were intermingled with endometrium). The myocytes from *Tgfbr1* cKO mice seemed to have clearly stained F-actin fibers when cultured *in vitro* (Figure 6L).

### 2.3.5 Production of ECM proteins associated with the basement membrane is impaired in uteri in which *Tgfbr1* is conditionally ablated

The ECM components undergo constant remodeling (i.e., synthesis, deposition, and degradation), which is implicated in normal development and diseases [268, 269]. To determine the expression pattern of ECM components associated with the basement membrane zone, we analyzed the expression of type IV collagen (*Col4a1*, *Col4a2*, *Col4a3*, *Col4a4*, *Col4a5*, and *Col4a6*), laminin (*Lama1*, *Lama2*, *Lama3*, *Lama4*, *Lama5*, *Lamb1*, *Lamb2*, *Lamb3*, *Lamc1*, *Lamc2*, and *Lamc3*), and fibronectin (*Fn1*) genes. We found that expression of collagen IV genes in the mouse uterus was developmentally up-regulated after birth and plateaued at P5 (*Col4a1* and *Col4a2*; Figure 7A and B), P10

(*Col4a4, Col4a5*, and *Col4a6*; Figure 7D-F), or P15 (*Col4a3*; Figure 7C). The laminin genes were also regulated during development and the transcript levels of the majority of laminin genes (*Lama3*, *Lama4*, *Lama5*, *Lamb2*, *Lamb3*, *Lamc1*, *Lamc2*) peaked at P10 (Figure 7H-J and L-O) and P15 (*Lama2* and *Lamc3*; Figure 7G and P). *Lama1* mRNA levels were close to the detection limit and thus *Lama1* was excluded from this analysis. In contrast, no significant changes in *Lamb1* and *Fn1* were found at the examined time points (Figure 7K and Appendix A-3A).

**Table 5.** Relative expression of mRNAs for collagen IV genes in uteri of control and *Tgfbr1* cKO mice at P5 and P10

| Gene | P5 Ctrl ($n$ = 5) Mean ± SEM | P5 cKO ($n$ = 5) Mean ± SEM | P10 Ctrl ($n$ = 5) Mean ± SEM | P10 cKO ($n$ = 3) Mean ± SEM |
|---|---|---|---|---|
| *Col4a1* | 1.00 ± 0.03 | 0.81 ± 0.04* | 1.03 ± 0.13 | 0.98 ± 0.16 |
| *Col4a2* | 1.12 ± 0.30 | 1.22 ± 0.17 | 1.00 ± 0.05 | 0.73 ± 0.19 |
| *Col4a3* | 1.01 ± 0.06 | 0.90 ± 0.13 | 1.01 ± 0.06 | 0.64 ± 0.13* |
| *Col4a4* | 1.01 ± 0.08 | 0.82 ± 0.03* | 1.00 ± 0.03 | 0.70 ± 0.03* |
| *Col4a5* | 1.01 ± 0.05 | 0.74 ± 0.07* | 1.01 ± 0.08 | 0.66 ± 0.05* |
| *Col4a6* | 1.01 ± 0.05 | 1.03 ± 0.04 | 1.01 ± 0.06 | 0.85 ± 0.02 |

*$P < 0.05$ vs. age-matched controls

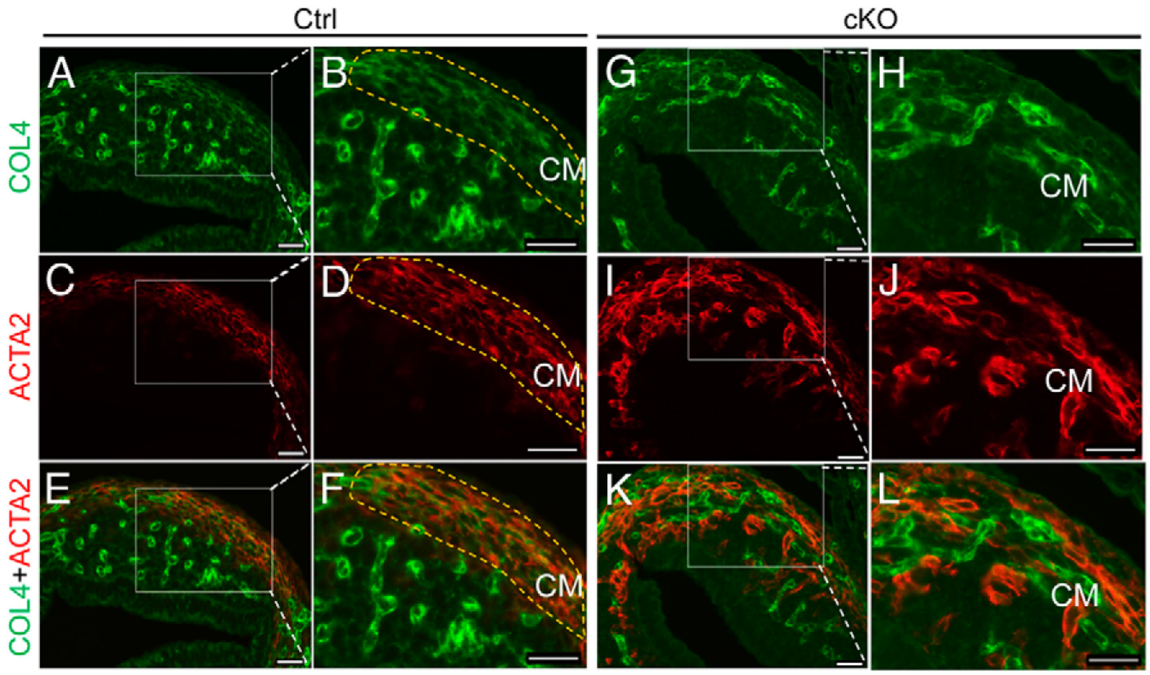


**Figure 8.** Conditional ablation of *Tgfbr1* reduces expression of collagen IV in the mouse uterus during early development. (A-F) Subcellular localization of collagen IV (Green; A and B), ACTA2 (Red; C and D), and collagen IV and ACTA2 (E and F) in uteri of control mice at P5. (G-L) Subcellular localization of collagen IV (Green; G and H), ACTA2 (Red; I and J), and collagen IV and ACTA2 (K and L) in uteri of *Tgfbr1* cKO mice at P5. Note the diminished immunofluorescence signals for collagen IV in the smooth muscle cells of *Tgfbr1* cKO mice (G-L) compared with control mice (A-F). Representative images are shown for each group ($n = 3$). The yellow dotted lines indicate that the circular smooth muscle layers developed at P5. CM, circular smooth muscle layer; COL4, collagen IV. Scale bar = 20 μm.

Based on the fact that postnatal uterine development involves extensive ECM remodeling and the role of TGFβ in this process [270, 271], we hypothesized that the production of type IV collagen chains and other ECM components associated with the basement membrane is impaired in the *Tgfbr1* cKO uteri. To test this hypothesis, we performed qPCR to compare the transcript levels of genes encoding collagen IV, laminin, and fibronectin between control and *Tgfbr1* cKO mice at P5 and P10, two

critical time points of myometrial formation. Our results showed a reduction in expression of *Col4a1*, *Col4a4*, and *Col4a5* mRNAs in the *Tgfbr1* cKO mice compared with control mice at P5 (Table 5). Analysis of P10 samples revealed down-regulation of *Col4a3*, *Col4a4*, and *Col4a5* transcripts in mice with conditionally deleted *Tgfbr1* (Table 5). To further examine the subcellular localization and potential alterations in collagen IV protein in *Tgfbr1* cKO mice, we performed immunofluorescence analyses and found that collagen IV was strongly associated with microvessels (Figure 8A, B, E, F, G, H, K, and L). A signal for collagen IV was also detected in the newly formed circular smooth muscle layers in the control mice at P5 (Figure 8A-F). However, immunofluorescence signals for collagen IV in the disrupted uterine smooth muscle layers of the *Tgfbr1* cKO mice were diminished (Figure 8G-L). Meanwhile, we observed a change in the distribution of endometrial blood vessels in the *Tgfbr1* cKO uteri compared with controls using CD31/PECAM-1 to label endothelial cells within the endometrium (Appendix A-4).

A significant reduction in transcript levels for laminin genes was not detected in the *Tgfbr1* cKO mice at P5 or P10 with the exception of *Lama2* and *Lamc2* for which the mRNA levels were reduced at P10 (data not shown). Since the qPCR was performed using whole uterine tissues that could potentially mask the cell-specific changes in expression of laminin, we further examined laminin protein localization in the uterine tissue sections. Immunofluorescence analyses demonstrated that the predominant sites of laminin expression were microvessels and uterine smooth muscle layers (Appendix A-

5A, B, E, F, G, H, K, and L). Well-organized circular myometrial layers with abundant laminin expression were found in control mice (Appendix A-5A-F). However, disruption of the uterine smooth muscle layer formation was accompanied by a reduction in laminin signals in the uterine smooth muscle cells of *Tgfbr1* cKO mice (Appendix A-5G-L). In contrast to the dysregulation of collagen IV and laminin, the expression of FN1 was not different between control and *Tgfbr1* cKO uteri (Appendix A-3B-F). These data suggest that the compromised synthesis of basement membrane components resulting from conditional deletion of *Tgfbr1* may disrupt basement membrane deposition and interfere with myometrial organization/formation.

### 2.3.6 Altered platelet-derived growth factor (PDGF) expression in *Tgfbr1* cKO uteri and the role in uterine stromal cell migration

PDGFs are well-established migratory factors [272, 273]. In the *Tgfbr1* cKO uteri, we found greater expression of mRNAs for *Pdgfa* and *Pdgfb* during early uterine developmental stages (Figure 9A). Western blot analysis demonstrated the increased expression of PDGFAA in the *Tgfbr1* cKO uteri (Figure 9B). To explore the implication of the increased PDGFs in the uterus of *Tgfbr1* cKO mice, we first analyzed the PDGF receptor (PDGFRA and PDGFRB) localization during postnatal uterine development. We found that PDGFRA (Figure 9C-F) and PDGFRB (Figure 9G-J) were predominantly localized to uterine stromal cells, with no expression in the epithelium. In the myometrial compartment, PDGFRA signals were close to background level, while PDGFRB expression was low, but detectable (Figure 9C-J).

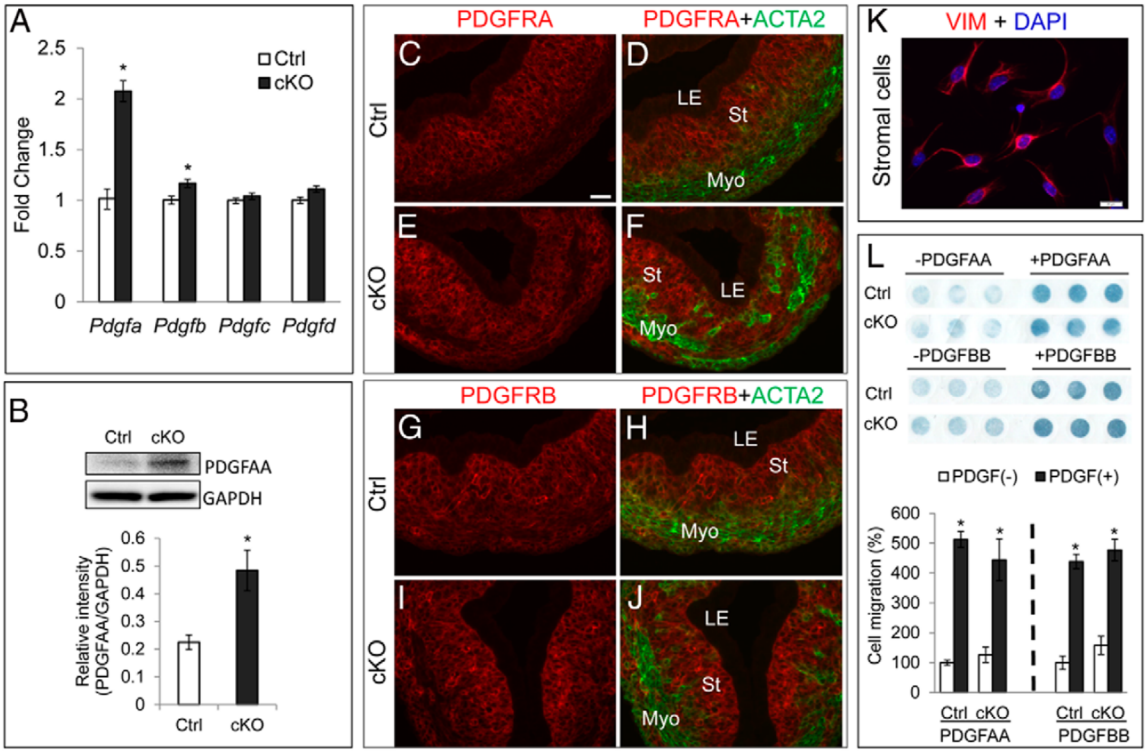


**Figure 9.** Altered PDGF expression in *Tgfbr1* cKO uteri and its role in uterine stromal cell migration. (A) Relative expression of mRNAs for *Pdgfa*, *Pdgfb*, *Pdgfc*, and *Pdgfd* in the uteri of control and *Tgfbr1* cKO mice at P5 ($n$ = 5 per group). (B) Western blot analysis of PDGFAA protein in control and *Tgfbr1* cKO mice. Representative images are depicted in the upper panel and the lower panel shows the relative intensity of PDGFAA, which is expressed as a ratio of the density of PDGFAA to that of GAPDH ($n$ =3 per group). (C-F) Subcellular localization of PDGFRA in uteri of control (C and D) and *Tgfbr1* cKO mice (E and F) at P5. (G-J) Subcellular localization of PDGFRB in uteri of control (G and H) and *Tgfbr1* cKO mice (I and J) at P5. Representative images (C-J) are shown for each group ($n$ =3). Note the PDGFRA and PDGFRB signals were strongly present in the stromal cells but absent from the uterine epithelium. LE, luminal epithelium; St, stroma; Myo, myometrium. Scale bar (20 μm) is representatively denoted in (C). (K) Primary uterine stromal cells express vimentin (VIM). Isolated uterine stromal cells were cultured for 24 h and stained with anti-vimentin antibody. Scale bar = 20 μm. (L) PDGFAA and PDGFBB induce uterine stromal cell migration in control and *Tgfbr1* cKO mice. Representative images of cells in the Boyden chamber assay are depicted in the upper panel, and the lower panel shows the quantification data from three independent assays. Data are mean ± SEM. *$P < 0.05$ vs. corresponding controls.

Based on the cellular distribution of PDGF receptors in the uterus, we postulated that PDGFs regulate/control cell migration during postnatal uterine development. To test this hypothesis, we isolated mouse primary uterine stromal cells, which are positive for vimentin (Figure 9K). Using a Boyden chamber assay, we found that PDGFAA and PDGFBB (20 ng/mL) induced uterine stromal cell migration ($P < 0.05$) in both control and *Tgfbr1* cKO mice to similar levels, and the ability of stromal cells to migrate was not altered in the *Tgfbr1* cKO mice (Figure 9L). Hence, elevated PDGFs could potentially enhance uterine stromal cell migration via paracrine action in the *Tgfbr1* cKO mice during postnatal uterine development.

## 2.4 Discussion

### 2.4.1 Role of TGFBR1 in myometrial development and pathology

Accumulating evidence indicates an obligatory role for TGFβ superfamily signaling in female reproduction [142, 274]. TGFβ superfamily members and signaling components including TGFβs [153, 154], activin [167], myostatin [168] and TGFBRs and SMADs [152, 154] are present in the myometrium. TGFβs modulate the rate of DNA synthesis of human myometrial smooth muscle cells [154], while activin and myostatin inhibit human myometrial cell growth/proliferation [167, 168]. These studies provide circumstantial evidence that TGFβ superfamily signaling is involved in the development and/or function of the myometrium. However, the *in vivo* function of TGFβ ligands/receptors and their associated signaling cascades in the myometrium are poorly defined.

The essential role of TGFβ signaling in the female reproductive tract was demonstrated in the *Tgfbr1* conditional knockout mouse model [179]. Conditional deletion of *Tgfbr1* in the mesenchymal compartments of the female reproductive tract using *Amhr2*-Cre renders the mice infertile [179]. The *Tgfbr1* cKO mice are viable and the infertility is not attributed to ovarian dysfunction, but caused by the development of oviductal diverticulum [179]. Remarkably, these mice develop smooth muscle defects in the oviduct and uterus [179]. By focusing on a critical time window of postnatal uterine development, we found that uterine smooth muscle defects in *Tgfbr1* cKO mice occurred during early development. The developmental expression of TGFβ isoforms and the localization of TGFBR1 in the myometrial cells provided further evidence in support of the involvement of TGFβ signaling in the myometrium. Although the myometrial defects and alteration in basement membrane components were primarily caused by loss of TGFBR1 in uterine smooth muscle cells, our results did not rule out the potential contribution of the *Amhr2-Cre* expression in endometrial stromal cells to the observed phenotype/molecular alterations.

In contrast to the myometrial disruption, development of uterine glands seemed to be initiated and progressed normally during early uterine development in the *Tgfbr1* cKO mice. However, in adult mice, the *Tgfbr1* cKO myometrium showed reduced continuity and the presence of endometrium and uterine glands within the myometrium, resembling adenomyosis observed in mice exposed to tamoxifen, an estrogen receptor antagonist, during the neonatal period [123, 275]. The incorrect spatial localization of uterine glands

during adenogenesis owing to the myometrial lesions supports the emerging concept that myometrial defects may contribute to the etiology of uterine adenomyosis [123]. Of note, aged *Tgfbr1* cKO mice had glandular defects in the uterus [179], which was potentially secondary to the disruption of uterine smooth muscle development and/or altered uterine mesenchymal-epithelial interactions.

### 2.4.2 Implications of TGFβ signaling in uterine smooth muscle differentiation, basement membrane protein synthesis, and myometrial integrity

In mice, uterine mesenchymal cells remain randomly oriented and undifferentiated until after birth. Between birth and P3, myometrial layers are differentiated from the mesenchyme [121], marking the beginning of myometrial development. Formation of the circular myometrial layer precedes that of the longitudinal layer and is evident by P5. The essential structure of myometrium is well developed by P15 [121]. TGFβ signaling regulates the *in vivo* differentiation of vascular smooth muscle [276]. To determine whether conditional deletion of *Tgfbr1* affected uterine smooth muscle cell differentiation, we examined transcript levels of a number of known smooth muscle genes and regulators in *Tgfbr1* cKO uteri. Surprisingly, mRNA levels of most examined genes were comparable between control and *Tgfbr1* cKO uteri at P5 and P10, two critical time points of myometrial development. However, expression of *Tagln* mRNA was reduced (~30%) in the *Tgfbr1* cKO mice at P5, but not at P15 (data not shown). TAGLN and ACTG2 seem to be more specific markers for smooth muscle than ACTA2, which is also expressed in non-smooth muscle cells and myofibroblast-like cells [277,

278]. However, *Tagln* knockout mice are viable and fertile [279]. Although the role of TAGLN remains to be identified, it is tempting to speculate that reduced expression of TAGLN is associated with delayed/reduced myofibroblast differentiation. Furthermore, the cytoskeleton of uterine smooth muscle cells seemed to be intact in the *Tgfbr1* cKO mice. Altogether, our data suggest that the myometrial defects may not directly arise from an intrinsic deficiency in uterine smooth muscle cell differentiation.

ECM components undergo constant remodeling and regulate smooth muscle development by influencing essential cellular funcitons [268, 269]. Collagen IV and laminin are critically invloved in smooth muscle cell differentiation [280, 281]. Regulation of smooth muscle cell phenotype by basement membrane components has been reported [252, 282]. Based on those findings, we asked whether the myometrial defects in *Tgfbr1* cKO mice were associated with dysregulation of ECM proteins, especially basement membrane components.

Vascular smooth muscle cells are enclosed with basement membranes that regulate their functions [252, 253]. However, the formation, regulation, and function of basement membranes of uterine smooth muscle cells within the myometrium are not well defined, despite evidence that mouse uterine smooth muscle cells express several collagen genes [254]. The finding of reduced synthesis of collagen IV and laminin in *Tgfbr1* cKO mice during early uterine development suggests a potential defect in basement membrane deposition. Of note, loss of *Smad4* causes altered basement membrane deposition during

early development in mice [283]. Our findings support the notion that smooth muscle cells regulate the development of their basement membranes [284]. On the other hand, the altered production of key basement membrane proteins may profoundly affect uterine smooth muscle differentiation (e.g., timing) and myometrial structural development. Understanding the dynamics of synthesis of basement membrane proteins and their role in regulating cell fate and function during postnatal uterine development remains a future goal.

### 2.4.3 Platelet-derived growth factors as potential regulators of uterine development

Further efforts toward exploring mechanisms underlying the developmental failure of the myometrium in *Tgfbr1* cKO mice identified PDGF signaling as a potentially important contributing factor. PDGFs are known migratory regulators for cells including endometrial stromal cells and vascular smooth muscle cells [272, 273]. The increased expression of PDGFs in the *Tgfbr1* cKO mice is a manifestation of a potentially indirect effect of loss of TGFBR1 in the uterus because induction of PDGFs by TGFβ1 *in vitro* was reported [285]. Interestingly, PDGFAA and PDGFBB promoted the migration of uterine stromal cells from both control and *Tgfbr1* cKO mice, consistent with the expression of PDGF receptors by these cells. Although stromal cells isolated from *Tgfbr1* cKO and control mice migrated identically in response to PDGFs, increases in PDGFs could potentially enhance cell migration via paracrine action *in vivo*. Indeed, both *Pdgfa* and *Pdgfb* mRNAs were expressed by uterine stromal cells and smooth muscle cells (Gao Y, unpublished results). Furthermore, the altered abundance of

PDGFs may also affect the uterine vasculature, as PDGFs are known to regulate angiogenesis and vascular stabilization [286, 287]. Collectively, the deficiency in production of extracellular matrix components and abnormal uterine cell migration may contribute to the disrupted myometrial formation in *Tgfbr1* cKO mice during postnatal uterine development.

In summary, this study identified an important role for TGFBR1 in regulating myometrial configuration and synthesis of basement membrane components during early postnatal uterine development, highlighting TGFBR1 as an essential regulator of myometrial development.

# 3. CONSTITUTIVE ACTIVATION OF TRANSFORMING GROWTH FACTOR BETA RECEPTOR 1 IN THE MOUSE UTERUS IMPAIRS UTERINE MORPHOLOGY AND FUNCTION*

## 3.1 Introduction

Transforming growth factor beta (TGFB) superfamily signaling plays a pleiotropic role in fundamental cellular and developmental processes [288]. TGFB superfamily ligands [e.g., TGFBs, activins, and bone morphogenetic proteins (BMPs)] interact with their membrane bound type 2 and type 1 receptors to form a heteromeric complex. Subsequent phosphorylation of the type 1 receptor at the glycine and serine (GS) domains by the constitutively active type 2 receptor activates receptor-regulated intracellular SMAD proteins, which modulate gene transcription in concert with the common SMAD (i.e., SMAD4), co-activators, and co-repressors [44, 289].

TGFB superfamily signaling activity is precisely controlled under normal physiological conditions. Multiple regulatory factors including ligand traps (e.g., follistatin), ligand activators (e.g., tenascin-X), inhibitory SMADs (i.e., SMAD6 and SMAD7), and agonistic/antagonistic pathways may cooperate to govern the normal activity and function of this pathway [289-295]. Accumulating evidence indicates that TGFB

---

* Partially reprinted with permission from "Constitutive activation of transforming growth factor beta receptor 1 in the mouse uterus impairs uterine morphology and function" by Gao Y, Duran S, Lydon JP, DeMayo FJ, Burghardt RC, *et al*. Biol Reprod 2015; 92(2):34.

superfamily members are key regulators of female reproduction, including, but not limited to, follicular development, ovulation, oocyte-cumulus cell communications, uterine decidualization, and conceptus development [138-149, 179].

TGFB ligands (i.e., TGFB1-3) are founding members of the TGFB superfamily. TGFBs signal via TGFB receptor 1 (TGFBR1/ALK5) and receptor 2 (TGFBR2) and downstream SMAD2/3 proteins. Identification of the *in vivo* function of TGFB signaling in the uterus remains a challenging puzzle, partially because of the potential redundancy of the ligands [232, 233] and the lack of appropriate animal models. TGFB signaling components including TGFB ligands, receptors, and SMADs are expressed in the mouse and human myometrium and regulate DNA synthesis in human myometrial cells [152-154]. In the rat uterus, myometrial expression of TGFB1 and TGFB3 is increased from mid-gestation, with TGFB3 strongly localized to the circular myometrial layer at late pregnancy [155]. Interestingly, *TGFB3* levels are higher in human leiomyoma cells versus myometrial cells, and TGFB3 is expected to promote leiomyoma development via stimulating cell growth and fibrogenic process [212]. By taking advantage of a conditional knockout approach, we have shown that ablation of *Tgfbr1* in the female reproductive tract using anti-Müllerian hormone receptor type 2 (*Amhr2*)-Cre recombinase leads to smooth muscle defects and reproductive failure [179, 242], suggesting an essential role for TGFB signaling in myometrial development.

That TGFB signaling is finely tuned argues for the need to use both loss-of-function and gain-of-function approaches to fully understand its physiologic and pathologic roles. Constitutively active receptors can be used to investigate the impact of sustained elevation of a signaling pathway on the pathogenesis of diseases. To our knowledge, mouse models with enhanced TGFB signaling in the female reproductive tract are lacking. Notably, overactivation of TGFB signaling is linked to the development of diseases, including cancer [296-298]. Therefore, in the current study, we created a mouse model harboring a constitutively active TGFBR1 in the uterus whose expression is conditionally induced by the progesterone receptor (*Pgr*)-Cre. Over-activation of TGFB signaling causes infertility and striking phenotypic alterations in the uteri of these mice. Our results highlight the importance of a precisely controlled TGFB signaling system in establishing a uterine microenvironment conducive to normal development and function.

## 3.2 Materials and methods

### 3.2.1 Animals and treatment

All protocols using laboratory mice were approved by the Institutional Animal Care and Use Committee (IACUC) at Texas A&M University. Mice were maintained on a mixed C57BL/6/129SvEv genetic background. Mice were exposed to a 12h dark/12h light cycle with access to food and water ad libitum during the entire experimental period. The *Pgr*-Cre mice were created as described [299]. Mice harboring constitutively active TGFBR1 were generated previously, where strategies including genetic modifications

were described [300]. Briefly, constitutive activation of the receptor in the absence of ligand results from three missense mutations: T204D that constitutively activates the TGFBR1 kinase [46] and L193A/P194A that prevent binding of the TGFBR1 inhibitor, FKBP12 [301]. Mice harboring the *Rosa26-LacZ* allele [Gt(ROSA)26Sor$^{tm1Sor}$/J] [302] were purchased from the Jackson Laboratory and used as a reporter for *Pgr*-Cre expression. Fertility testing was performed by breeding the control and experimental female mice with proven fertile males for a period of 3-months. Superovulation of immature females was performed as described previously [145]. Analysis of uterine decidualization was conducted as reported [179, 303]. Briefly, ovariectomized mice received subcutaneous injections of estradiol (E2; 100 ng/mouse for 3 days; Sigma). The mice were rested for 2 days and then treated with E2 (6.7 ng/mouse) and progesterone (P4; 1.0 mg/mouse; Sigma). After 2 days of injection, one uterine horn was traumatized using a burred needle, while the other served as unstimulated control. Two days after the decidual stimulus, mice were sacrificed and uterine samples collected. The uterine horns were weighed and total RNA was prepared for real-time PCR analysis as described below. Alkaline phosphatase staining was performed to examine uterine stromal cell differentiation as described previously [240].

### 3.2.2 Mouse breeding, genotyping, and DNA recombination analysis

To generate mice with conditionally activated TGFBR1 (TGFBR1$^{CA}$), mice containing a latent constitutively active TGFBR1 were bred with *Pgr*-Cre mice. Genomic DNA was isolated from mouse tails using NaOH buffer. Genotyping and DNA recombination

analyses of the *TGFBR1*$^{CA}$ allele were carried out using polymerase chain reaction (PCR) [300, 304, 305]. Primers used for genotyping of *Pgr*-Cre have been described elsewhere [147]. PCR products were separated on 1% agarose gels containing ethidium bromide and digital images captured using a VWR Gel Imager.

### 3.2.3 Histological analysis

Uterine and ovarian samples were collected from control and experimental mice at defined ages (1 week or 1-3 months) and fixed in neutral buffered formalin. The histology core facility of the Department of Veterinary Integrative Biosciences at Texas A&M University was used for sample processing and embedding. Paraffin sections (5 μm) were serially generated, and hematoxylin and eosin (HE) staining was conducted using a standard protocol. After staining, slides were mounted and examined with a microscope and images were captured using a digital camera (DP25; Olympus) with cellSens® Digital Imaging Software.

### 3.2.4 X-gal staining

Uteri from mice harboring *Rosa26-LacZ* and *Pgr*-Cre were collected and fixed as described [179]. The samples were washed and stained using staining buffer containing 1 mg/ml X-gal, 5 mM potassium ferricyanide, and 5 mM potassium ferrocyanide (Sigma). Samples were then sequentially processed for post-fixation, paraffin embedding, sectioning, and fast red counterstaining [179].

### 3.2.5 Human uterine smooth muscle cell line culture and treatment

A well-characterized human myometrial cell line, PHM1-41 [306-308] was used to determine the effect of TGFB ligands on alpha smooth muscle actin (*ACTA2*) expression in uterine smooth muscle cells. Briefly, PHM1-41 cells were cultured in DMEM supplemented with 10% fetal bovine serum (FBS), penicillin-streptomycin, and 0.1 mg/ml G418 sulfate. Prior to the experiment, G418 was omitted. The cells were serum-starved overnight before treatment. For the SMAD2/3 phosphorylation study, the cells were treated with TGFB1 (2.5 ng/ml; R&D) and collected after 40 min of treatment. The cells were then processed for immunofluorescence as described [242]. Briefly, the cells were fixed with 4% paraformaldehyde in cold PBS for 15 min and permeabilized with 0.1% Triton X-100 for another 15 min. The cells were then blocked with 10% normal goat serum and incubated with rabbit anti-SMAD2/3 antibody (Cell Signaling; 1:100) overnight at 4°C. After washing, the cells were incubated with Alexa Fluor 594 conjugated anti-rabbit IgG (Invitrogen) for 1 h. The nuclei were labeled with DAPI using ProLong Gold Antifade Reagent (Invitrogen). For gene expression analysis, the cells were treated with 2.5 ng/ml of TGFB1 (R&D Systems), TGFB2 (HumanZyme), and TGFB3 (HumanZyme). Selection of the dosage for TGFBs was based on a pilot experiment. Cells were collected after 20 h of treatment and processed for RNA isolation and real-time PCR analysis.

### 3.2.6 Immunofluorescence microscopy

Immunofluorescence microscopy was performed using serial paraffin sections [179]. Antigen retrieval was performed to expose the hidden antigenic sites by boiling the sections for 20 min in 10 mM citrate buffer (pH 6.0) using a microwave oven. Following antigen retrieval, the sections were blocked with 5% bovine serum albumin (BSA; Sigma) and incubated with the following primary antibodies overnight at 4°C in a humid box: mouse anti-ACTA2 (Abcam; 1:2,000), rat anti-cytokeratin 8 (KRT8) (Developmental Studies Hybridoma Bank; 1:100), rabbit anti-vimentin (VIM) (Cell Signaling; 1:200), and goat anti-3-beta-hydroxysteroid dehydrogenase (HSD3B) (Santa Cruz; 1:1000). The slides were next incubated with secondary antibodies conjugated with Alexa Fluor 488 or 594 (Invitrogen) at room temperature for 1 h and the sections were mounted using ProLong Gold Slowfade media with DAPI. The slides were examined using an IX73 microscope (Olympus) interfaced with an XM10 CCD camera and cellSens® Digital Imaging Software. To determine the background levels of the above assays, controls where primary antibodies were replaced by isotype-matched IgGs purified from the same species as the primary antibodies were included.

### 3.2.7 Western blot

Protein lysates were prepared using radioimmunoprecipitation assay (RIPA) buffer [145] containing proteinase and phosphatase inhibitors (Roche) and quantified using a bicinchoninic acid (BCA) Protein Assay Kit (Thermo Scientific). Protein samples (~30 μg) were separated on 10% Tris gel, transferred to polyvinylidene difluoride (PVDF)

membranes (Bio-Rad), and incubated overnight at 4°C with the following primary antibodies: mouse anti- hemagglutinin (HA) (Santa Cruz; 1: 200), rabbit anti-phospho-SMAD2 (Millipore; 1:500); rabbit anti-SMAD2 (Cell Signaling; 1:1000), and mouse anti-beta actin (ACTB) (Sigma; 1:50000). Then, the membranes were washed and further incubated with horseradish peroxidase (HRP)-conjugated donkey anti-rabbit antibody (Jackson ImmunoResearch; 1:20,000) at room temperature for 1 h. The signals were developed with Immobilon Western Chemiluminescent HRP Substrate (Millipore) and scanned using a Kodak Image Station 4000 mm PRO. ACTB was used as an internal control. ImageJ (NIH, 1.47v) was used for western blot quantification, where the intensity of target bands was normalized to that of ACTB to correct for variations in sample loading.

### 3.2.8 RNA isolation and real-time PCR

Mouse uterine tissues were homogenized and total RNA was isolated using an RNeasy Mini Kit (Qiagen) according to the manufacturer's instruction. On column DNase digestion was performed during the procedure to eliminate potential DNA contamination. Total RNA was quantified using a NanoDrop Spectrophotometer ND 1000 (NanoDrop Technologies). Two hundred ng of total RNA were reverse transcribed to generate complementary DNA (cDNA) [242]. Then real-time PCR was performed using CFX Connect Real-time PCR Detection System (Bio-Rad) and iTaq Universal SYBR Green Supermix (Bio-Rad) [242].

Quantification of matrix metalloproteinase 9 (*Mmp9*), *Acta2*, calponin 1(*Cnn1*), desmin (*Des*), smoothelin (*Smtn*), transgelin (*Tagln*), smooth muscle actin gamma (*Actg2*), myosin heavy chain 11(*Myh11*), *Bmp2*, follistatin (*Fst*), and *ACTA2* was conducted as described [242, 309, 310]. Primers used for serine (or cysteine) peptidase inhibitor clade E member 1 (*Serpine1*), connective tissue growth factor (*Ctgf*), *Bmp2*, *Fst* and TGFB-induced factor homeobox 1 (*TGIF1*) are listed below: *Serpine1* (Forward: 5'-TTCAGCCCTTGCTTGCCTC-3', Reverse: 5'- ACACTTTTACTCCGAAGTCGGT-3'; ID# 6679373a1), *Ctgf* (Forward: 5'- GGGCCTCTTCTGCGATTTC-3', Reverse: 5'-ATCCAGGCAAGTGCATTGGTA-3'; ID#6753878a1), *Bmp2* (Forward: 5'-GGGACCCGCTGTCTTCTAGT-3', Reverse: 5'-TCAACTCAAATTCGCTGAGGAC-3; ID# 6680794a1), *Fst* (Forward: 5'-TGCTGCTACTCTGCCAGTTC-3', Reverse: 5'-GTGCTGCAACACTCTTCCTTG-3'; ID# 6679867a1), and *TGIF1* (Forward: 5'-GGGATCAGTTTTGGCTCGTCC-3', Reverse: 5'-GCAGTCACAGTGGTATGGCAG-3'). *Serpine1*, *Ctgf*, *Bmp2*, and *Fst* primers were obtained from PrimerBank [311]. *Rpl19* [242] and *RPLP0/36B4* [119] were used as internal controls for the respective mouse and human gene expression analyses. The assays were performed in duplicate for each biological replicate. Relative levels of gene expression were calculated as described [255].

### 3.2.9 Statistical analysis

The statistical analysis was performed using Statistical Package for the Social Sciences (SPSS; Version 21). A one-way analysis of variance (ANOVA) was applied to

determine the differences in means among treatment groups, followed by a Bonferroni post-hoc test. Comparisons of mean values from two groups were made using the student's *t*-test. Data are presented as mean ± standard error of the mean (SEM). Significance was defined when a *P* value is less than 0.05.

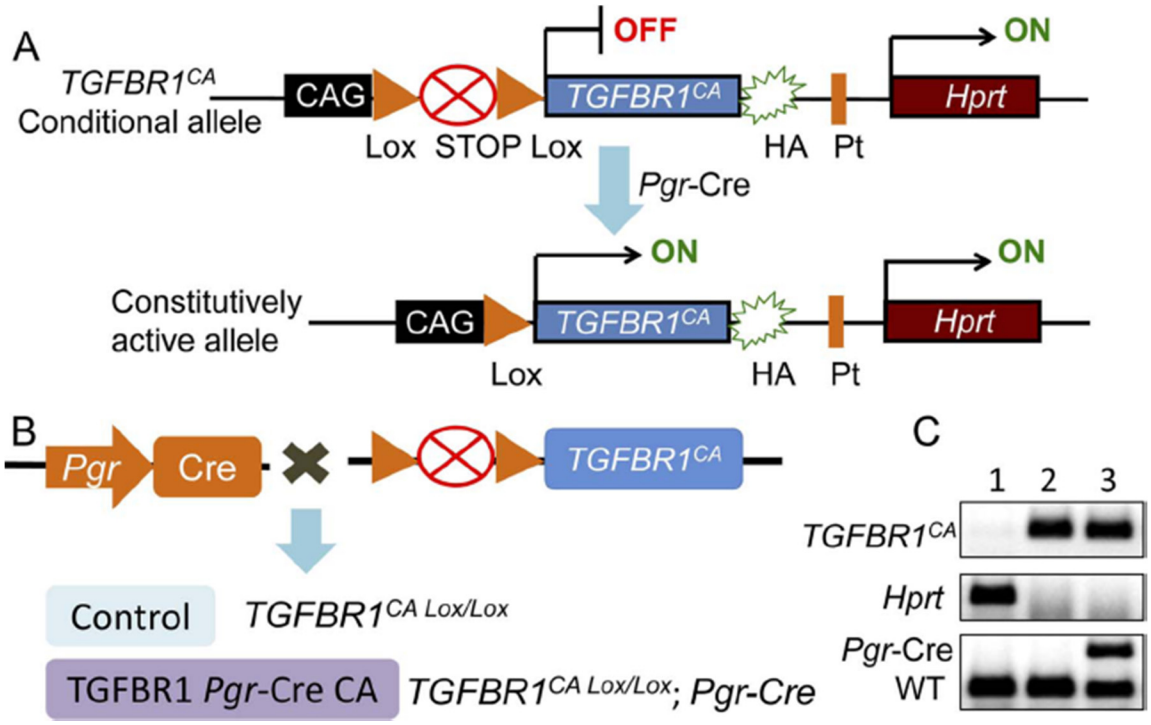


**Figure 10.** Generation of mice containing a constitutively active TGFBR1 gene in the uterus. (**A**) Schematic representation of the latent constitutively active *TGFBR1* allele. Pt, *Hprt* promoter; HA, hemagglutinin tag; CAG, composite constitutive CAG (human cytomegalovirus enhancer and chicken beta actin); *Hprt*, hypoxanthine-guanine phosphoribosyl transferase. (**B**) The *TGFBR1*$^{CA\ Lox/Lox}$ mice were bred with *Pgr*-Cre mice to produce control (*TGFBR1*$^{CA\ Lox/Lox}$; Ctrl) and experimental mice (*TGFBR1*$^{CA\ Lox/Lox}$; *Pgr*-Cre; TGFBR1 *Pgr*-Cre CA). (**C**) Illustration of genotyping PCR of female pups. Lanes 1-3 represent WT, *TGFBR1*$^{CA\ Lox/Lox}$, and *TGFBR1*$^{CA\ Lox/Lox}$; *Pgr*-Cre, respectively.

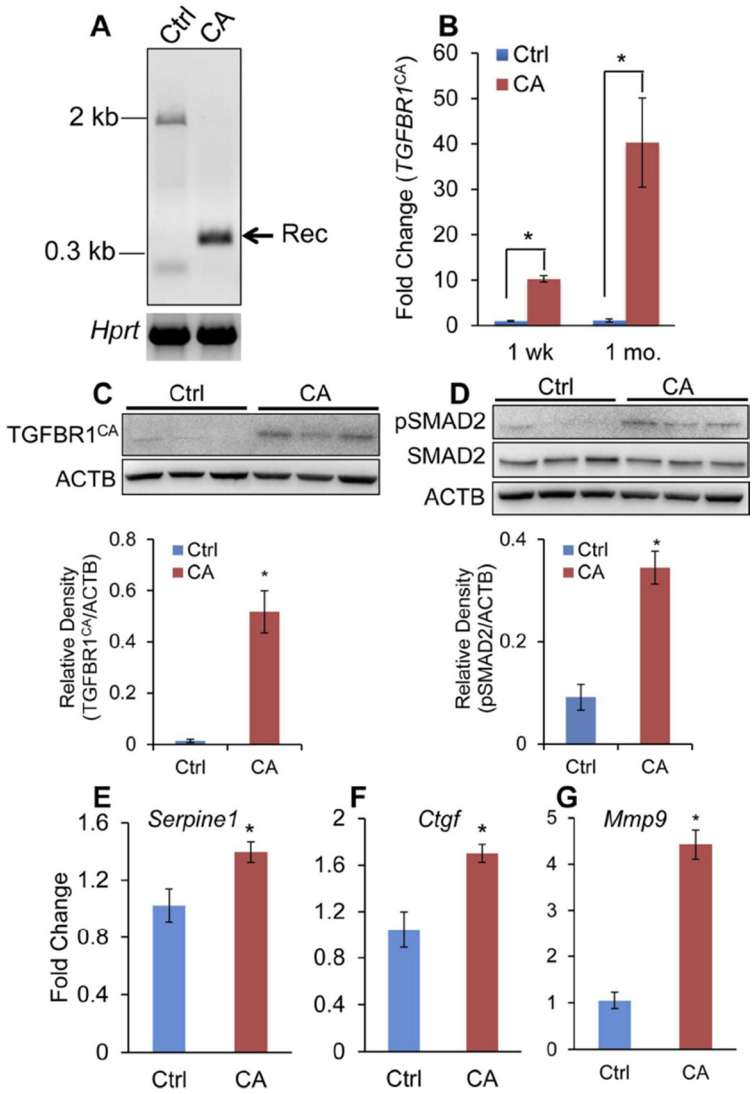


**Figure 11.** Constitutively active TGFBR1 enhances TGFB signaling in the mouse uterus. (**A**) DNA recombination. Rec, recombination. (**B**) *TGFBR1*$^{CA}$ mRNA levels were significantly higher in mice containing a constitutively active TGFBR1. Real-time PCR was performed using uteri samples from control (Ctrl) and *TGFBR1*$^{CA\ Lox/Lox}$; *Pgr*-Cre (CA) mice at the age of 1 week and 1 month ($n = 4$). Note that the primers amplify the transgene. (**C** and **D**) Western blot analysis of TGFBR1-HA fusion protein, phospho-SMAD2, and SMAD2 in the uteri of control and *TGFBR1*$^{CA\ Lox/Lox}$; *Pgr*-Cre mice. Note that upper panels show the representative western blot images, while the lower panels depict the results of quantification for TGFBR1$^{CA}$ (C) and phospho-SMAD2 (D). Each lane represents an independent sample. Uterine samples were collected from mice at the age of 6 wk ($n = 3$-5). (**E**-**G**) Increased mRNA expression of *Serpine1*, *Ctgf*, and *Mmp9* in the uteri of *TGFBR1*$^{CA\ Lox/Lox}$; *Pgr*-Cre mice compared with controls. Uterine samples were collected from mice at 1 wk of age ($n = 4$). Data are mean ± SEM. *$P < 0.05$ versus controls.

## 3.3 Results

### 3.3.1 Generation of mice harboring a constitutively active TGFBR1 in the uterus

To create a gain-of-function model of TGFBR1 in the mouse uterus, we took advantage of a latent constitutively active *TGFBR1* allele (*TGFBR1*$^{CA}$), where a constitutively active *TGFBR1* was knocked into the hypoxanthine guanine phosphoribosyl transferase (*Hprt*) locus [300] (Figure 10A). We created mice harboring the *TGFBR1*$^{CA}$ whose expression was conditionally induced by *Pgr*-Cre recombinase (TGFBR1 *Pgr*-Cre CA) (Figure 10B and C). *Pgr*-Cre is expressed in the uterus [312] and has been extensively utilized as a Cre deletor for genes expressed in the uterus [104, 147, 313, 314]. By crossing the *Pgr*-Cre mice with *Rosa26 LacZ* reporter mice [302], we verified the expression of *Pgr*-Cre in the uterus (data not shown). *Pgr*-Cre recombinase can remove the "stop" sequence of the constitutively active *TGFBR1* allele in the uterus, leading to the expression of the constitutively active TGFBR1.

To validate this model, we first determined whether *TGFBR1*$^{CA}$ allele could be recombined at the genomic DNA level. Using specific recombination primers for *TGFBR1*$^{CA}$ [304] and uterine DNA isolated from control and TGFBR1 *Pgr*-Cre CA mice, a band with the expected size was detected in the uterus of TGFBR1 *Pgr*-Cre CA mice, but not control mice (Figure 11A). Next, we performed quantitative real-time PCR and demonstrated that *TGFBR1*$^{CA}$ mRNA was significantly greater in uteri of *TGFBR1* *Pgr*-Cre CA mice compared with control mice (Figure 11B). Using an antibody directed against HA, we further showed that TGFBR1$^{CA}$-HA fusion protein expression was

induced in the *TGFBR1 Pgr*-Cre CA uterus (Figure 11C) and correlated with increased abundance of phospho-SMAD2, an indicator of TGFB signaling activity (Figure 11D). Consistent with enhanced TGFB signaling activity in the uterus, mRNA levels of TGFB targets including *Serpine1* (Figure 11E), *Ctgf* (Figure 11F), and *Mmp9* (Figure 11G) were up-regulated in uteri of TGFBR1 *Pgr*-Cre CA mice at the age of 1 week, a critical time-point for early postnatal uterine development. Therefore, we created a mouse model with enhanced TGFB signaling in the uterus.

**Table 6.** Fertility tests for TGFBR1 *Pgr*-Cre CA and control mice

| Genotype | n | Pups/litter | Litter/month |
|---|---|---|---|
| *TGFBR1*$^{CA\ Lox/Lox}$ | 4 | 10.0 ± 0.5 | 1.0 ± 0.0 |
| *TGFBR1*$^{CA\ Lox/Lox}$; *Pgr-Cre* | 6 | 0 | 0 |

* The fertility test was conducted during a 3-month period. Data are mean ± SEM.

### 3.3.2 Mice harboring a constitutively active TGFBR1 in the uterus are infertile and develop myometrial and glandular defects

TGFBR1 *Pgr*-Cre CA mice were sterile during a 3-month fertility test period compared with control mice (Table 6). To determine the potential causes of the infertility and investigate the effect of activation of TGFB signaling in the uterus, we first performed immunofluorescence microscopy using antibodies against ACTA2, a smooth muscle cell marker. Hypermuscled uteri were identified in sexually immature TGFBR1 *Pgr*-Cre CA mice (Figure 12D and F) compared with control mice (Figure 12A and C). Immunofluorescence examination of keratin 8 (KRT8), an epithelial marker, was

performed to evaluate the integrity of uterine epithelia in the TGFBR1 overactivation mice. Interestingly, a marked reduction in uterine glands was detected in *TGFBR1*$^{CA\ Lox/Lox}$; *Pgr*-Cre mice (Figure 12B, C, E, and F).

To determine whether these morphological alterations were preserved in older mice, circular and longitudinal layers were examined in adult mice at the age of 2-3 months (Figure 12G-R and Appendix A-6). While organized myometrial layers were evident in control mice (Figure 12G and J and Appendix A-6A and B), an increased thickness of the myometrium and a disorientation of the inner circular layer of myometrium with gaps between smooth muscle bundles was observed in the TGFBR1 *Pgr*-Cre CA mice (Figure 12H and K and Appendix A-6C and D). Longitudinal orientation of muscle structures could also be found within the circular layer region in TGFBR1 *Pgr*-Cre CA mice (Figure 12I and L). In contrast to the circular myometrium, defects in the longitudinal layer were less pronounced at the examined time stages (Figure 12M, N, P, and Q). Altogether, these results showed that constitutive activation of TGFBR1 in the mouse uterus promoted the development of hypermuscled uteri with a disorganized myometrial structure.

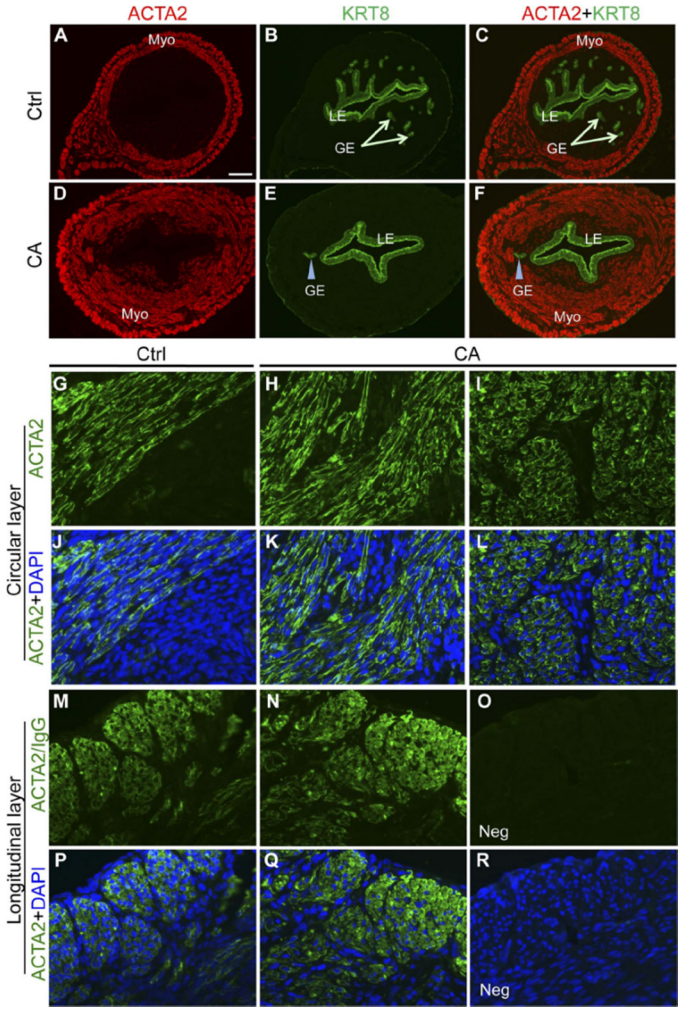


**Figure 12.** Constitutively active TGFBR1 in the mouse uterus causes myometrial and glandular defects. (**A-F**) Immunofluorescence detection of ACTA2 (red) and KRT8 (green) in uterine samples from control and *TGFBR1*$^{\text{CA Lox/Lox}}$; *Pgr*-Cre mice. Note the increased thickness of the myometrium (D and F), reduced uterine glands (E and F), and myofibroblast-like cells within stroma (D and F) in TGFBR1 *Pgr*-Cre CA mice compared with age-matched control mice (A-C). Uterine samples from 1 month old control and *TGFBR1*$^{\text{CA Lox/Lox}}$; *Pgr*-Cre mice ($n$ = 3) were analyzed and representative images are shown. (**G-R**) Immunofluorescence of ACTA2 in the uteri of control and *TGFBR1*$^{\text{CA Lox/Lox}}$; *Pgr*-Cre mice. Note the disorganized smooth muscle cell orientation (green; H and K) and the presence of muscle structures with longitudinal orientation within the circular myometrial layer region (I and L) compared with controls (G and J). Less pronounced alterations of longitudinal muscle structure was found in *TGFBR1*$^{\text{CA Lox/Lox}}$; *Pgr*-Cre mice (N and Q) versus control mice (M and P). (**O** and **R**) Representative negative controls where the primary antibody for ACTA2 was replaced with mouse IgG. LE, luminal epithelium; GE, glandular epithelium; Myo, myometrium; Neg, negative controls. The scale bars is representatively shown in (A) and equals 100 µm (A-F) and 25 µm (G-R).

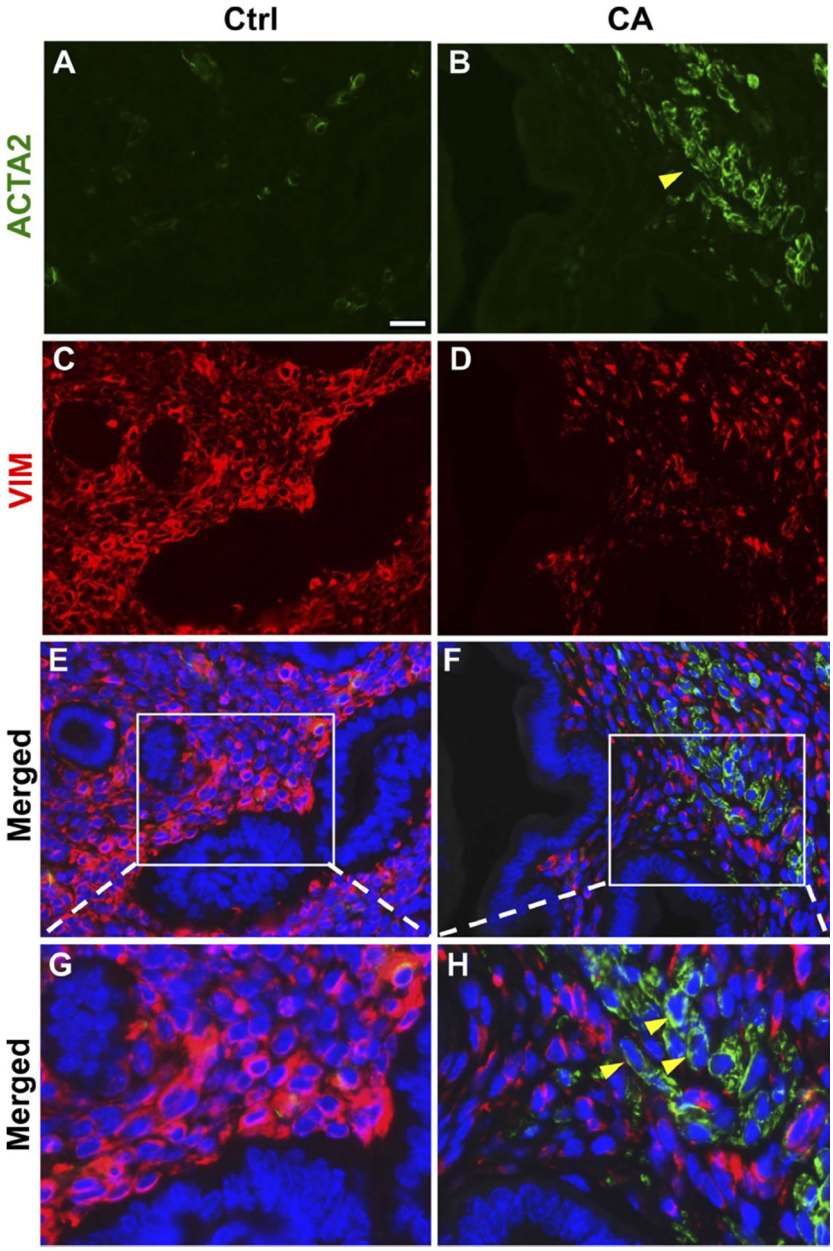


**Figure 13.** Co-localization of ACTA2 and vimentin in the endometrium. (**A-H**) Representative images of immunofluorescence for ACTA2 and vimentin using uterine samples from control and *TGFBR1*$^{\text{CA Lox/Lox}}$; *Pgr*-Cre mice. Note the presence of abundant ACTA2-positive cells (green) in the stroma (B), and those cells did not express vimentin (red; F and H). (G) and (H) are higher power images for (E) and (F), respectively. DAPI (blue) was used to counterstain the nucleus. VIM, vimentin. Scale bar = 20 μm (A-F) and 10 μm (G and H).

We next examined whether development of the endometrium was altered in TGFBR1 *Pgr*-Cre CA mice. In contrast to control mice (Figure 13A and E), the endometrium of the *TGFBR1*$^{\text{CA Lox/Lox}}$; *Pgr*-Cre mice contained abundant ACTA2-positive cells (Figure 13B and F), suggesting a potential increase in the myofibroblast-like cells. These ACTA2-positive cells were negative for vimentin as demonstrated by double immunofluorescence of ACTA2 and vimentin (Figure 13F and H), the latter of which was predominantly expressed in normal uterine fibroblasts (Figure 13C, E, and G). Therefore, over-activation of TGFB signaling appears to promote myofibroblast-like cell differentiation in the endometrium of the uterus.

### 3.3.3 Increased smooth muscle gene expression in uteri of mice with constitutively active TGFBR1

Along with the hypermuscled uterine phenotype, the expression of a battery of smooth muscle genes including *Acta2*, *Cnn1*, *Des*, *Smtn*, *Tagln*, *Actg2*, and *Myh11* was up-regulated in uteri of TGFBR1 *Pgr*-Cre CA mice at 1 wk of age compared with age-matched controls (Figure 14A). To independently test whether TGFB signaling enhanced expression of smooth muscle genes in myometrial cells *in vitro*, we utilized a well-characterized uterine smooth muscle cell line, PHM1. TGFB1 activated SMAD2/3 in PHM1 cells, evidenced by the nuclear accumulation of SMAD2/3 in TGFB1-treated cells versus vehicle control cells (VEHL; Figure 14B). The addition of multiple TGFB isoforms stimulated the expression of *ACTA2* (Figure 14C). *TGIF1*, a known TGFB-induced gene in human myometrial cells [270], was included as a positive control

(Figure 14D). These results suggest that TGFB signaling promotes expression of smooth muscle genes in uterine myometrial cells.

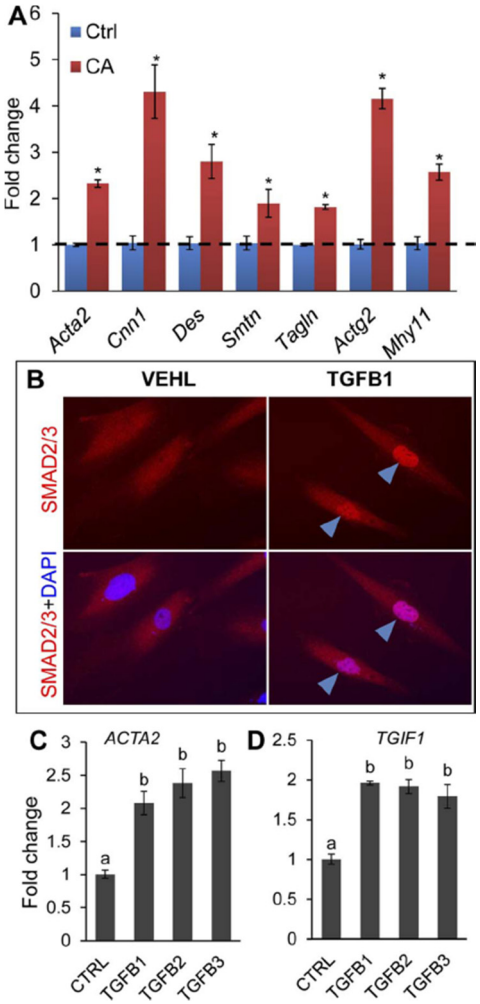


**Figure 14.** TGFB signaling promotes expression of uterine smooth muscle genes. (**A**) Increased expression of smooth muscle genes in uteri of TGFBR1 *Pgr*-Cre CA mice at 1 week of age compared with age-matched controls ($n = 4$). Data are mean ± SEM. *$P <$ 0.05 versus corresponding controls. The dotted line marks gene expression levels for controls mice. (**B**) TGFB1 activated SMAD2/3 in PHM1 cells. DAPI was used to counterstain the nuclei of PHM1 cells. Images are representative for immunofluorescence staining from two independent culture experiments. (**C** and **D**) TGFB ligands stimulated *ACTA2* and *TGIF1* expression in PHM1 cells. Data are mean ± SEM from three independent cell culture experiments. Bars without a common letter are significantly different ($P < 0.05$).

### 3.3.4 Dysregulation of TGFB signaling alters uterine fibroblast function

To define the timing of the glandular defects during postnatal uterine development, we performed immunofluorescence analysis of KRT8 to compare adenogenesis in TGFBR1 *Pgr*-Cre CA and control mice on postnatal days (D) 5, 7, and 15. Uterine glands were formed normally in control uteri on D5, 7 and 15, which is consistent with previous studies [315, 316]. In contrast, formation of uterine glands were impaired in the uteri of TGFBR1 *Pgr*-Cre CA mice (Appendix A-7), suggesting that glandular defects occur during the initiation of adenogenesis.

Adenogenesis involves epithelial cell proliferation and epithelial-mesenchymal interactions which are regulated by growth factors such as WNT signaling and cell-extracellular matrix interactions [132, 315, 317]. Immunohistochemical analysis of Ki67 expression indicated that adenogenic defects occurred in spite of the unimpeded proliferation of uterine luminal epithelial cells at D7 (Appendix A-8). Analysis of genes encoding the WNT signaling pathway components at various developmental time-points using quantitative real-time PCR revealed that the majority of WNT signaling components were comparable between control and TGFBR1 *Pgr*-Cre CA uteri at D7 except for *Wnt11* (Appendix A-9). However, *Wnt11 Pgr*-Cre cKO mice have normal uterine adenogenesis [317]. Dysregulation of *Wnt4*, *Wnt7a*, *Wnt16* and catenin beta 1 (*Ctnnb1*) was found at D15 and/or D31 in the TGFBR1 *Pgr*-Cre CA uteri compared with control uteri (Appendix A-9).

TGFB signaling is known to induce tissue fibrosis by regulating extracellular matrix deposition and integrin expression [318, 319]. As expected, we observed increased expression of genes associated with fibrosis such as *Ctgf*, the extracellular matrix gene laminin alpha 1 (*Lama1*) and integrin alpha 1 (*Itga1*), in TGFBR1 *Pgr*-Cre CA uteri at D7 and collagen type I alpha 1 (*Col1a1*) and *Itgb1* at D15 and D31 (Appendix A-10) [318-321]. To test whether TGFB signaling regulates the expression of these genes *in vitro*, we isolated primary stromal cells which were serum starved and treated with TGFB1. TGFB1 treatment induced the expression of pro-fibrotic genes and smooth muscle genes (Appendix A-11), suggesting that enhanced TGFB signaling may hamper adenogenesis by promoting fibrotic changes of endometrial stroma.

### 3.3.5 Impaired uterine decidualization in mice with constitutively active TGFBR1

The significantly altered endometrial phenotype of TGFBR1 *Pgr*-Cre CA mice pointed to potential defects in uterine function. To test this possibility, we assessed the ability of the uterus to undergo decidualization, a process wherein endometrial stromal cells differentiate into decidual cells to support implanted blastocysts during pregnancy. An artificial decidualization experiment was performed using a well-established protocol (Figure 15A) to determine whether constitutively active TGFBR1 in the mouse uterus compromised the uterine decidual response. Two days after the deciduagenic stimulus, the ratio of the weight of the stimulated and unstimulated uterine horns of the TGFBR1 *Pgr*-Cre CA mice was significantly lower than that of control mice (Figure 15B-D), suggesting decidualization defects in mice with enhanced TGFB signaling in the uterus.

Further histological analysis and results of an alkaline phosphatase (AP) staining assay (Figure 15E-J) demonstrated impaired decidualization and uterine stromal cell differentiation in the TGFBR1 *Pgr*-Cre CA mice, as evidenced by low levels of AP staining (Figure 15J), compared with controls (Figure 15G).

To further explore the molecular mechanism responsible for the defective decidualization, we assessed the ability of a deciduagenic stimulus to induce the expression of critical regulators of uterine decidualization in the TGFBR1 *Pgr*-Cre CA uteri by examining whether expression and induction of *Bmp2* and *Fst* were altered. Interestingly, we found that the deciduagenic stimulus failed to induce *Bmp2* and *Fst* expression in the TGFBR1 *Pgr*-Cre CA mice, whereas expression of those genes increased following the deciduagenic stimulation in uteri of control mice (Figure 15K and L). Moreover, a marked reduction in *Bmp2* transcript abundance occurred in the decidualized horns of TGFBR1 *Pgr*-Cre CA mice compared with controls (Figure 15K). No significant differences in *Fst* mRNA levels between decidualized horns of TGFBR1 *Pgr*-Cre CA and control mice were detected (Figure 15L). Therefore, enhanced TGFB signaling compromises uterine decidualization.

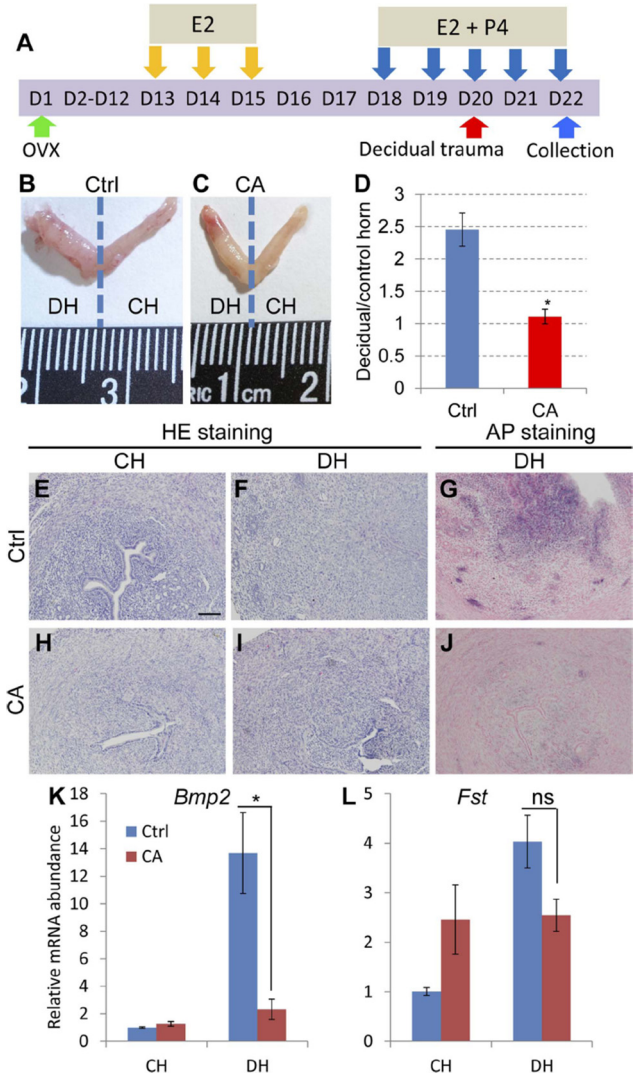


**Figure 15.** Constitutively active TGFBR1 in the uterus impairs uterine decidualization. (**A**) Illustration of the artificial decidualization procedure. OVX, ovariectomy. (**B** and **C**) Gross morphology of control (B) and TGFBR1 *Pgr*-Cre CA (C) uteri collected 2 days after decidual stimulation. DH, decidualized uterine horn; CH, control uterine horn that was not stimulated. (**D**) Ratio of wet uterine weight between stimulated and unstimulated uterine horns of control and TGFBR1 *Pgr*-Cre CA mice ($n$ = 4-5). (**E-J**) Histological analysis and alkaline phosphatase (AP) staining of uterine tissues from TGFBR1 *Pgr*-Cre CA and control mice. Note the strong AP signals in the decidualized horns of control mice (G) versus those of TGFBR1 *Pgr*-Cre CA mice (J). The scale bar is representatively depicted in panel (E) and equals 100 μm (E-J). (**K** and **L**) Expression of *Bmp2* and *Fst* in TGFBR1 *Pgr*-Cre CA and control uteri during artificial decidualization. Note that *Bmp2* and *Fst* transcripts were upregulated by decidual stimulus in control mice, but not TGFBR1 *Pgr*-Cre CA mice. In the decidualized uterine horns, significantly lower *Bmp2* mRNA levels were detected in the TGFBR1 *Pgr*-Cre CA mice compared with controls ($n$ = 3-4). Ns, not significant. Data are mean ± SEM. *$P < 0.05$.

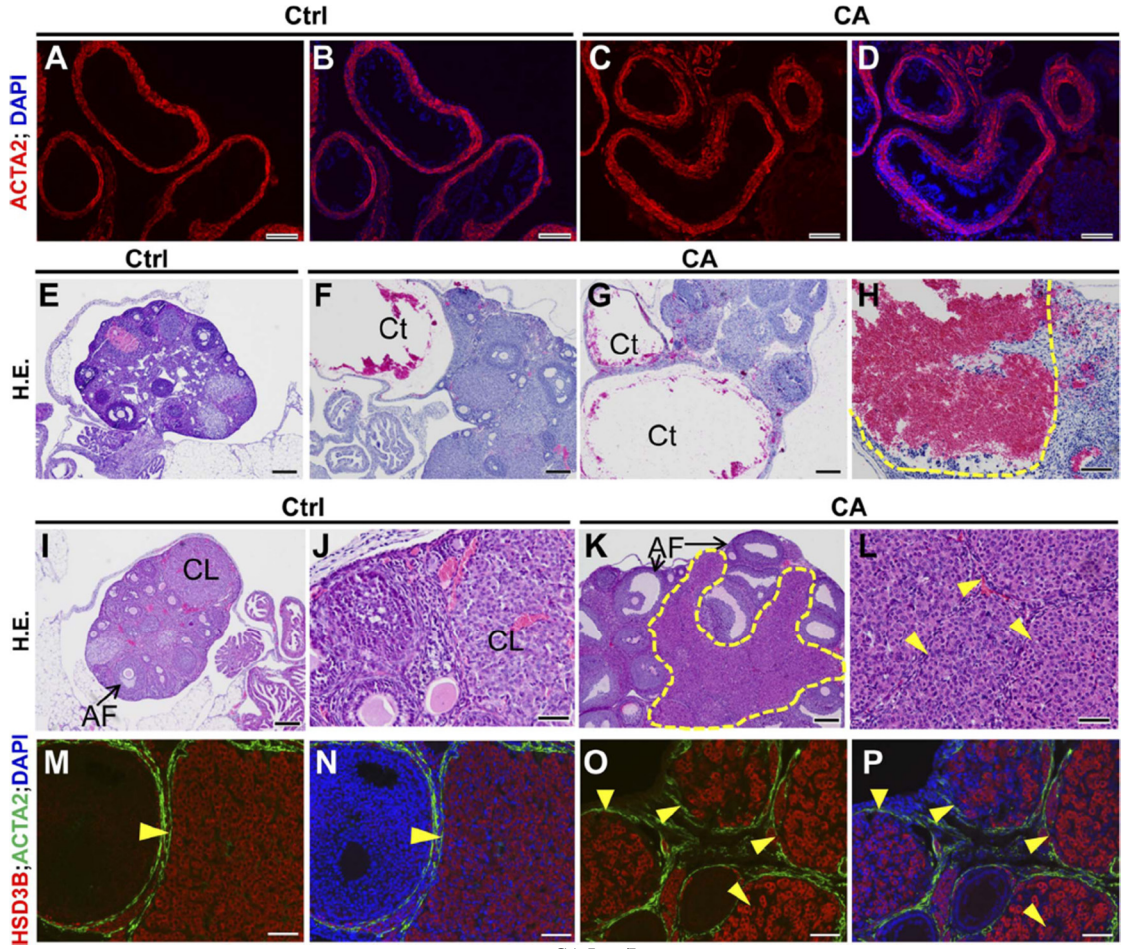


**Figure 16.** Ovarian pathology of *TGFBR1*$^{CA\ Lox/Lox}$; *Pgr*-Cre mice. (**A-D**) Intact smooth muscle structure of the oviduct in *TGFBR1*$^{CA\ Lox/Lox}$; *Pgr*-Cre mice. Immunofluorescence of ACTA2 (red) using oviduct collected from 2 month old control (A and B) and *TGFBR1*$^{CA\ Lox/Lox}$; *Pgr*-Cre mice (C and D). (**E-H**) Hemorrhagic cystic structure in the ovary of *TGFBR1*$^{CA\ Lox/Lox}$; *Pgr*-Cre mice. (G) and (H; dotted yellow line) demonstrate the different cystic structures in the same ovary. (**I-P**) *TGFBR1*$^{CA\ Lox/Lox}$; *Pgr*-Cre mice contained abnormal luteinized structures (K and L; dotted yellow line and yellow arrow heads) that were positive for HSD3B (red) (O and P; yellow arrow heads). HSD3B was localized mainly to the corpus luteum (yellow arrow heads), but not granulosa cells within an adjacent follicle in the control mice (M and N). ACTA2 (green) was used to mark the outer theca layer of follicles. DAPI (blue) was used to counterstain the nucleus. Ct, cystic structure; CL, corpus luteum; AF, antral follicle. Scale bar = 100 μm (A-D and H), 200 μm (E-G, I, and K), and 50 μm (J, L, and M-P).

### 3.3.6 Ovarian defects in mice harboring a constitutively active TGFBR1

Because *Pgr*-Cre is also expressed in the oviduct and preovulatory follicles in the ovary after the gonadotropin surge, the histology of the oviduct and ovaries was analyzed to determine the effects of over-activation of TGFBR1 in these tissues. The histological structure of the oviduct of TGFBR1 *Pgr*-Cre CA mice was comparable to controls, as demonstrated by immunofluorescence staining of ACTA2 (Figure 16A-D). However, histological studies of the ovary showed that three of eight TGFBR1 *Pgr*-Cre CA mice developed cystic structures filled with blood (Figure 16F-H). In contrast, none of the control mice developed that pathology (Figure 16E). Further analysis of mice at 2-3 months of age showed the presence of abnormal luteinized structures within the ovary of the TGFBR1 transgenic mice versus control mice (Figure 16I-L). These structures were positive for HSD3B (Figure 16O and P), which was localized to corpora lutea, but not ovarian granulosa cells in the control mice (Figure 16M and N). To evaluate the ovulatory potential of mice containing a constitutively active TGFBR1, we performed a superovulation experiment and demonstrated that immature TGFBR1 *Pgr*-Cre CA mice ovulated a similar number of oocytes as controls in response to exogenous gonadotropin injection (39.3 ± 5.9 vs. 40.0 ± 3.9 oocytes/mouse; n = 3-4; $P > 0.05$). These results collectively suggest that over-activation of TGFB signaling profoundly affects ovarian cell differentiation and/or function although the ovulation potential in prepubertal mice is not altered.

### 3.4 Discussion

In mice, Müllerian duct formation starts from the specification of coelomic epithelial cells that express LIM homeobox protein 1 (*Lim1*) at embryonic day E11.75 [120]. Subsequent invagination of coelomic epithelium into the mesonephros and elongation of the duct to the urogenital sinus are completed by E13.5 [120]. The Müllerian duct further develops into the female reproductive tract including oviduct, uterus, cervix, and the upper part of vagina. The uterus contains simple epithelium and supporting mesenchyme at birth, and gradually acquires basic myometrial structures by D15 [121, 244]. The role of TGFB signaling in myometrial development was revealed in our early studies using a *Tgfbr1* conditional knockout mouse model. We showed that conditional deletion of TGFBR1 in the female reproductive tract disrupts the formation of uterine smooth muscle layers [179, 242]. The current study was aimed at developing a gain-of-function model to achieve further insight into the roles of TGFB signaling in uterine development and function.

The role of TGFB superfamily signaling has been identified in many reproductive processes using a functional genomics approach. However, the majority of currently available mouse models were generated to induce loss-of-function of genes encoding the components of TGFB signaling pathway [145, 179, 322-324]. It is noteworthy that over-activation of TGFB signaling has been associated with diseases including fibrosis, Marfan syndrome, and late stage cancers [296-298]. Because TGFB signaling is fine-tuned and controls homeostatic cellular processes in a highly contextual manner [325],

the use of loss-of-function and gain-of-function mouse models is complementary and beneficial to a more comprehensive understanding of TGFB signaling in both physiological and pathological conditions. Until now, there have been no available mouse models with over-activation of TGFB signaling in the female reproductive tract. Several strategies have been utilized to develop mouse models with over-activation of TGFB signaling. Targeting inhibitors of TGFB signaling such as inhibitory SMADs (SMAD6 and SMAD7) [326] and fibrillin [296] can enhance TGFB signaling activity. Transgenic mice expressing TGFB1 or having a constitutively active TGFBR1 driven by a fibroblast-specific promoter have been reported [327, 328]. By utilizing a latent conditional constitutively active TGFBR1 allele [300, 304] and *Pgr*-Cre, we created a mouse model containing a constitutively active TGFBR1 in the uterus. To our knowledge, this is the first mouse model with over-activation of TGFB signaling in the uterus.

The most striking phenotype of the TGFBR1 *Pgr*-Cre CA mice is the development of hypermuscled uteri, supporting a clear role for TGFB signaling in uterine smooth muscle biology. The role of TGFB signaling in smooth muscle cell differentiation and function has been unambiguously demonstrated in vascular smooth muscle cells [246, 276, 329, 330]. While TGFB signaling promotes gene expression in smooth muscle cells and formation of smooth muscle in the TGFBR1 gain-of-function model, our studies using *Tgfbr1* conditional knockout mice [242] suggested that TGFBR1 may not be required for the lineage commitment of uterine smooth muscle cells because loss of TGFBR1 allows

continued expression of smooth muscle genes in myometrial cells. It is conceivable that compensatory mechanisms operate in the absence of TGFB signaling in the TGFBR1 loss-of-function model. As direct *in vitro* evidence that TGFB signaling regulates smooth muscle gene expression in myometrial cells, we herein demonstrated that TGFB signaling activated SMAD2/3 and induced *ACTA2* expression in human uterine smooth muscle cells. This result suggests a common regulatory mechanism in response to TGFB signaling in uterine smooth muscle cells. TGFB signaling induces the differentiation of mesenchymal stem cells into smooth muscle cells [331]. It is tempting to speculate that enhanced TGFB signaling resulting from constitutively active TGFBR1 may cause endometrial stem cell differentiation. Recent evidence suggests the existence of stromal stem/progenitor cells in the mouse endometrium, although the properties of these cells are incompletely defined [329, 332]. Thus, it remains to be determined whether enhanced TGFB signaling affects endometrial stem/progenitor cell differentiation and promotes smooth muscle cell formation.

TGFB signaling is involved in myofibroblast differentiation [333]. Myofibroblasts are cells that differentiate from quiescent fibroblasts in response to a number of stimuli including injury. They are characterized by development of contractile machinery induced by changes in the composition and mechanical properties of the extracellular matrix [334]. Myofibroblasts express ACTA2 and can be differentiated/transdifferentiated from several potential precursor cells including local fibroblasts, epithelial cells, and blood-borne cells [335]. Myofibroblasts are generally

absent in most tissues, but their differentiation can be induced during tissue repair [336]. Human decidual stromal cells resemble myofibroblasts and express ACTA2 [337]. The presence, origin, and role of myofibroblasts in the mouse uterus are poorly understood. TGFB signaling is a key regulator of myofibroblast differentiation in other systems [338]. Supporting a role for TGFB signaling in uterine myofibroblast differentiation, we found that overactivation of TGFB signaling led to the differentiation of myofibroblast-like cells in mouse endometrium, accompanied by an increased expression of smooth muscle genes. These ACTA2 positive cells could also potentially be smooth muscle cells migrating from the disorganized myometrium of the TGFBR1 *Pgr*-Cre CA mice. Furthermore, our results showed that TGFBR1 *Pgr*-Cre CA mice had a compromised decidualization ability, coincident with uterine morphological aberrations. Uterine gland development supports decidualization [339]. It is not known whether reduced uterine glands in the TGFBR1 *Pgr*-Cre CA mice affect decidualization induced by an artificial stimulus. The potential contribution of myofibroblast-like cells to the observed decidualization defects also awaits elucidation.

Uterine glands are essential for fertility and pregnancy in multiple species of females including rodents [132]. Mouse uterine glands develop postnatally. The mechanisms underlying uterine gland development are not well understood although recent studies using mouse models have identified a few important genes in this developmental process such as forkhead box A2 (*Foxa2*), *Wnt4*, *Wnt5a*, *Wnt7a*, and cadherin 1 (*Cdh1*) [124, 127, 133-137]. Elegant studies have utilized progestin treatment to disrupt uterine gland

development and fertility in both sheep and mouse models [131, 263]. Likewise, the synthetic estrogen, diethylstilbestrol (DES), can also block adenogenesis when administered within an appropriate time-frame during postnatal uterine development [317]. The exact mechanisms of how these endocrine disruptors suppress uterine gland development are not clear, but may be partially associated with reduced uterine epithelial cell proliferation and/or altered expression of *Wnt* genes [317]. TGFB signaling regulates multiple developmental events, and several lines of evidence suggest a link between estrogen action and TGFB signaling pathways in various types of cells including uterine cells [340-343]. In addition, TGFB signaling interacts with Wnts [344]. Since overactivation of TGFB signaling reduces uterine gland formation, it is tantalizing to speculate that TGFB signaling may partially mediate the adverse effect of endocrine disruptors on uterine gland development through regulating adenogenic genes. However, further investigation is warranted to identify a potential link.

Although the primary focus of this study targeted uterine development and function, we noted histological alterations of the adult ovary. The role of TGFB signaling in the ovary remains largely unknown. To determine whether potential ovarian defects contribute to the observed infertility phenotype of TGFBR1 *Pgr*-Cre CA mice, we performed a timed mating study and found that no blastocysts could be recovered from the TGFBR1 *Pgr*-Cre CA uteri, but there were a reduced number of morula stage embryos (data not shown). Therefore, the ovarian defects of TGFBR1 *Pgr*-Cre mice could be a contributing factor to the reproductive failure observed in these mice. Counterintuitively,

the ovulatory potential seems to be integral in sexually immature mice based on a superovulation experiment. Of note, *Pgr*-Cre is expressed in granulosa cells within the preovulatory follicles and interpretation of the ovarian phenotype of TGFBR1 *Pgr*-Cre CA mice should take into account the differentiation status of granulosa cells and the timing of Cre expression. Therefore, the observed ovarian defect in adult mice may reflect a cumulative effect of constitutive activation of TGFBR1, as opposed to the superovulation results obtained from pre-pubertal mice where *Pgr*-Cre activity is expected to be minimal before gonadotropin stimulation. An independent study is currently ongoing to characterize the role of over-activation of TGFBR1 in the mouse ovary.

Collectively, our results show that constitutive activation of TGFBR1 in the uterus leads to morphological abnormalities and functional deficiencies in the uterus. These findings further reinforce the importance of a precisely controlled TGFB signaling system in normal uterine development and function.

# 4. CONDITIONAL ABROGATION OF TRANSFORMING GROWTH FACTOR BETA RECEPTOR 1 IN PTEN-INACTIVATED ENDOMETRIUM PROMOTES ENDOMETRIAL CANCER PROGRESSION IN MICE*

## 4.1 Introduction

Approximately 61,380 new cases and 10,920 deaths from uterine corpus cancers, the majority of which are endometrial cancers, are projected to occur in 2017 in the United States [223]. There are two major types of endometrial cancer. Type I cancers are mostly endometrioid adenocarcinomas that are associated with excess estrogen. Type II cancers are mainly composed of serous carcinomas which are estrogen independent, with overall poorer prognoses [345]. The mechanisms of endometrial cancer development are not well defined and effective prophylactic and therapeutic approaches are needed. Therefore, understanding the molecular mechanisms underlying the pathogenesis of endometrial cancer is an essential step toward developing novel targeted therapies [346].

Phosphatase and tensin homolog (*PTEN*), a tumor suppressor gene, is mutated in a variety of human cancers including endometrioid adenocarcinoma. PTEN suppresses activity of the phosphoinositide 3-kinase (PI3K)-AKT signaling pathway by dephosphorylating phosphatidylinositol (3, 4, 5)-trisphosphate (PIP3) that participates in

---

* Reprinted in slight modified form with permission from "Conditional abrogation of transforming growth factor beta receptor 1 in PTEN-inactivated endometrium promotes endometrial cancer progression in mice" by Gao Y, Lin P, Lydon JP, Li Q. J Pathol 2017; 10.1002/path.4930

AKT activation. The PI3K-AKT signaling pathway regulates diverse cellular functions including, but not limited to, growth, survival, and metabolism and its abnormal activation is associated with cancer development [347]. Heterozygous *Pten* mice develop neoplasms in multiple organs [348]. Conditional deletion of *Pten* in the mouse uterus using progesterone receptor (*Pgr*)-Cre leads to endometrial cancer formation, supporting a pivotal role of PTEN in endometrial oncogenesis [349].

Cancer cells, particularly those arising from advanced malignancies, can metastasize from the primary site to secondary site(s). Metastasis, consisting of a series of events including local invasion, intravasation, circulation, extravasation, and colonization, is the major cause of morbidity and mortality in cancer patients [350]. To establish distant metastasis, cancer cells originating from the primary site acquire an enhanced ability to migrate and invade. Myometrial invasion is an important factor for the diagnosis and staging of endometrial cancer. The depth of myometrial invasion has been used as a criterion for staging endometrial cancers by the International Federation of Gynecology and Obstetrics (FIGO), where FIGO stages IA and IB refer to endometrial cancers with no or less than half myometrial invasion and those with half or more than half myometrial invasion, respectively [351]. Moreover, a higher risk of extra-uterine metastases has been found in endometrial cancer patients with more than 50% myoinvasion compared to those with less than 50% myoinvasion [352]. Endometrial cancer can metastasize to other organs, with the common sites being lymph nodes, vagina, peritoneum, and lung [353, 354]. It has been increasingly recognized that the

cancer microenvironment is critical for metastasis by promoting adhesion, survival, extracellular matrix proteolysis, cell migration/invasion, immune escape, and angiogenesis [355]. Chemokines and their receptors are important regulators of many cancer cell properties such as proliferation, invasion, apoptosis, and metastasis [356]. Moreover, tumor-associated macrophages (TAMs), a major population of infiltrating leukocytes and well-known immunosuppressive cells, promote cancer growth, invasion, and metastasis [357]. Of note, metastasis has not been reported in the mouse model of endometrial cancer with uterine *Pten* depletion [349, 358], indicating a need to create additional models to study the metastatic process and associated mechanisms of this gynecologic malignancy.

Transforming growth factor beta (TGFB) signaling is known to be tumor suppressive. Many essential elements of this pathway including the ligands, receptors, and SMAD transducers are mutated and/or altered in human diseases including cancers [359]. *In vitro* studies suggest that TGFB signaling regulates endometrial cancer cell proliferation, survival, invasion, and metastasis [360-362]. However, the contribution of TGFB signaling to the pathogenesis of endometrial cancer at the organismic level remains to be uncovered. Therefore, this study explores the role of TGFB signaling in endometrial cancer development and progression by creating a mouse model that harbors concurrent deletion of *Tgfbr1* and *Pten* in the uterus.

## 4.2 Materials and methods

### 4.2.1 Animals

Mice were on a mixed C57BL/6/129 genetic background and the use of mice for this study was approved by the Institutional Animal Care and Use Committee at Texas A&M University. The *Pgr*-Cre and *Tgfbr1*$^{flox}$ mice were generated previously [238, 299]. The *Pgr*-Cre mice were obtained from Drs. John Lydon and Francesco DeMayo, while the *Tgfbr1*$^{flox}$ mice were contributed by Dr. Stefan Karlsson and imported from the laboratory of Dr. Martin Matzuk at Baylor College of Medicine. The *Pten*$^{flox}$ mice were purchased from The Jackson Laboratory (stock # 006440; Bar Harbor, ME, USA) [363]. Genotypes of mice and DNA recombination were analyzed by genomic PCR (Appendix B-1) [238, 363].

### 4.2.2 Histology, immunohistochemistry, and immunofluorescence

Tissue samples were fixed in 10% neutral buffered formalin (Sigma, St. Louis, MO, USA), embedded in paraffin, and cut into 5 μm sections for hematoxylin-eosin (H & E) staining, immunohistochemistry, or immunofluorescence as described [364]. Antibody information is listed in Appendix B-2.

### 4.2.3 Western blots

Western blots were conducted as described [364] using primary antibodies (Appendix B-2). Quantification of western blot was performed using NIH Image J (version 1.50i).

Data are presented as percentage, where the levels of target protein in *Pten*$^{d/d}$ mice were set to 100%.

### 4.2.4 Enzyme-linked immunosorbent assay (ELISA)

Concentrations of CXCL5 in serum were measured using the Quantikine ELISA kit (R&D, Minneapolis, MN, USA) according to the manufacturer's instructions. Briefly, mouse serum samples were diluted 1:20 and assayed in duplicate, along with CXCL5 controls and working standards. Upon completion of the assay, the optical density (OD) value of each well was measured by a microplate reader (BioTek, Winooski, VT, USA) at the wavelength of 450 nm and 540 nm. The OD values were corrected by subtracting readings at 540 nm from those at 450 nm. Concentrations of CCL2 in serum were determined using a mouse MCP-1/CCL2 ELISA Kit (Sigma) according to manufacturer's protocol. The concentration of CCL2 in each sample was calculated using an online software (http://elisaanalysis.com).

### 4.2.5 RNAscope

The RNAscope 2.5 HD detection reagent (brown) and mouse *Tgfbr1* probe (catalog No. 406201) were purchased from Advanced Cell Diagnostics (ACD, Newark, CA, USA) and the analysis was performed according to the manufacturer's instructions. Briefly, paraffin sections were deparaffinized, pretreated by boiling, and digested using protease before hybridization. Hybridization of *Tgfbr1* probe was carried out at 40°C for 2 h,

followed by a series of amplification steps. The signals were detected using 3,3'-diaminobenzidine (DAB).

### 4.2.6 RNA isolation, reverse transcription, and quantitative real-time PCR

Mouse uterine tissues were homogenized in RNA lysis tissue (RLT) buffer (Qiagen, Redwood City, CA, USA). Total RNA was isolated using a RNeasy Mini Kit (Qiagen) based on the manufacturer's protocol, with on-column DNase digestion. The resultant RNA was dissolved in ribonuclease-free water. Reverse transcription was carried out using 200 ng (uterus) or 1 μg (lung) RNA and superscript III reverse transcriptase (ThermoFisher Scientific, Waltham, MA, USA). Quantitative real-time PCR was conducted using Bio-Rad Real-time PCR Detection System (Hercules, CA, USA). Each assay was performed at least in duplicate using primers (Appendix B-1) and iTaq Universal SYBR Green Supermix (Bio-Rad) [242].

### 4.2.7 Statistical analysis

Statistical analysis was performed using GraphPad Prism (version 7.01). Data are mean ± standard error of the mean (s.e.m.). Comparisons between two means were performed using two-tailed *t*-tests (unpaired). Comparisons of means among multiple groups were performed by one-way analysis of variance (ANOVA) followed by Holm-Sidak pairwise comparisons. Survival curve was analyzed by Log-rank/Mantel-Cox test. Significantly skewed data were log transformed prior to ANOVA. Statistical significance was defined as $^{*}P < 0.05$, $^{**}P < 0.01$, and $^{***}P < 0.001$.

## 4.3 Results

### 4.3.1 Generation of mice harboring simultaneous deletion of the *Pten* and *Tgfbr1* genes

*Pten Pgr*-Cre conditional knockout (termed *Pten*$^{d/d}$) mice develop endometrial cancer [349]. To define the function of TGFB signaling in endometrial cancer, we simultaneously ablated the *Pten* and *Tgfbr1* genes in the mouse uterus using *Pgr*-Cre. To examine the expression of *Tgfbr1* in *Pten*$^{d/d}$ uteri, we performed RNAscope and demonstrated the localization of *Tgfbr1* mRNA to the hyperplastic uterine epithelia in *Pten*$^{d/d}$ uteri (Appendix A-12A, B). Positive and negative controls were used (Appendix A-12C, D). To validate these models, we demonstrated that *Pten* and *Tgfbr1* conditional alleles were recombined in the uteri, but not the tails, of *Pten*$^{d/d}$ and/or *Pten*$^{d/d}$; *Tgfbr1*$^{d/d}$ mice (Appendix A-13A). A significant reduction in expression of *Pten* and/or *Tgfbr1* mRNAs was detected in uteri of *Pten*$^{d/d}$, *Tgfbr1*$^{d/d}$, and *Pten*$^{d/d}$; *Tgfbr1*$^{d/d}$ mice by real-time PCR analysis (Appendix A-13B-D). Reductions in abundance of PTEN in the uteri of *Pten*$^{d/d}$; *Tgfbr1*$^{d/d}$ mice was demonstrated using immunohistochemistry and western blot analyses (Appendix A-13E-G, K). Consistent with the loss of inhibition of the PI3K-AKT pathway, phospho-AKT (pAKT) levels were increased in PTEN-depleted uteri (Appendix A-13H-K). Thus, we successfully created a mouse model with conditional deletion of *Pten* and *Tgfbr1* in the uterus.

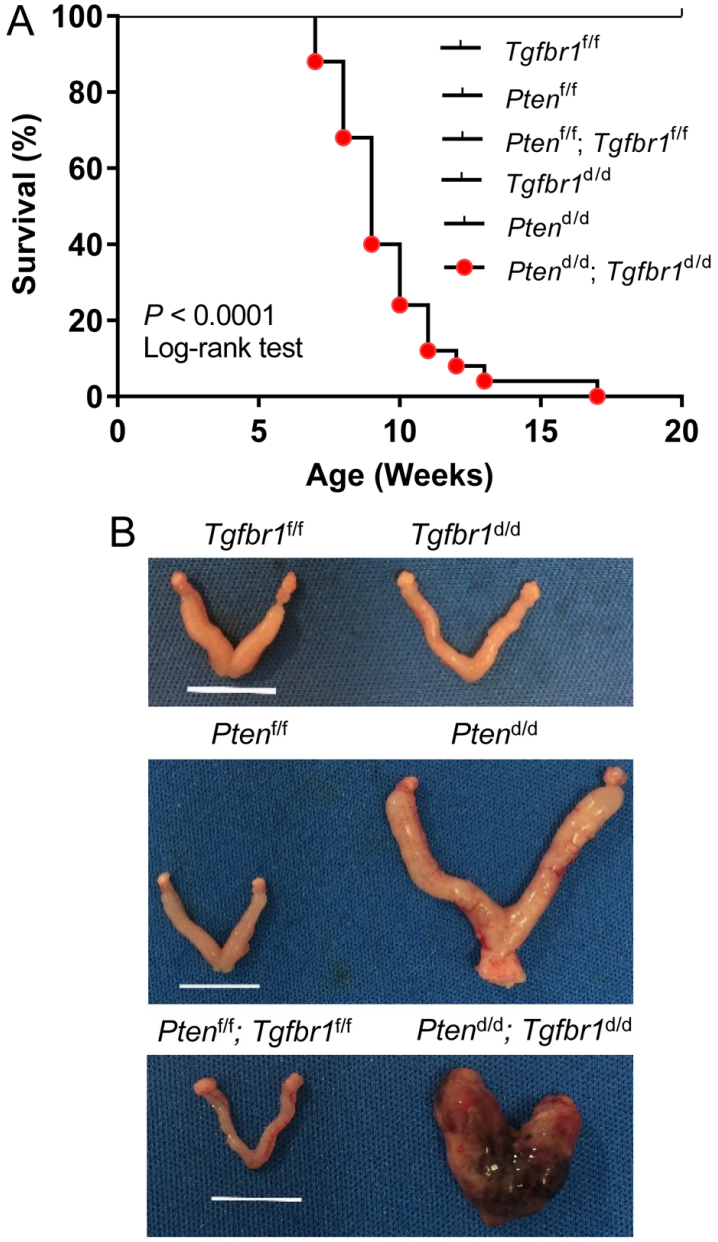


**Figure 17.** Simultaneous deletion of *Pten* and *Tgfbr1* in the uterus leads to severe endometrial lesions at an early age. (A) Survival rates for *Tgfbr1*$^{f/f}$ ($n$ = 14), *Pten*$^{f/f}$ ($n$ = 12), *Pten*$^{f/f}$; *Tgfbr1*$^{f/f}$ ($n$ = 10), *Tgfbr1*$^{d/d}$ ($n$ = 19), *Pten*$^{d/d}$ ($n$ = 13), and *Pten*$^{d/d}$; *Tgfbr1*$^{d/d}$ ($n$ = 25) mice. Note the reduced lifespan of *Pten*$^{d/d}$; *Tgfbr1*$^{d/d}$ mice compared with *Tgfbr1*$^{f/f}$, *Pten*$^{f/f}$, *Pten*$^{f/f}$; *Tgfbr1*$^{f/f}$, *Tgfbr1*$^{d/d}$, and *Pten*$^{d/d}$ mice. $P < 0.0001$ (Log-rank/Mantel-Cox test). (B) Macroscopic analysis of uterine cancer from 8-week-old *Pten*$^{d/d}$ and *Pten*$^{d/d}$; *Tgfbr1*$^{d/d}$ mice. Note that the uterine cancer from *Pten*$^{d/d}$; *Tgfbr1*$^{d/d}$ mice was hemorrhagic and locally invasive compared with that from *Pten*$^{d/d}$ mice. *Tgfbr1*$^{f/f}$, *Tgfbr1*$^{d/d}$, *Pten*$^{f/f}$, and *Pten*$^{f/f}$; *Tgfbr1*$^{f/f}$ uteri were morphologically normal. Scale bar = 10 mm.

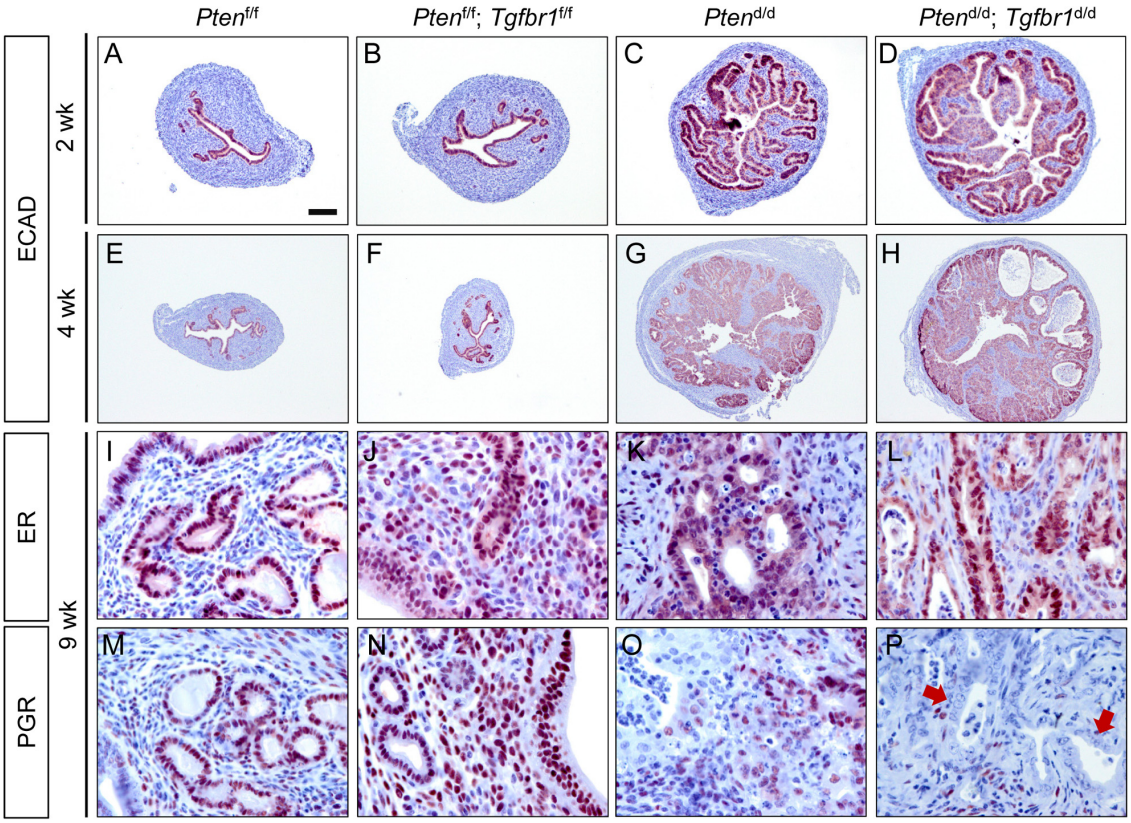


**Figure 18.** Enhanced tumor progression in mice with uterine ablation of TGFBR1 and PTEN. (A-H) Immunostaining for ECAD in the uteri of *Pten*$^{f/f}$, *Pten*$^{f/f}$; *Tgfbr1*$^{f/f}$, *Pten*$^{d/d}$, and *Pten*$^{d/d}$; *Tgfbr1*$^{d/d}$ mice at 2 and 4 weeks of age. Note the increased epithelial hyperplasia at 2 weeks of age (D) and formation of adenocarcinoma foci with necrosis at 4 weeks of age in some *Pten*$^{d/d}$; *Tgfbr1*$^{d/d}$ mice (H) versus *Pten*$^{d/d}$ mice (C, G). A lower magnification was used for E-H versus A-D to capture full images of uterine sections at 4 weeks of age. (I-P) Immunostaining of ER and PGR in the uteri of *Pten*$^{f/f}$, *Pten*$^{f/f}$; *Tgfbr1*$^{f/f}$, *Pten*$^{d/d}$, and *Pten*$^{d/d}$; *Tgfbr1*$^{d/d}$ mice. Signals were developed using NovaRED. Sections were counterstained with hematoxylin. Arrows indicate epithelial components lacking PGR expression (P). Immunohistochemistry was performed using at least three independent samples per genotype. Scale bar is representatively depicted in (A) and equals 100 µm (A-D), 250 µm (E-H), and 25 µm (I-P).

### 4.3.2 *Pten*$^{d/d}$; *Tgfbr1*$^{d/d}$ mice develop severe endometrial lesions that progress more rapidly compared to mice with *Pten* deletion alone

Endometrial cancer affects the lifespan of *Pten* $^{d/d}$ mice beginning around 5 months of age [349]. While all *Pten*$^{d/d}$, *Tgfbr1*$^{d/d}$, *Tgfbr1*$^{f/f}$, *Pten*$^{f/f}$, and *Pten*$^{f/f}$; *Tgfbr1*$^{f/f}$ mice survived past 17 weeks, the *Pten*$^{d/d}$; *Tgfbr1*$^{d/d}$ mice had significantly shortened lifespans (Figure 17A). Consistent with cancer development, the uterus/body weight ratio was increased in both *Pten*$^{d/d}$ and *Pten*$^{d/d}$; *Tgfbr1*$^{d/d}$ mice versus *Tgfbr1*$^{f/f}$, *Pten*$^{f/f}$, *Pten*$^{f/f}$; *Tgfbr1*$^{f/f}$, and *Tgfbr1*$^{d/d}$ mice at both 4 and 9 weeks of age (Appendix A-14A, B). The uterine cancer in *Pten*$^{d/d}$; *Tgfbr1*$^{d/d}$ mice was generally more hemorrhagic and/or locally invasive (Figure 17B). *Tgfbr1*$^{d/d}$ mice did not develop endometrial cancer despite the presence of cystic endometrial glands and adenomyosis in 8-month-old mice (data not shown). Thus, this mouse line was not included in subsequent studies.

To determine potential phenotypic differences in endometrial cancer development between *Pten*$^{d/d}$ and *Pten*$^{d/d}$; *Tgfbr1*$^{d/d}$ mice, we performed H & E staining and immunohistochemical analyses of E-cadherin (ECAD), an epithelial marker, using uteri from *Pten*$^{d/d}$, *Pten*$^{d/d}$; *Tgfbr1*$^{d/d}$, and corresponding control mice at various ages. Atypical endometrial hyperplasia was found at the age of 10 days (not shown) and at 2 weeks in both *Pten*$^{d/d}$ and *Pten*$^{d/d}$; *Tgfbr1*$^{d/d}$ mice (Appendix A-15A-F). Dramatic differences between *Pten*$^{d/d}$; *Tgfbr1*$^{d/d}$ and *Pten*$^{d/d}$ mice were not found at 2 weeks of age, except for the presence of more hyperplastic epithelia in some *Pten*$^{d/d}$; *Tgfbr1*$^{d/d}$ mice (Figure 18A-D; Appendix A-15A-F). At the age of 4 weeks, the atypical endometrial hyperplasia in

*Pten*$^{d/d}$ mice progressed to carcinoma. In contrast, *Pten*$^{d/d}$; *Tgfbr1*$^{d/d}$ mice developed more severe lesions with the presence of large foci of adenocarcinoma accompanied by degenerating cells within its central region in some mice (Figure 18E-H; Appendix A-15G-L). Of note, endometrial cancers in both *Pten*$^{d/d}$ and *Pten*$^{d/d}$; *Tgfbr1*$^{d/d}$ mice were positive for estrogen receptor (ER) and PGR at this stage (Appendix A-16A-H). However, a reduction of PGR, but not ER signals was observed in *Pten*$^{d/d}$; *Tgfbr1*$^{d/d}$ mice at a later stage (Figure 18I-P; Appendix A-16I). At the age of 2 months, although myoinvasion could be observed in both *Pten*$^{d/d}$ and *Pten*$^{d/d}$; *Tgfbr1*$^{d/d}$ mice (Appendix A-17A-D), *Pten*$^{d/d}$; *Tgfbr1*$^{d/d}$ uteri demonstrated a haphazard glandular pattern, desmoplastic stroma, and more severe myometrial disruption (Appendix A-17E, F; Figure 19A-E). Immunohistochemical analysis using a smooth muscle marker, calponin 1 (CNN1), revealed that *Pten*$^{d/d}$ mice had recognizable myometrial layers at 2 months of age (Figure 19A, B, E), while severely disrupted myometrial layers intermingled with epithelial cancer cells were found in approximately 69% of *Pten*$^{d/d}$; *Tgfbr1*$^{d/d}$ mice (Figure 19C, D, E). No myometrial abnormality was found in *Tgfbr1*$^{d/d}$ and*Tgfbr1*$^{f/f}$ mice at the examined time stages (data not shown). To better visualize epithelial and myometrial compartments, we performed double immunofluorescence using anti-cytokeratin 8 (KRT8) and CNN1 antibodies to label the respective epithelium and smooth muscle (Figure 19F-M). The results revealed that cancer epithelia breached the uterine wall in *Pten*$^{d/d}$; *Tgfbr1*$^{d/d}$ mice (Figure 19J-M) versus *Pten*$^{d/d}$ mice (Figure 19F-I). Thus, these results provide *in vivo* evidence of accelerated endometrial cancer

progression and enhanced cell invasion in mice with conditional deletion of *Pten* and *Tgfbr1*.

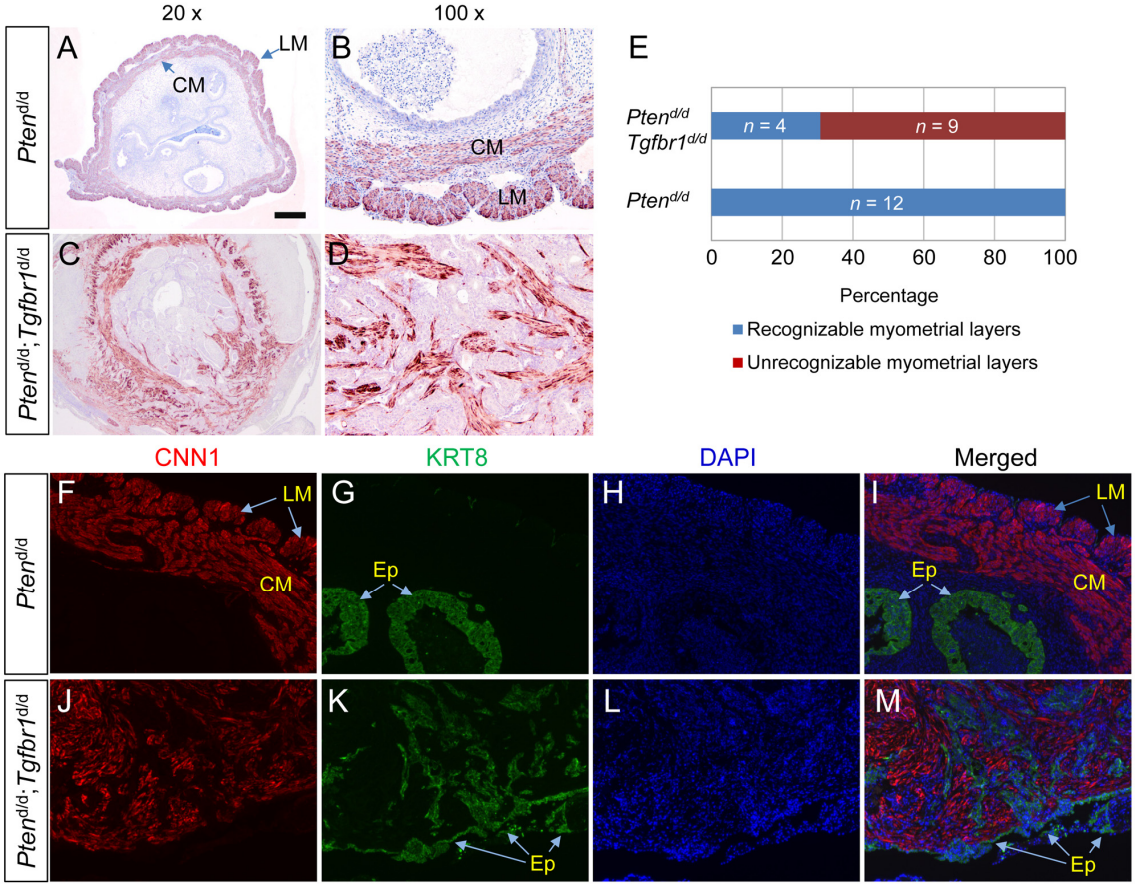


**Figure 19.** Myometrial invasion in *Pten*$^{d/d}$; *Tgfbr1*$^{d/d}$ mice. (A-E) Immunohistochemical analysis of myometrial integrity using uteri from *Pten*$^{d/d}$ and *Pten*$^{d/d}$; *Tgfbr1*$^{d/d}$ mice. Representative images of CNN1 staining (9 wk) are shown in panels (A-D) and a summary chart is provided in panel (E). *Pten*$^{d/d}$ (n = 12) and *Pten*$^{d/d}$; *Tgfbr1*$^{d/d}$ (n = 13) mice at 8 and 9 weeks of age were utilized. (F-M) Double immunofluorescence of KRT8 and CNN1 using uteri of 9-week-old *Pten*$^{d/d}$ and *Pten*$^{d/d}$; *Tgfbr1*$^{d/d}$ mice. Note the severe myometrial invasion/disruption in *Pten*$^{d/d}$; *Tgfbr1*$^{d/d}$ mice compared with *Pten*$^{d/d}$ mice. LM, longitudinal muscle layer; CM, circular muscle layer; Ep, epithelial cells. DAPI was used to counterstain nuclei. Scale bar is representatively depicted in (A) and equals 100 µm (B, D, F-M) and 500 µm (A, C).

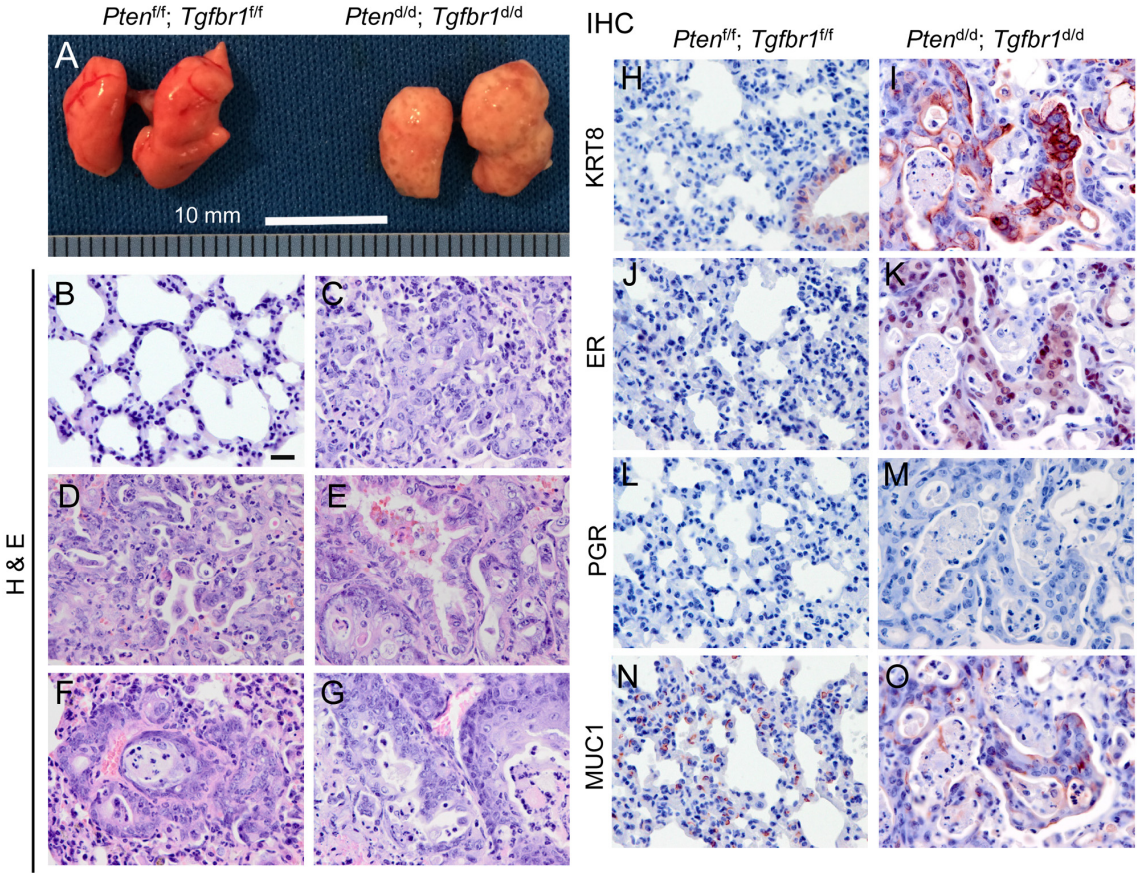


**Figure 20.** Conditional deletion of *Pten* and *Tgfbr1* promotes endometrial cancer metastasis. (A) Gross analysis of lung metastases in 7-week-old *Pten*$^{d/d}$; *Tgfbr1*$^{d/d}$ mice versus age-matched *Pten*$^{f/f}$; *Tgfbr1*$^{f/f}$ *mice*. Note the lungs from *Pten*$^{d/d}$; *Tgfbr1*$^{d/d}$ mice were occupied with tumor foci versus those from *Pten*$^{f/f}$; *Tgfbr1*$^{f/f}$ mice. Scale bar = 10 mm. (B-G) Histological analysis of the lungs from *Pten*$^{d/d}$; *Tgfbr1*$^{d/d}$ and *Pten*$^{f/f}$; *Tgfbr1*$^{f/f}$ mice. Note the presence of highly organized alveoli structures (B) and metastatic nodules containing neoplasms with variable differentiation status (C-G) in the lungs of *Pten*$^{f/f}$; *Tgfbr1*$^{f/f}$ and *Pten*$^{d/d}$; *Tgfbr1*$^{d/d}$ mice, respectively. (H-O) Immunohistochemical staining of lungs from *Pten*$^{f/f}$; *Tgfbr1*$^{f/f}$ *and Pten*$^{d/d}$; *Tgfbr1*$^{d/d}$ mice at 9 weeks of age. Note the metastatic sites were positive for KRT8 (I), ER (K), and MUC1 (O), but not PGR (M). Immunohistochemistry was performed using at least 4 independent lung samples per genotype. The scale bar is representatively depicted in (B) and equals 20 μm (B-O).

### 4.3.3 *Pten*$^{d/d}$; *Tgfbr1*$^{d/d}$ mice develop pulmonary metastasis

Metastasis is a major cause of death in endometrial cancer patients [353, 354]. In contrast to the *Pten*$^{d/d}$ mice where visible metastasis in distant organs was not observed even at 25-36 weeks of age (Appendix B-3), *Pten*$^{d/d}$; *Tgfbr1*$^{d/d}$ mice developed distant organ metastasis, preferentially in the lung. At the advanced stage of disease development (i.e., 7-16 weeks), no grossly visible metastases were observed in the bladder, heart, kidney, and spleen (Appendix B-3), although microscopically detectable metastases positive for KRT8 and ER could be found in the lymph nodes of *Pten*$^{d/d}$; *Tgfbr1*$^{d/d}$ and *Pten*$^{d/d}$ mice (Appendix A-18*)*. In contrast, grossly visible metastases were evident in the lungs of *Pten*$^{d/d}$; *Tgfbr1*$^{d/d}$ mice (Figure 20A; Appendix A-19A, Appendix B-3). Unlike the lungs of *Pten*$^{d/d}$ mice comprising highly organized alveoli structures (Figure 20B), the lungs of *Pten*$^{d/d}$; *Tgfbr1*$^{d/d}$ mice demonstrated multiple metastatic sites, consisting of pathological lesions with variable differentiation status (Figure 20C-G). In addition, the metastasis was frequently accompanied by hemorrhage and loss of morphologically normal alveoli (Appendix A-19A; Figure 20C-G). Using immunohistochemistry, we further verified that the metastatic nodules were positive for KRT8 (Figure 20I; Appendix A-19C) and ER (Figure 20K), but were negative for PGR (Figure 20M). Of note, analysis of ER expression in the lungs of *Pten*$^{d/d}$; *Tgfbr1*$^{d/d}$ mice demonstrated the formation of endometrial gland-like lesions within the metastatic nodules (Appendix A-19D, E). Furthermore, recombined *Tgfbr1/Pten* conditional alleles were detected in the lung metastases of *Pten*$^{d/d}$*; Tgfbr1*$^{d/d}$ mice, but not in the lung tissues of *Pten*$^{d/d}$ *mice* (Appendix A-19F). The metastatic nodules also expressed mucin 1

(MUC1; Figure 20O), a protein that is frequently over-expressed in metastatic cancers [365]. Immunostaining of the lungs from *Pten*$^{f/f}$; *Tgfbr1*$^{f/f}$ controls were representatively shown (Figure 20H, J, L, N). To confirm that pulmonary metastasis was specific to *Pten*$^{d/d}$; *Tgfbr1*$^{d/d}$ mice, we analyzed age-matched lungs from *Pten*$^{d/d}$ and *Pten*$^{f/f}$ mice and did not find metastasis in those mice (data not shown).

### 4.3.4 Loss of TGFBR1 increases the production of pro-inflammatory chemokines associated with cancer metastasis

Chemoattractant cytokines, or chemokines, and their receptors play important roles in many carcinogenic events [366]. To determine the potential mechanism of metastasis resulting from ablation of TGFBR1, we compared uterine expression of mRNAs for chemokines including C-X-C motif ligand 1 (*Cxcl1*), *Cxcl5*, *Cxcl12*, chemokine (C-C motif) ligand 2 (*Ccl2*), and *Ccl9* and a chemokine receptor *Cxcr2* that are involved in metastasis [367-370] between *Pten*$^{d/d}$; *Tgfbr1*$^{d/d}$ and *Pten*$^{d/d}$ mice, along with *Pten*$^{f/f}$; *Tgfbr1*$^{f/f}$ and *Pten*$^{f/f}$ controls. Results showed that the transcript levels of *Cxcl5* and its receptor *Cxcr2* were increased in the uteri of *Pten*$^{d/d}$; *Tgfbr1*$^{d/d}$ mice versus *Pten*$^{d/d}$ and control mice at 2 weeks of age (Figure 21B, D), while those of *Cxcl1* (Figure 21A), *Cxcl12* (Figure 21C), *Ccl2* (Figure 21E), and *Ccl9* (Figure 21F) were comparable between *Pten*$^{d/d}$; *Tgfbr1*$^{d/d}$ and *Pten*$^{d/d}$ mice at this time-point. To determine whether there was a correlation between concentrations of CXCL5 in serum and cancer progression and metastasis, we performed ELISA and demonstrated significantly greater

concentrations of CXCL5 in serum of *Pten*$^{d/d}$; *Tgfbr1*$^{d/d}$ mice versus *Pten*$^{d/d}$ and control mice at 9 weeks of age (Figure 21G).

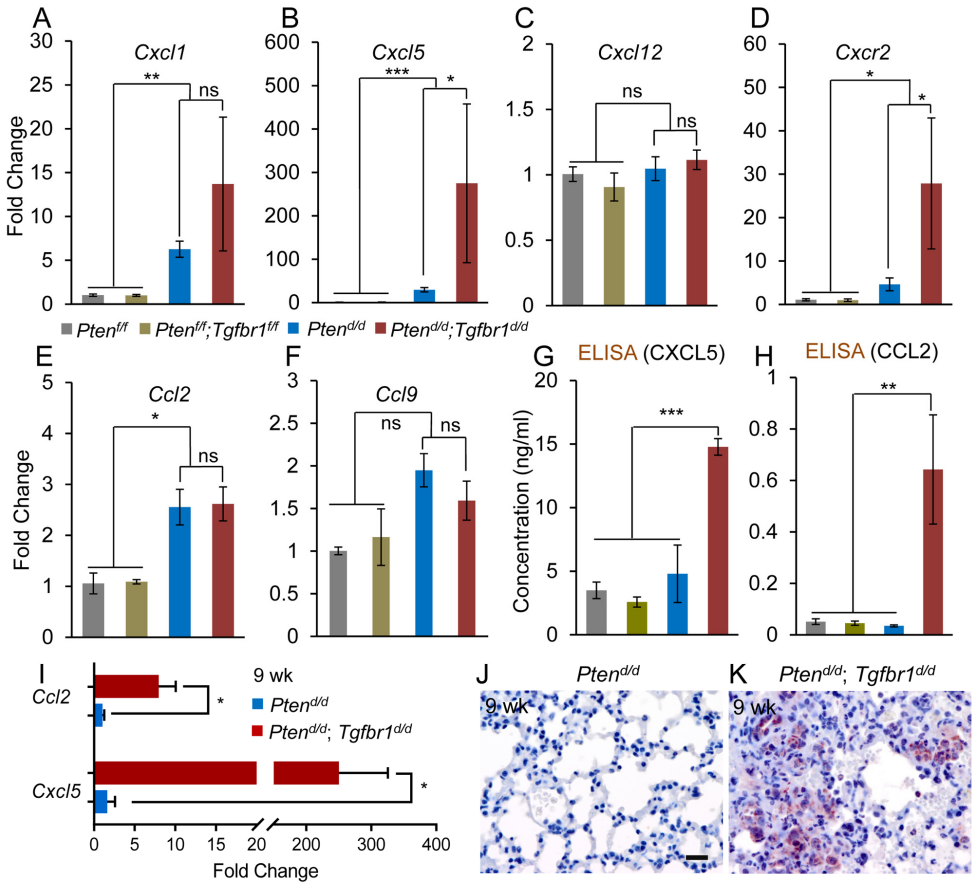


**Figure 21.** Alteration of pro-inflammatory chemokine and receptor in *Pten*$^{d/d}$; *Tgfbr1*$^{d/d}$ uteri. (A-F) Expression of select chemokines and receptor in the mouse uterus. Note that expression of *Cxcl5* and *Cxcr2* mRNA was increased in 2-week-old *Pten*$^{d/d}$; *Tgfbr1*$^{d/d}$ mice versus *Pten*$^{d/d}$ and control mice. *Pten*$^{f/f}$ and *Pten*$^{f/f}$*; Tgfbr1*$^{f/f}$ mice were included as normal controls. Real-time PCR was performed using ΔΔCT method. *Rpl19* was used as internal control. $n$ = 4-9. (G, H) Serum CXCL5 and CCL2 levels in 9-week-old mice measured by ELISA. $n$ = 5. Data are mean ± s.e.m. $^{*}P < 0.05$, $^{**}P < 0.01$, and $^{***}P < 0.001$. Ns, $P \geq 0.05$. (I) Increased mRNA levels of *Ccl2* and *Cxcl5* in the lungs of *Pten*$^{d/d}$; *Tgfbr1*$^{d/d}$ mice versus *Pten*$^{d/d}$ mice at 9 weeks of age. $n$ = 4. Data are mean ± s.e.m. $^{*}P < 0.05$. (J, K) Immunostaining of CXCL5 in the lungs of 9-week-old *Pten*$^{d/d}$ and *Pten*$^{d/d}$; *Tgfbr1*$^{d/d}$ mice. Immunohistochemistry was performed using at least four independent lung samples per genotype. Scale bar is representatively shown in (J) and equals 20 μm (J, K).

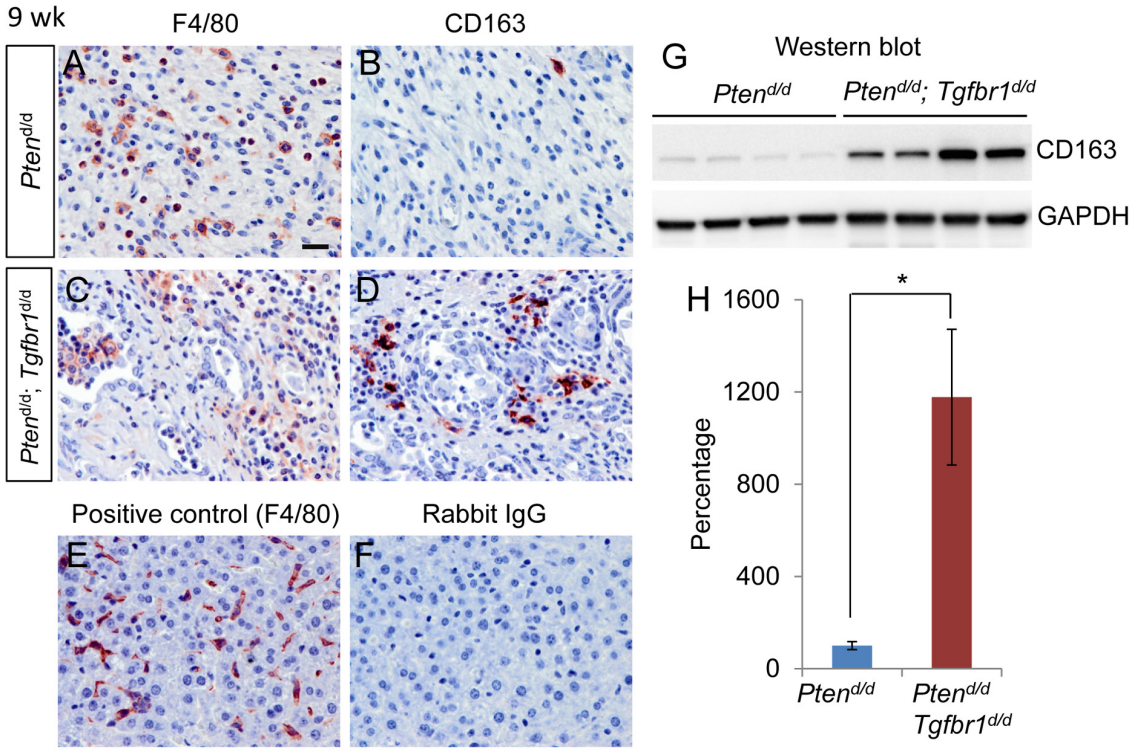


**Figure 22.** Expression of F4/80 and CD163 in mice with uterine deletion of *Tgfbr1* and *Pten*. (A-D) Immunostaining of F4/80 and CD163 in the uteri of *Pten*$^{d/d}$ and *Pten*$^{d/d}$; *Tgfbr1*$^{d/d}$ mice at 9 weeks of age. Five independent samples per genotype were examined. (E, F) Representative positive and negative controls for immunohistochemistry. Panel (E) shows a positive control for F4/80 antibody using liver tissues from 9-week-old *Pten*$^{f/f}$ mice, while panel (F) is a negative control using rabbit IgG. The scale bar is representatively depicted in (A) and equals 20 μm (A-F). (G, H) Western blot analysis of CD163 protein expression in uteri of 9-week-old *Pten*$^{d/d}$ and *Pten*$^{d/d}$; *Tgfbr1*$^{d/d}$ mice. Images for CD163 and GAPDH (internal control) are depicted in panel (G) and quantification results are shown in panel (H). Each lane represents an independent sample. Data are presented as percentages, where CD163 protein levels in *Pten*$^{d/d}$ mice were set to 100%. $n = 4$. Data are mean ± s.e.m. $^{*}P < 0.05$.

Interestingly, serum CCL2 levels were also increased in 9-week-old *Pten*$^{d/d}$; *Tgfbr1*$^{d/d}$ mice (Figure 21H). Further analysis revealed significantly up-regulated expression of *Ccl2* and *Cxcl5* mRNAs in the lung metastases of 9-week-old *Pten*$^{d/d}$; *Tgfbr1*$^{d/d}$ mice versus age-matched *Pten*$^{d/d}$ mice (Figure 21I), suggesting that lung metastases may serve

as a potential source of the elevated serum levels of these chemokines. Furthermore, CXCL5 was localized to the metastatic nodules within the lungs of *Pten*$^{d/d}$; *Tgfbr1*$^{d/d}$ mice versus *Pten*$^{d/d}$ mice (Figure 21J, K). These results suggest involvement of CXCL5/CCL2 in endometrial cancer progression in *Pten*$^{d/d}$; *Tgfbr1*$^{d/d}$ mice.

### 4.3.5 Recruitment of tumor-associated macrophages in *Pten*$^{d/d}$; *Tgfbr1*$^{d/d}$ uteri

TGFB signaling regulates CXCL5 secretion in mammary cancer cells and recruits immune cells including TAMs to promote tumor progression [368, 369]. TAMs can acquire a polarized M2 phenotype (i.e., M2 macrophage or alternatively activated macrophage) and promote tumor progression [371]. We therefore examined the potential involvement of TAMs in tumor progression in *Pten*$^{d/d}$; *Tgfbr1*$^{d/d}$ mice by immunohistochemistry using antibodies directed to CD163 (a marker for M2 macrophages) [372]. F4/80, a well-established marker of murine macrophage [373], was used to monitor the macrophage population in the uteri. The presence of F4/80$^{+}$ macrophages was revealed in the stroma of both *Pten*$^{d/d}$ and *Pten*$^{d/d}$; *Tgfbr1*$^{d/d}$ tumors at 9 weeks of age (Figure 22A, C). Interestingly, cells positive for CD163 were readily detectable in the uteri of *Pten*$^{d/d}$; *Tgfbr1*$^{d/d}$ mice versus *Pten*$^{d/d}$ mice (Figure 22B, D). Positive and negative controls were included (Figure 22E, F). Consistent with this immunohistochemical observation, western blot analysis showed that CD163 expression was increased significantly in *Pten*$^{d/d}$; *Tgfbr1*$^{d/d}$ mice compared with *Pten*$^{d/d}$ mice (Figure 22G, H). Immunostaining for F4/80 and CD163 using age-matched *Pten*$^{f/f}$ and *Pten*$^{f/f}$;

*Tgfbr1*$^{f/f}$ mice was done and results are presented in Appendix A-20. These findings suggest a role for TAMs in endometrial cancer progression in *Pten*$^{d/d}$; *Tgfbr1*$^{d/d}$ mice.

### 4.4 Discussion

Mutation or inactivation of TGFB signaling components has been associated with the development of a broad array of cancers [374]. Although a putative role for TGFB signaling in the pathogenesis of human endometrial cancer has long been proposed [375], the precise function of TGFB signaling in endometrial cancer development has remained elusive. *PTEN* mutations have been identified in a variety of cancers. Loss of PTEN, a negative regulator of the PI3K-AKT pathway, is involved in the oncogenesis of endometrial carcinoma [376]. Conditional deletion of *Pten* in the mouse uterus using *Pgr*-Cre leads to the development of endometrial malignancy, which phenocopies many pathological characteristics of the human endometrial cancer [349]. As a result, the *Pten*$^{d/d}$ mouse model has been used to study endometrial cancer development [358, 377, 378]. However, *Pten*$^{d/d}$ mice do not develop visible organ metastasis, a cause of recurrence after surgical intervention for primary cancers. Recurrence of endometrial cancer resulting from either local or distant metastases is devastating. Endometrial cancer results in the highest frequency of pulmonary metastases (20-25%) versus other gynecologic cancers [353, 354]. Therefore, development of an endometrial cancer model with organ metastases mimicking human endometrial cancer is critical to understanding of metastatic initiation and progression.

Little is known about the potential interplay between TGFB signaling and PTEN during endometrial carcinogenesis although their interactions have been documented in other tumors [379, 380]. Inactivation of TGFB signaling and loss of growth inhibition are associated with the development of human endometrial cancer [228, 381]. It has been shown that mutations of TGFB signaling components including TGFB receptors and SMADs and alteration of TGFB signaling activity reflected by changes in gene expression and/or phosphorylation of key signaling proteins play a role in the pathoetiology of human endometrial cancer [205, 206, 228]. TGFBR1 has a 5.6% mutation and alteration rate in human endometrial cancer [206, 224]. As reported, cancerous human endometrium expresses lower levels of TGFBR1 protein [227, 228]. TGFBR2 is mutated/altered in 6.5% endometrial tumors [206, 224]. Results of studies from The Cancer Genome Atlas (TCGA) Research Network have also suggested alterations of several SMADs in human endometrial cancer [206, 224]. Of particular importance is the availability of the two endometrial cancer models (i.e., *Pten*$^{d/d}$ and *Pten*$^{d/d}$; *Tgfbr1*$^{d/d}$ mice) that demonstrated distinct pulmonary metastatic outcomes depending on the status of a known TGFB signaling component (i.e., TGFBR1) in the PTEN-inactivated uterus. Therefore, the aforementioned mutations and/or dysregulation of TGFB signaling components in endometrial cancer and the development of pulmonary metastasis in *Pten*$^{d/d}$; *Tgfbr1*$^{d/d}$ mice make this model a valuable tool to study the pathogenesis and progression of endometrioid adenocarcinoma, the most frequent type of endometrial cancer in women. However, it needs to be pointed out that due to the expression of *Pgr*-Cre in uterine stromal cells and the myometrium, a potential impact of

TGFBR1 and/or PTEN loss in these cellular compartments on the tumor phenotype cannot be excluded, which may represent a limitation of the current study. Future investigations are needed to address this question using Cre lines targeting distinct cellular compartments of the uterus.

Metastasis is a complex process where cancer cells can disseminate via the bloodstream and/or lymphatics to establish secondary tumors at the metastatic sites. Because of the invlovment of chemokines in the process of metastasis, therapeutic strategies targeting the action of chemokines may block/attenuate metastasis. A functional link between TGFB signaling and chemokines during cancer metastasis has emerged [367, 382, 383]. In one study, conditional ablation of TGFBR2 in mammary fibroblasts increased the secretion of CCL2, which promoted mammary cancer progression at least partially through a TAM-dependent mechanism [367]. Enhanced production of CCL9 resulting from loss of TGFB signaling promotes immature myeloid cell infiltration and the development of invasive intestinal tumors [384]. Loss of TGFB signaling in mouse mammary epithelial cells promotes metastasis by recruiting myeloid-derived suppressor cells into tumor tissues via the CXCL5-CXCR2 and CXCL12-CXCR4 axes [368]. The increased transcript levels of *Cxcl5* and its receptor *Cxcr2* in uteri of *Pten*$^{d/d}$; *Tgfbr1*$^{d/d}$ mice suggest a potential common mechanism for CXCL5/CCL2 up-regulation in the absence of TGFB receptor-mediated signaling in epithelial cancer cells [368]. This finding, together with the role of CXCL5 in cell invasion and metastasis in several types of cancers including bladder cancer [385], mammary cancer [368], and liver cancer

[386], suggests that activation of the CXCL5-CXCR2 axis due to loss of TGFBR1 may contribute to the pulmonary metastasis of endometrial cancer induced by conditional abrogation of PTEN in the uterus. Importantly, we showed that serum levels of CXCL5 and CCL2 were elevated in *Pten*$^{d/d}$; *Tgfbr1*$^{d/d}$ mice compared with *Pten*$^{d/d}$ mice. Since *CXCL5* expression is increased in human endometrial cancer tissues compared with normal endometrium [387], it is plausible to further explore the potential of CXCL5 and CCL2 as biomarkers for endometrial cancer patients.

Studies using genetically modified mice have revealed the emerging role of TAMs in the development of invasive endometrial cancer [388, 389]. However, the involvement of uterine TGFB signaling in TAM recruitment and polarization and the contribution of TAMs to the development of endometrial cancer remains to be elucidated. At advanced stages of tumor development, CD163$^{+}$ cells were readily detectable and the expression of CD163 was increased in the uteri of *Pten*$^{d/d}$; *Tgfbr1*$^{d/d}$ mice versus *Pten*$^{d/d}$ mice, suggesting the involvement of TAMs in promoting endometrial cancer progression in *Pten*$^{d/d}$; *Tgfbr1*$^{d/d}$ mice. Future studies are warranted to define the mechanism of action of pro-inflammatory chemokines, particularly CXCL5 and CCL2, and the function of TAMs within the tumor microenvironment in our model. It is noteworthy that TGFB signaling may act as tumor suppressor in pre-malignant cells, but tumor promoter during advanced tumor development [325]. That deletion of *Tgfbr1* in the PTEN-inactivated uterus accelerates endometrial cancer progression and also highlights the complex role

of TGFB signaling *in vivo*, where compensatory pathways may function to promote cancer invasion/metastasis in the absence of TGFBR1.

In summary, conditional deletion of *Pten* and *Tgfbr1* leads to a disease that recapitulates invasive and lethal endometrial cancer. This new mouse model is potentially valuable for preclinical testing of targeted therapies to treat endometrial cancer with metastasis.

# 5. SUMMARY

Uterine dysfunction can cause infertility. Therefore, understanding the mechanisms underlying the uterine development and function is an important issue. A variety of reproductive and developmental processes are regulated by a family of growth factors named as transforming growth factor beta (TGFβ) superfamily. These growth factors signal through the receptor complexes and intracellular canonical and/or noncanonical signaling to regulate multiple cellular events. Conditional knockout (cKO) of TGFβ type 1 receptor (TGFBR1) in the female reproductive tract using anti-Müllerian hormone receptor type 2 (*Amhr2*)-Cre results in disrupted myometrial formation, suggesting that TGFβ signaling is critical for uterine development and function

The first study of this dissertation was aimed at defining the cellular and molecular basis for myometrial defects in the *Tgfbr1* cKO mice. We found that TGFBR1 is required for myometrial configuration/formation during early development. Despite the well-established role of TGFβ signaling in vascular smooth muscle cell differentiation, the majority of smooth muscle genes were expressed in *Tgfbr1* cKO uteri at similar levels as controls, coinciding with the presence but abnormal distribution of proteins for select smooth muscle markers. Importantly, the uteri of these mice had impaired synthesis of key extracellular matrix proteins collagen IV and laminin, and dysregulated expression of platelet-derived growth factors. Furthermore, platelet-derived growth factors induced the migration of uterine stromal cells from both control and *Tgfbr1* cKO mice *in vitro*.

Our results suggest that the myometrial defects in *Tgfbr1* cKO mice may not directly arise from an intrinsic deficiency in uterine smooth muscle cell differentiation, but are linked to the impaired production of key extracellular matrix components and abnormal uterine cell migration during a critical time window of postnatal uterine development. These findings will potentially aid in the design of novel therapies for reproductive disorders associated with myometrial defects.

In the second study, to complement the loss of function model in the first study, we generated a gain-of-function mouse model harboring a constitutively active (CA) TGFBR1, the expression of which was conditionally induced by the progesterone receptor (*Pgr*)-Cre recombinase. Over-activation of TGFβ signaling was verified by enhanced phosphorylation of SMAD2 and increased expression of TGFβ target genes in the uterus. TGFBR1 *Pgr*-Cre CA mice were sterile. Histological, cellular, and molecular analyses demonstrated that constitutive activation of TGFBR1 in the mouse uterus promoted the formation of thicker myometrium. Accompanying this phenotype was the upregulation of a battery of smooth muscle genes in the uterus. Furthermore, TGFβ ligands activated SMAD2/3 and stimulated the expression of a smooth muscle maker gene, *ACTA2*, in human uterine smooth muscle cells. Immunofluorescence microscopy identified a marked reduction of uterine glands in TGFBR1 *Pgr*-Cre CA mice within the endometrial compartment that contained myofibroblast-like cells. We then demonstrated decidualization defects in the TGFBR1 *Pgr*-Cre CA mice using artificial decidualization approaches. Thus, constitutive activation of TGFBR1 in the mouse uterus leads to

morphological abnormalities and functional deficiency of the uterus. These results suggest a balanced TGFβ signaling system is required for normal uterine development and function.

Although a putative role for TGFβ signaling in the pathogenesis of human endometrial cancer has long been proposed, the precise function of TGFβ signaling in the development and progression of endometrial cancer remains elusive. Depletion of PTEN in the mouse uterus causes endometrial cancer. In the third study, we focused on identifying the role of TGFB signaling in PTEN-inactivated uterine epithelial cells by deleting *Tgfbr1* and *Pten* in the mouse uterus using *Pgr*-Cre (termed *Pten*$^{d/d}$; *Tgfbr1*$^{d/d}$). We found that *Pten*$^{d/d}$; *Tgfbr1*$^{d/d}$ mice developed severe endometrial lesions that progressed more rapidly compared with those resulting from conditional deletion of *Pten* alone, suggesting that TGFβ signaling synergizes with PTEN to suppress endometrial cancer progression. Remarkably, the *Pten*$^{d/d}$; *Tgfbr1*$^{d/d}$ mice developed distant pulmonary metastases. Mechanistically, the uteri and lung metastases of *Pten*$^{d/d}$; *Tgfbr1*$^{d/d}$ mice had increased production of pro-inflammatory chemokines such as CXCL5 and CCL2. The severe myometrial invasion and disruption in *Pten*$^{d/d}$; *Tgfbr1*$^{d/d}$ mice suggested enhanced epithelial cell migration/invasion in *Pten*$^{d/d}$; *Tgfbr1*$^{d/d}$ mice. Furthermore, tumor-associated macrophages were recruited to the endometrial compartment of *Pten*$^{d/d}$; *Tgfbr1*$^{d/d}$ mice that might promote tumor progression. Thus, conditional deletion of *Tgfbr1* in PTEN-inactivated endometrium leads to more invasive

endometrial cancer. This mouse model may be valuable for preclinical testing of new cancer therapies targeting tumor cell motility.

## REFERENCES


1. Sporn MB. The early history of TGF-beta, and a brief glimpse of its future. Cytokine Growth Factor Rev 2006; 17:3-7.
2. Moses HL, Roberts AB, Derynck R. The Discovery and Early Days of TGF-beta: A Historical Perspective. Cold Spring Harb Perspect Biol 2016; 8.
3. de Larco JE, Todaro GJ. Growth factors from murine sarcoma virus-transformed cells. Proc Natl Acad Sci U S A 1978; 75:4001-4005.
4. Moses HL, Branum EL, Proper JA, Robinson RA. Transforming growth factor production by chemically transformed cells. Cancer Res 1981; 41:2842-2848.
5. Roberts AB, Anzano MA, Lamb LC, Smith JM, Sporn MB. New class of transforming growth factors potentiated by epidermal growth factor: isolation from non-neoplastic tissues. Proc Natl Acad Sci U S A 1981; 78:5339-5343.
6. Assoian RK, Komoriya A, Meyers CA, Miller DM, Sporn MB. Transforming growth factor-beta in human platelets. Identification of a major storage site, purification, and characterization. J Biol Chem 1983; 258:7155-7160.
7. Derynck R, Jarrett JA, Chen EY, Eaton DH, Bell JR, et al. Human transforming growth factor-beta complementary DNA sequence and expression in normal and transformed cells. Nature 1985; 316:701-705.
8. Burt DW, Law AS. Evolution of the transforming growth factor-beta superfamily. Prog Growth Factor Res 1994; 5:99-118.

9. Massague J. The transforming growth factor-beta family. Annu Rev Cell Biol 1990; 6:597-641.

10. Burt DW. Evolutionary grouping of the transforming growth factor-beta superfamily. Biochem Biophys Res Commun 1992; 184:590-595.

11. Mason AJ, Hayflick JS, Ling N, Esch F, Ueno N, et al. Complementary DNA sequences of ovarian follicular fluid inhibin show precursor structure and homology with transforming growth factor-beta. Nature 1985; 318:659-663.

12. Cate RL, Mattaliano RJ, Hession C, Tizard R, Farber NM, et al. Isolation of the bovine and human genes for Mullerian inhibiting substance and expression of the human gene in animal cells. Cell 1986; 45:685-698.

13. Wozney JM, Rosen V, Celeste AJ, Mitsock LM, Whitters MJ, et al. Novel regulators of bone formation: molecular clones and activities. Science 1988; 242:1528-1534.

14. Chang H, Brown CW, Matzuk MM. Genetic analysis of the mammalian transforming growth factor-beta superfamily. Endocr Rev 2002; 23:787-823.

15. Weiskirchen R, Meurer SK, Gressner OA, Herrmann J, Borkham-Kamphorst E, et al. BMP-7 as antagonist of organ fibrosis. Front Biosci (Landmark Ed) 2009; 14:4992-5012.

16. Gentry LE, Lioubin MN, Purchio AF, Marquardt H. Molecular events in the processing of recombinant type 1 pre-pro-transforming growth factor beta to the mature polypeptide. Mol Cell Biol 1988; 8:4162-4168.

17. Khalil N. TGF-beta: from latent to active. Microbes Infect 1999; 1:1255-1263.

18. Lioubin MN, Madisen L, Marquardt H, Roth R, Kovacina KS, et al. Characterization of latent recombinant TGF-beta 2 produced by Chinese hamster ovary cells. J Cell Biochem 1991; 45:112-121.

19. Paetzel M, Karla A, Strynadka NC, Dalbey RE. Signal peptidases. Chem Rev 2002; 102:4549-4580.

20. Munger JS, Harpel JG, Gleizes PE, Mazzieri R, Nunes I, et al. Latent transforming growth factor-beta: structural features and mechanisms of activation. Kidney Int 1997; 51:1376-1382.

21. Dubois CM, Laprise MH, Blanchette F, Gentry LE, Leduc R. Processing of transforming growth factor beta 1 precursor by human furin convertase. J Biol Chem 1995; 270:10618-10624.

22. Annes JP, Munger JS, Rifkin DB. Making sense of latent TGFbeta activation. J Cell Sci 2003; 116:217-224.

23. Lyons RM, Keski-Oja J, Moses HL. Proteolytic activation of latent transforming growth factor-beta from fibroblast-conditioned medium. J Cell Biol 1988; 106:1659-1665.

24. Lyons RM, Gentry LE, Purchio AF, Moses HL. Mechanism of activation of latent recombinant transforming growth factor beta 1 by plasmin. J Cell Biol 1990; 110:1361-1367.

25. Sato Y, Rifkin DB. Inhibition of endothelial cell movement by pericytes and smooth muscle cells: activation of a latent transforming growth factor-beta 1-like molecule by plasmin during co-culture. J Cell Biol 1989; 109:309-315.

26. Yee JA, Yan L, Dominguez JC, Allan EH, Martin TJ. Plasminogen-dependent activation of latent transforming growth factor beta (TGF beta) by growing cultures of osteoblast-like cells. J Cell Physiol 1993; 157:528-534.

27. Yu Q, Stamenkovic I. Cell surface-localized matrix metalloproteinase-9 proteolytically activates TGF-beta and promotes tumor invasion and angiogenesis. Genes Dev 2000; 14:163-176.

28. Murphy-Ullrich JE, Schultz-Cherry S, Hook M. Transforming growth factor-beta complexes with thrombospondin. Mol Biol Cell 1992; 3:181-188.

29. Schultz-Cherry S, Murphy-Ullrich JE. Thrombospondin causes activation of latent transforming growth factor-beta secreted by endothelial cells by a novel mechanism. J Cell Biol 1993; 122:923-932.

30. Murphy-Ullrich JE, Poczatek M. Activation of latent TGF-beta by thrombospondin-1: mechanisms and physiology. Cytokine Growth Factor Rev 2000; 11:59-69.

31. Barcellos-Hoff MH, Dix TA. Redox-mediated activation of latent transforming growth factor-beta 1. Mol Endocrinol 1996; 10:1077-1083.

32. Jobling MF, Mott JD, Finnegan MT, Jurukovski V, Erickson AC, et al. Isoform-specific activation of latent transforming growth factor beta (LTGF-beta) by reactive oxygen species. Radiat Res 2006; 166:839-848.

33. Munger JS, Huang X, Kawakatsu H, Griffiths MJ, Dalton SL, et al. The integrin alpha v beta 6 binds and activates latent TGF beta 1: a mechanism for regulating pulmonary inflammation and fibrosis. Cell 1999; 96:319-328.

34. Mu D, Cambier S, Fjellbirkeland L, Baron JL, Munger JS, et al. The integrin alpha(v)beta8 mediates epithelial homeostasis through MT1-MMP-dependent activation of TGF-beta1. J Cell Biol 2002; 157:493-507.

35. Brown PD, Wakefield LM, Levinson AD, Sporn MB. Physicochemical activation of recombinant latent transforming growth factor-beta's 1, 2, and 3. Growth Factors 1990; 3:35-43.

36. Durbec P, Marcos-Gutierrez CV, Kilkenny C, Grigoriou M, Wartiowaara K, et al. GDNF signalling through the Ret receptor tyrosine kinase. Nature 1996; 381:789-793.

37. Jing S, Wen D, Yu Y, Holst PL, Luo Y, et al. GDNF-induced activation of the ret protein tyrosine kinase is mediated by GDNFR-alpha, a novel receptor for GDNF. Cell 1996; 85:1113-1124.

38. Saarma M. GDNF - a stranger in the TGF-beta superfamily? Eur J Biochem 2000; 267:6968-6971.

39. Lin HY, Moustakas A. TGF-beta receptors: structure and function. Cell Mol Biol (Noisy-le-grand) 1994; 40:337-349.

40. Massague J. Receptors for the TGF-beta family. Cell 1992; 69:1067-1070.

41. Hinck AP. Structural studies of the TGF-betas and their receptors - insights into evolution of the TGF-beta superfamily. FEBS Lett 2012; 586:1860-1870.

42. Blobe GC, Schiemann WP, Pepin MC, Beauchemin M, Moustakas A, et al. Functional roles for the cytoplasmic domain of the type III transforming growth

factor beta receptor in regulating transforming growth factor beta signaling. J Biol Chem 2001; 276:24627-24637.

43. Esparza-Lopez J, Montiel JL, Vilchis-Landeros MM, Okadome T, Miyazono K, et al. Ligand binding and functional properties of betaglycan, a co-receptor of the transforming growth factor-beta superfamily. Specialized binding regions for transforming growth factor-beta and inhibin A. J Biol Chem 2001; 276:14588-14596.

44. Massague J. TGF-beta signal transduction. Annu Rev Biochem 1998; 67:753-791.

45. Wrana JL, Tran H, Attisano L, Arora K, Childs SR, et al. Two distinct transmembrane serine/threonine kinases from Drosophila melanogaster form an activin receptor complex. Mol Cell Biol 1994; 14:944-950.

46. Wieser R, Wrana JL, Massague J. GS domain mutations that constitutively activate T beta R-I, the downstream signaling component in the TGF-beta receptor complex. EMBO J 1995; 14:2199-2208.

47. Souchelnytskyi S, ten Dijke P, Miyazono K, Heldin CH. Phosphorylation of Ser165 in TGF-beta type I receptor modulates TGF-beta1-induced cellular responses. EMBO J 1996; 15:6231-6240.

48. Weis-Garcia F, Massague J. Complementation between kinase-defective and activation-defective TGF-beta receptors reveals a novel form of receptor cooperativity essential for signaling. EMBO J 1996; 15:276-289.

49. Fukuda T, Scott G, Komatsu Y, Araya R, Kawano M, et al. Generation of a mouse with conditionally activated signaling through the BMP receptor, ALK2. Genesis 2006; 44:159-167.

50. Shore EM, Xu M, Feldman GJ, Fenstermacher DA, Cho TJ, et al. A recurrent mutation in the BMP type I receptor ACVR1 causes inherited and sporadic fibrodysplasia ossificans progressiva. Nat Genet 2006; 38:525-527.

51. Willis SA, Zimmerman CM, Li LI, Mathews LS. Formation and activation by phosphorylation of activin receptor complexes. Mol Endocrinol 1996; 10:367-379.

52. Goumans MJ, Valdimarsdottir G, Itoh S, Lebrin F, Larsson J, et al. Activin receptor-like kinase (ALK)1 is an antagonistic mediator of lateral TGFbeta/ALK5 signaling. Mol Cell 2003; 12:817-828.

53. Medici D, Shore EM, Lounev VY, Kaplan FS, Kalluri R, et al. Conversion of vascular endothelial cells into multipotent stem-like cells. Nat Med 2010; 16:1400-1406.

54. Miyazono K. Signal transduction by bone morphogenetic protein receptors: functional roles of Smad proteins. Bone 1999; 25:91-93.

55. Fujii M, Takeda K, Imamura T, Aoki H, Sampath TK, et al. Roles of bone morphogenetic protein type I receptors and Smad proteins in osteoblast and chondroblast differentiation. Mol Biol Cell 1999; 10:3801-3813.

56. Derynck R, Feng XH. TGF-beta receptor signaling. Biochim Biophys Acta 1997; 1333:F105-150.

57. Lin HY, Moustakas A, Knaus P, Wells RG, Henis YI, et al. The soluble exoplasmic domain of the type II transforming growth factor (TGF)-beta receptor. A heterogeneously glycosylated protein with high affinity and selectivity for TGF-beta ligands. J Biol Chem 1995; 270:2747-2754.

58. Lopez-Casillas F, Wrana JL, Massague J. Betaglycan presents ligand to the TGF beta signaling receptor. Cell 1993; 73:1435-1444.

59. Wang XF, Lin HY, Ng-Eaton E, Downward J, Lodish HF, et al. Expression cloning and characterization of the TGF-beta type III receptor. Cell 1991; 67:797-805.

60. Lopez-Casillas F, Cheifetz S, Doody J, Andres JL, Lane WS, et al. Structure and expression of the membrane proteoglycan betaglycan, a component of the TGF-beta receptor system. Cell 1991; 67:785-795.

61. Sankar S, Mahooti-Brooks N, Centrella M, McCarthy TL, Madri JA. Expression of transforming growth factor type III receptor in vascular endothelial cells increases their responsiveness to transforming growth factor beta 2. J Biol Chem 1995; 270:13567-13572.

62. Wiater E, Harrison CA, Lewis KA, Gray PC, Vale WW. Identification of distinct inhibin and transforming growth factor beta-binding sites on betaglycan: functional separation of betaglycan co-receptor actions. J Biol Chem 2006; 281:17011-17022.

63. Cheifetz S, Bellon T, Cales C, Vera S, Bernabeu C, et al. Endoglin is a component of the transforming growth factor-beta receptor system in human endothelial cells. J Biol Chem 1992; 267:19027-19030.

64. Massague J, Seoane J, Wotton D. Smad transcription factors. Genes Dev 2005; 19:2783-2810.

65. Attisano L, Wrana JL. Smads as transcriptional co-modulators. Curr Opin Cell Biol 2000; 12:235-243.

66. Makkar P, Metpally RP, Sangadala S, Reddy BV. Modeling and analysis of MH1 domain of Smads and their interaction with promoter DNA sequence motif. J Mol Graph Model 2009; 27:803-812.

67. Shi Y, Wang YF, Jayaraman L, Yang H, Massague J, et al. Crystal structure of a Smad MH1 domain bound to DNA: insights on DNA binding in TGF-beta signaling. Cell 1998; 94:585-594.

68. Lo RS, Chen YG, Shi Y, Pavletich NP, Massague J. The L3 loop: a structural motif determining specific interactions between SMAD proteins and TGF-beta receptors. EMBO J 1998; 17:996-1005.

69. Tsukazaki T, Chiang TA, Davison AF, Attisano L, Wrana JL. SARA, a FYVE domain protein that recruits Smad2 to the TGFbeta receptor. Cell 1998; 95:779-791.

70. Hata A, Lo RS, Wotton D, Lagna G, Massague J. Mutations increasing autoinhibition inactivate tumour suppressors Smad2 and Smad4. Nature 1997; 388:82-87.

71. Wu RY, Zhang Y, Feng XH, Derynck R. Heteromeric and homomeric interactions correlate with signaling activity and functional cooperativity of Smad3 and Smad4/DPC4. Mol Cell Biol 1997; 17:2521-2528.

72. Itoh S, Ericsson J, Nishikawa J, Heldin CH, ten Dijke P. The transcriptional co-activator P/CAF potentiates TGF-beta/Smad signaling. Nucleic Acids Res 2000; 28:4291-4298.

73. Kretzschmar M, Liu F, Hata A, Doody J, Massague J. The TGF-beta family mediator Smad1 is phosphorylated directly and activated functionally by the BMP receptor kinase. Genes Dev 1997; 11:984-995.

74. Souchelnytskyi S, Tamaki K, Engstrom U, Wernstedt C, ten Dijke P, et al. Phosphorylation of Ser465 and Ser467 in the C terminus of Smad2 mediates interaction with Smad4 and is required for transforming growth factor-beta signaling. J Biol Chem 1997; 272:28107-28115.

75. Abdollah S, Macias-Silva M, Tsukazaki T, Hayashi H, Attisano L, et al. TbetaRI phosphorylation of Smad2 on Ser465 and Ser467 is required for Smad2-Smad4 complex formation and signaling. J Biol Chem 1997; 272:27678-27685.

76. Heldin CH, Miyazono K, ten Dijke P. TGF-beta signalling from cell membrane to nucleus through SMAD proteins. Nature 1997; 390:465-471.

77. Hariharan R, Pillai MR. Structure-function relationship of inhibitory Smads: Structural flexibility contributes to functional divergence. Proteins 2008; 71:1853-1862.

78. Imamura T, Takase M, Nishihara A, Oeda E, Hanai J, et al. Smad6 inhibits signalling by the TGF-beta superfamily. Nature 1997; 389:622-626.

79. Nakao A, Afrakhte M, Moren A, Nakayama T, Christian JL, et al. Identification of Smad7, a TGFbeta-inducible antagonist of TGF-beta signalling. Nature 1997; 389:631-635.

80. Guo X, Wang XF. Signaling cross-talk between TGF-beta/BMP and other pathways. Cell Res 2009; 19:71-88.

81. Luo K. Signaling Cross Talk between TGF-beta/Smad and Other Signaling Pathways. Cold Spring Harb Perspect Biol 2017; 9.

82. Attisano L, Wrana JL. Signal integration in TGF-beta, WNT, and Hippo pathways. F1000Prime Rep 2013; 5:17.

83. Butz H, Racz K, Hunyady L, Patocs A. Crosstalk between TGF-beta signaling and the microRNA machinery. Trends Pharmacol Sci 2012; 33:382-393.

84. Zhang W, Liu HT. MAPK signal pathways in the regulation of cell proliferation in mammalian cells. Cell Res 2002; 12:9-18.

85. Pearson G, Robinson F, Beers Gibson T, Xu BE, Karandikar M, et al. Mitogen-activated protein (MAP) kinase pathways: regulation and physiological functions. Endocr Rev 2001; 22:153-183.

86. Plotnikov A, Zehorai E, Procaccia S, Seger R. The MAPK cascades: signaling components, nuclear roles and mechanisms of nuclear translocation. Biochim Biophys Acta 2011; 1813:1619-1633.

87. Mulder KM, Morris SL. Activation of p21ras by transforming growth factor beta in epithelial cells. J Biol Chem 1992; 267:5029-5031.

88. Hartsough MT, Mulder KM. Transforming growth factor beta activation of p44mapk in proliferating cultures of epithelial cells. J Biol Chem 1995; 270:7117-7124.

89. Mucsi I, Skorecki KL, Goldberg HJ. Extracellular signal-regulated kinase and the small GTP-binding protein, Rac, contribute to the effects of transforming growth factor-beta1 on gene expression. J Biol Chem 1996; 271:16567-16572.

90. Frey RS, Mulder KM. TGFbeta regulation of mitogen-activated protein kinases in human breast cancer cells. Cancer Lett 1997; 117:41-50.

91. Yamaguchi K, Shirakabe K, Shibuya H, Irie K, Oishi I, et al. Identification of a member of the MAPKKK family as a potential mediator of TGF-beta signal transduction. Science 1995; 270:2008-2011.

92. Moriguchi T, Kuroyanagi N, Yamaguchi K, Gotoh Y, Irie K, et al. A novel kinase cascade mediated by mitogen-activated protein kinase kinase 6 and MKK3. J Biol Chem 1996; 271:13675-13679.

93. Shirakabe K, Yamaguchi K, Shibuya H, Irie K, Matsuda S, et al. TAK1 mediates the ceramide signaling to stress-activated protein kinase/c-Jun N-terminal kinase. J Biol Chem 1997; 272:8141-8144.

94. Zavadil J, Bitzer M, Liang D, Yang YC, Massimi A, et al. Genetic programs of epithelial cell plasticity directed by transforming growth factor-beta. Proc Natl Acad Sci U S A 2001; 98:6686-6691.

95. Davies M, Robinson M, Smith E, Huntley S, Prime S, et al. Induction of an epithelial to mesenchymal transition in human immortal and malignant keratinocytes by TGF-beta1 involves MAPK, Smad and AP-1 signalling pathways. J Cell Biochem 2005; 95:918-931.

96. Wendt MK, Allington TM, Schiemann WP. Mechanisms of the epithelial-mesenchymal transition by TGF-beta. Future Oncol 2009; 5:1145-1168.

97. Franke TF. PI3K/Akt: getting it right matters. Oncogene 2008; 27:6473-6488.

98. Hemmings BA, Restuccia DF. PI3K-PKB/Akt pathway. Cold Spring Harb Perspect Biol 2012; 4:a011189.

99. Wilkes MC, Mitchell H, Penheiter SG, Dore JJ, Suzuki K, et al. Transforming growth factor-beta activation of phosphatidylinositol 3-kinase is independent of Smad2 and Smad3 and regulates fibroblast responses via p21-activated kinase-2. Cancer Res 2005; 65:10431-10440.

100. Shin I, Bakin AV, Rodeck U, Brunet A, Arteaga CL. Transforming growth factor beta enhances epithelial cell survival via Akt-dependent regulation of FKHRL1. Mol Biol Cell 2001; 12:3328-3339.

101. Bakin AV, Tomlinson AK, Bhowmick NA, Moses HL, Arteaga CL. Phosphatidylinositol 3-kinase function is required for transforming growth factor beta-mediated epithelial to mesenchymal transition and cell migration. J Biol Chem 2000; 275:36803-36810.

102. Wood GA, Fata JE, Watson KL, Khokha R. Circulating hormones and estrous stage predict cellular and stromal remodeling in murine uterus. Reproduction 2007; 133:1035-1044.

103. Tabibzadeh S. The signals and molecular pathways involved in human menstruation, a unique process of tissue destruction and remodelling. Mol Hum Reprod 1996; 2:77-92.

104. Li Q, Kannan A, DeMayo FJ, Lydon JP, Cooke PS, et al. The antiproliferative action of progesterone in uterine epithelium is mediated by Hand2. Science 2011; 331:912-916.

105. Stewart CL, Kaspar P, Brunet LJ, Bhatt H, Gadi I, et al. Blastocyst implantation depends on maternal expression of leukaemia inhibitory factor. Nature 1992; 359:76-79.

106. Thathiah A, Carson DD. Mucins and blastocyst attachment. Rev Endocr Metab Disord 2002; 3:87-96.

107. Spencer TE, Dunlap KA, Filant J. Comparative developmental biology of the uterus: insights into mechanisms and developmental disruption. Mol Cell Endocrinol 2012; 354:34-53.

108. Jones RL, Stoikos C, Findlay JK, Salamonsen LA. TGF-beta superfamily expression and actions in the endometrium and placenta. Reproduction 2006; 132:217-232.

109. Mesiano S, Chan EC, Fitter JT, Kwek K, Yeo G, et al. Progesterone withdrawal and estrogen activation in human parturition are coordinated by progesterone

receptor A expression in the myometrium. J Clin Endocrinol Metab 2002; 87:2924-2930.

110. Condon JC, Jeyasuria P, Faust JM, Wilson JW, Mendelson CR. A decline in the levels of progesterone receptor coactivators in the pregnant uterus at term may antagonize progesterone receptor function and contribute to the initiation of parturition. Proc Natl Acad Sci U S A 2003; 100:9518-9523.

111. Brainard AM, Miller AJ, Martens JR, England SK. Maxi-K channels localize to caveolae in human myometrium: a role for an actin-channel-caveolin complex in the regulation of myometrial smooth muscle K+ current. Am J Physiol Cell Physiol 2005; 289:C49-57.

112. Brainard AM, Korovkina VP, England SK. Potassium channels and uterine function. Semin Cell Dev Biol 2007; 18:332-339.

113. Pierce SL, Kresowik JD, Lamping KG, England SK. Overexpression of SK3 channels dampens uterine contractility to prevent preterm labor in mice. Biol Reprod 2008; 78:1058-1063.

114. Pierce SL, England SK. SK3 channel expression during pregnancy is regulated through estrogen and Sp factor-mediated transcriptional control of the KCNN3 gene. Am J Physiol Endocrinol Metab 2010; 299:E640-646.

115. Yallampalli C, Dong YL. Estradiol-17beta inhibits nitric oxide synthase (NOS)-II and stimulates NOS-III gene expression in the rat uterus. Biol Reprod 2000; 63:34-41.

116. Yallampalli C, Garfield RE, Byam-Smith M. Nitric oxide inhibits uterine contractility during pregnancy but not during delivery. Endocrinology 1993; 133:1899-1902.

117. Yallampalli C, Izumi H, Byam-Smith M, Garfield RE. An L-arginine-nitric oxide-cyclic guanosine monophosphate system exists in the uterus and inhibits contractility during pregnancy. Am J Obstet Gynecol 1994; 170:175-185.

118. Dong YL, Yallampalli C. Interaction between nitric oxide and prostaglandin E2 pathways in pregnant rat uteri. Am J Physiol 1996; 270:E471-476.

119. Renthal NE, Chen CC, Williams KC, Gerard RD, Prange-Kiel J, et al. miR-200 family and targets, ZEB1 and ZEB2, modulate uterine quiescence and contractility during pregnancy and labor. Proc Natl Acad Sci U S A 2010; 107:20828-20833.

120. Orvis GD, Behringer RR. Cellular mechanisms of Mullerian duct formation in the mouse. Dev Biol 2007; 306:493-504.

121. Brody JR, Cunha GR. Histologic, morphometric, and immunocytochemical analysis of myometrial development in rats and mice: I. Normal development. Am J Anat 1989; 186:1-20.

122. Brauer MM, Passaro M, Casanova G, Abeledo G, Barreiro P. Differentiation of smooth muscle in the genital tract of the female mouse and its temporal relation with the development of the Wolffian nerve. Anat Embryol (Berl) 1989; 179:403-410.

123. Mehasseb MK, Bell SC, Habiba MA. The effects of tamoxifen and estradiol on myometrial differentiation and organization during early uterine development in the CD1 mouse. Reproduction 2009; 138:341-350.

124. Miller C, Sassoon DA. Wnt-7a maintains appropriate uterine patterning during the development of the mouse female reproductive tract. Development 1998; 125:3201-3211.

125. Wang Y, Jia Y, Franken P, Smits R, Ewing PC, et al. Loss of APC function in mesenchymal cells surrounding the Mullerian duct leads to myometrial defects in adult mice. Mol Cell Endocrinol 2011; 341:48-54.

126. Arango NA, Szotek PP, Manganaro TF, Oliva E, Donahoe PK, et al. Conditional deletion of beta-catenin in the mesenchyme of the developing mouse uterus results in a switch to adipogenesis in the myometrium. Dev Biol 2005; 288:276-283.

127. Parr BA, McMahon AP. Sexually dimorphic development of the mammalian reproductive tract requires Wnt-7a. Nature 1998; 395:707-710.

128. Bellessort B, Bachelot A, Heude E, Alfama G, Fontaine A, et al. Role of Foxl2 in uterine maturation and function. Hum Mol Genet 2015; 24:3092-3103.

129. Gray CA, Bazer FW, Spencer TE. Effects of neonatal progestin exposure on female reproductive tract structure and function in the adult ewe. Biol Reprod 2001; 64:797-804.

130. Gray CA, Burghardt RC, Johnson GA, Bazer FW, Spencer TE. Evidence that absence of endometrial gland secretions in uterine gland knockout ewes

compromises conceptus survival and elongation. Reproduction 2002; 124:289-300.

131. Cooke PS, Ekman GC, Kaur J, Davila J, Bagchi IC, et al. Brief exposure to progesterone during a critical neonatal window prevents uterine gland formation in mice. Biol Reprod 2012; 86:63.

132. Cooke PS, Spencer TE, Bartol FF, Hayashi K. Uterine glands: development, function and experimental model systems. Mol Hum Reprod 2013; 19:547-558.

133. Jeong JW, Kwak I, Lee KY, Kim TH, Large MJ, et al. Foxa2 is essential for mouse endometrial gland development and fertility. Biol Reprod 2010; 83:396-403.

134. Franco HL, Dai D, Lee KY, Rubel CA, Roop D, et al. WNT4 is a key regulator of normal postnatal uterine development and progesterone signaling during embryo implantation and decidualization in the mouse. FASEB J 2011; 25:1176-1187.

135. Mericskay M, Kitajewski J, Sassoon D. Wnt5a is required for proper epithelial-mesenchymal interactions in the uterus. Development 2004; 131:2061-2072.

136. Dunlap KA, Filant J, Hayashi K, Rucker EB, 3rd, Song G, et al. Postnatal deletion of Wnt7a inhibits uterine gland morphogenesis and compromises adult fertility in mice. Biol Reprod 2011; 85:386-396.

137. Reardon SN, King ML, MacLean JA, 2nd, Mann JL, DeMayo FJ, et al. CDH1 is essential for endometrial differentiation, gland development, and adult function in the mouse uterus. Biol Reprod 2012; 86:141, 141-110.

138. Dong J, Albertini DF, Nishimori K, Kumar TR, Lu N, et al. Growth differentiation factor-9 is required during early ovarian folliculogenesis. Nature 1996; 383:531-535.

139. Galloway SM, McNatty KP, Cambridge LM, Laitinen MP, Juengel JL, et al. Mutations in an oocyte-derived growth factor gene (BMP15) cause increased ovulation rate and infertility in a dosage-sensitive manner. Nat Genet 2000; 25:279-283.

140. Tomic D, Miller KP, Kenny HA, Woodruff TK, Hoyer P, et al. Ovarian follicle development requires Smad3. Mol Endocrinol 2004; 18:2224-2240.

141. Hashimoto O, Moore RK, Shimasaki S. Posttranslational processing of mouse and human BMP-15: potential implication in the determination of ovulation quota. Proc Natl Acad Sci U S A 2005; 102:5426-5431.

142. Juengel JL, McNatty KP. The role of proteins of the transforming growth factor-beta superfamily in the intraovarian regulation of follicular development. Hum Reprod Update 2005; 11:143-160.

143. Dragovic RA, Ritter LJ, Schulz SJ, Amato F, Thompson JG, et al. Oocyte-secreted factor activation of SMAD 2/3 signaling enables initiation of mouse cumulus cell expansion. Biol Reprod 2007; 76:848-857.

144. Diaz FJ, Wigglesworth K, Eppig JJ. Oocytes determine cumulus cell lineage in mouse ovarian follicles. J Cell Sci 2007; 120:1330-1340.

145. Li Q, Pangas SA, Jorgez CJ, Graff JM, Weinstein M, et al. Redundant roles of SMAD2 and SMAD3 in ovarian granulosa cells in vivo. Mol Cell Biol 2008; 28:7001-7011.

146. Gong X, McGee EA. Smad3 is required for normal follicular follicle-stimulating hormone responsiveness in the mouse. Biol Reprod 2009; 81:730-738.

147. Nagashima T, Li Q, Clementi C, Lydon JP, DeMayo FJ, et al. BMPR2 is required for postimplantation uterine function and pregnancy maintenance. J Clin Invest 2013; 123:2539-2550.

148. Itoh H, Kishore AH, Lindqvist A, Rogers DE, Word RA. Transforming growth factor beta1 (TGFbeta1) and progesterone regulate matrix metalloproteinases (MMP) in human endometrial stromal cells. J Clin Endocrinol Metab 2012; 97:E888-897.

149. Quezada M, Mcgee E. Inhibitory SMAD7 expression is upregulated by treatment with TGFβ in granulosa cells. Fertil Steril 2010; 94:S59-S59.

150. Li Q. Inhibitory SMADs: potential regulators of ovarian function. Biol Reprod 2015; 92:50.

151. Li Q. Transforming growth factor beta signaling in uterine development and function. J Anim Sci Biotechnol 2014; 5:52.

152. Chegini N, Luo X, Ding L, Ripley D. The expression of Smads and transforming growth factor beta receptors in leiomyoma and myometrium and the effect of gonadotropin releasing hormone analogue therapy. Mol Cell Endocrinol 2003; 209:9-16.

153. Das SK, Flanders KC, Andrews GK, Dey SK. Expression of transforming growth factor-beta isoforms (beta 2 and beta 3) in the mouse uterus: analysis of the periimplantation period and effects of ovarian steroids. Endocrinology 1992; 130:3459-3466.

154. Tang XM, Dou Q, Zhao Y, McLean F, Davis J, et al. The expression of transforming growth factor-beta s and TGF-beta receptor mRNA and protein and the effect of TGF-beta s on human myometrial smooth muscle cells in vitro. Mol Hum Reprod 1997; 3:233-240.

155. Shynlova O, Tsui P, Dorogin A, Langille BL, Lye SJ. The expression of transforming growth factor beta in pregnant rat myometrium is hormone and stretch dependent. Reproduction 2007; 134:503-511.

156. Chegini N, Zhao Y, Williams RS, Flanders KC. Human uterine tissue throughout the menstrual cycle expresses transforming growth factor-beta 1 (TGF beta 1), TGF beta 2, TGF beta 3, and TGF beta type II receptor messenger ribonucleic acid and protein and contains [125I]TGF beta 1-binding sites. Endocrinology 1994; 135:439-449.

157. Luo X, Xu J, Chegini N. The expression of Smads in human endometrium and regulation and induction in endometrial epithelial and stromal cells by transforming growth factor-beta. J Clin Endocrinol Metab 2003; 88:4967-4976.

158. Takahashi T, Eitzman B, Bossert NL, Walmer D, Sparrow K, et al. Transforming growth factors beta 1, beta 2, and beta 3 messenger RNA and protein expression

in mouse uterus and vagina during estrogen-induced growth: a comparison to other estrogen-regulated genes. Cell Growth Differ 1994; 5:919-935.

159. Liu G, Lin H, Zhang X, Li Q, Wang H, et al. Expression of Smad2 and Smad4 in mouse uterus during the oestrous cycle and early pregnancy. Placenta 2004; 25:530-537.

160. Li Y, Wei QW, Feng JG, Xu ML, Huang RH, et al. Expression of bone morphogenetic protein 2, 4, and related components of the BMP signaling pathway in the mouse uterus during the estrous cycle. J Zhejiang Univ Sci B 2014; 15:601-610.

161. Erickson GF, Fuqua L, Shimasaki S. Analysis of spatial and temporal expression patterns of bone morphogenetic protein family members in the rat uterus over the estrous cycle. J Endocrinol 2004; 182:203-217.

162. Tanwar PS, McFarlane JR. Dynamic expression of bone morphogenetic protein 4 in reproductive organs of female mice. Reproduction 2011; 142:573-579.

163. Richards EG, El-Nashar SA, Schoolmeester JK, Keeney GL, Mariani A, et al. Abnormal Uterine Bleeding Is Associated With Increased BMP7 Expression in Human Endometrium. Reprod Sci 2017; 24:671-681.

164. Petraglia F, Florio P, Luisi S, Gallo R, Gadducci A, et al. Expression and secretion of inhibin and activin in normal and neoplastic uterine tissues. High levels of serum activin A in women with endometrial and cervical carcinoma. J Clin Endocrinol Metab 1998; 83:1194-1200.

165. Candeloro L, Zorn TM. Distribution and spatiotemporal relationship of activin a and follistatin in mouse decidual and placental tissue. Am J Reprod Immunol 2007; 58:415-424.

166. Jones RL, Kaitu'u-Lino TJ, Nie G, Sanchez-Partida LG, Findlay JK, et al. Complex expression patterns support potential roles for maternally derived activins in the establishment of pregnancy in mouse. Reproduction 2006; 132:799-810.

167. Ciarmela P, Wiater E, Vale W. Activin-A in myometrium: characterization of the actions on myometrial cells. Endocrinology 2008; 149:2506-2516.

168. Ciarmela P, Wiater E, Smith SM, Vale W. Presence, actions, and regulation of myostatin in rat uterus and myometrial cells. Endocrinology 2009; 150:906-914.

169. Stoikos CJ, Harrison CA, Salamonsen LA, Dimitriadis E. A distinct cohort of the TGFbeta superfamily members expressed in human endometrium regulate decidualization. Hum Reprod 2008; 23:1447-1456.

170. Monsivais D, Matzuk MM, Pangas SA. The TGF-beta Family in the Reproductive Tract. Cold Spring Harb Perspect Biol 2017.

171. Jamin SP, Arango NA, Mishina Y, Hanks MC, Behringer RR. Requirement of Bmpr1a for Mullerian duct regression during male sexual development. Nat Genet 2002; 32:408-410.

172. Soyal SM, Mukherjee A, Lee KY, Li J, Li H, et al. Cre-mediated recombination in cell lineages that express the progesterone receptor. Genesis 2005; 41:58-66.

173. Lee KY, Jeong JW, Wang J, Ma L, Martin JF, et al. Bmp2 is critical for the murine uterine decidual response. Mol Cell Biol 2007; 27:5468-5478.

174. Park CB, DeMayo FJ, Lydon JP, Dufort D. NODAL in the uterus is necessary for proper placental development and maintenance of pregnancy. Biol Reprod 2012; 86:194.

175. Clementi C, Tripurani SK, Large MJ, Edson MA, Creighton CJ, et al. Activin-like kinase 2 functions in peri-implantation uterine signaling in mice and humans. PLoS Genet 2013; 9:e1003863.

176. Monsivais D, Clementi C, Peng J, Titus MM, Barrish JP, et al. Uterine ALK3 is essential during the window of implantation. Proc Natl Acad Sci U S A 2016; 113:E387-395.

177. Peng J, Fullerton PT, Jr., Monsivais D, Clementi C, Su GH, et al. Uterine Activin-Like Kinase 4 Regulates Trophoblast Development During Mouse Placentation. Mol Endocrinol 2015; 29:1684-1693.

178. Peng J, Monsivais D, You R, Zhong H, Pangas SA, et al. Uterine activin receptor-like kinase 5 is crucial for blastocyst implantation and placental development. Proc Natl Acad Sci U S A 2015; 112:E5098-5107.

179. Li Q, Agno JE, Edson MA, Nagaraja AK, Nagashima T, et al. Transforming growth factor beta receptor type 1 is essential for female reproductive tract integrity and function. PLoS Genet 2011; 7:e1002320.

180. Segars JH, Parrott EC, Nagel JD, Guo XC, Gao X, et al. Proceedings from the Third National Institutes of Health International Congress on Advances in

Uterine Leiomyoma Research: comprehensive review, conference summary and future recommendations. Hum Reprod Update 2014; 20:309-333.

181. Yi SE, LaPolt PS, Yoon BS, Chen JY, Lu JK, et al. The type I BMP receptor BmprIB is essential for female reproductive function. Proc Natl Acad Sci U S A 2001; 98:7994-7999.

182. Rodriguez A, Tripurani SK, Burton JC, Clementi C, Larina I, et al. SMAD Signaling Is Required for Structural Integrity of the Female Reproductive Tract and Uterine Function During Early Pregnancy in Mice. Biol Reprod 2016; 95:44.

183. Ramathal CY, Bagchi IC, Taylor RN, Bagchi MK. Endometrial decidualization: of mice and men. Semin Reprod Med 2010; 28:17-26.

184. Rossant J, Cross JC. Placental development: lessons from mouse mutants. Nat Rev Genet 2001; 2:538-548.

185. Watson ED, Cross JC. Development of structures and transport functions in the mouse placenta. Physiology (Bethesda) 2005; 20:180-193.

186. Tamada H, McMaster MT, Flanders KC, Andrews GK, Dey SK. Cell type-specific expression of transforming growth factor-beta 1 in the mouse uterus during the periimplantation period. Mol Endocrinol 1990; 4:965-972.

187. Selick CE, Horowitz GM, Gratch M, Scott RT, Jr., Navot D, et al. Immunohistochemical localization of transforming growth factor-beta in human implantation sites. J Clin Endocrinol Metab 1994; 78:592-596.

188. Paria BC, Ma W, Tan J, Raja S, Das SK, et al. Cellular and molecular responses of the uterus to embryo implantation can be elicited by locally applied growth factors. Proc Natl Acad Sci U S A 2001; 98:1047-1052.

189. Ying Y, Zhao GQ. Detection of multiple bone morphogenetic protein messenger ribonucleic acids and their signal transducer, Smad1, during mouse decidualization. Biol Reprod 2000; 63:1781-1786.

190. Jones RL, Salamonsen LA, Findlay JK. Potential roles for endometrial inhibins, activins and follistatin during human embryo implantation and early pregnancy. Trends Endocrinol Metab 2002; 13:144-150.

191. Zhang YS, Xiong GF, Peng JP. Effects of TGF beta-1 on mouse embryo implantation and expression of H2-D1 and H2-DM. Front Biosci (Elite Ed) 2010; 2:351-360.

192. Kane NM, Jones M, Brosens JJ, Kelly RW, Saunders PT, et al. TGFbeta1 attenuates expression of prolactin and IGFBP-1 in decidualized endometrial stromal cells by both SMAD-dependent and SMAD-independent pathways. PLoS One 2010; 5:e12970.

193. Cheng JC, Chang HM, Leung PC. Transforming growth factor-beta1 inhibits trophoblast cell invasion by inducing Snail-mediated down-regulation of vascular endothelial-cadherin protein. J Biol Chem 2013; 288:33181-33192.

194. Morrish DW, Kudo Y, Caniggia I, Cross J, Evain-Brion D, et al. Growth factors and trophoblast differentiation--workshop report. Placenta 2007; 28 Suppl A:S121-124.

195. Li Q, Kannan A, Wang W, Demayo FJ, Taylor RN, et al. Bone morphogenetic protein 2 functions via a conserved signaling pathway involving Wnt4 to regulate uterine decidualization in the mouse and the human. J Biol Chem 2007; 282:31725-31732.

196. de Caestecker M. The transforming growth factor-beta superfamily of receptors. Cytokine Growth Factor Rev 2004; 15:1-11.

197. Attisano L, Carcamo J, Ventura F, Weis FM, Massague J, et al. Identification of human activin and TGF beta type I receptors that form heteromeric kinase complexes with type II receptors. Cell 1993; 75:671-680.

198. Ray S, Pollard JW. KLF15 negatively regulates estrogen-induced epithelial cell proliferation by inhibition of DNA replication licensing. Proc Natl Acad Sci U S A 2012; 109:E1334-1343.

199. Papageorgiou I, Nicholls PK, Wang F, Lackmann M, Makanji Y, et al. Expression of nodal signalling components in cycling human endometrium and in endometrial cancer. Reprod Biol Endocrinol 2009; 7:122.

200. Munir S, Xu G, Wu Y, Yang B, Lala PK, et al. Nodal and ALK7 inhibit proliferation and induce apoptosis in human trophoblast cells. J Biol Chem 2004; 279:31277-31286.

201. Park CB, Dufort D. Nodal expression in the uterus of the mouse is regulated by the embryo and correlates with implantation. Biol Reprod 2011; 84:1103-1110.

202. Reissmann E, Jornvall H, Blokzijl A, Andersson O, Chang C, et al. The orphan receptor ALK7 and the Activin receptor ALK4 mediate signaling by Nodal proteins during vertebrate development. Genes Dev 2001; 15:2010-2022.

203. Petraglia F. Inhibin, activin and follistatin in the human placenta--a new family of regulatory proteins. Placenta 1997; 18:3-8.

204. Jones RL, Salamonsen LA, Critchley HO, Rogers PA, Affandi B, et al. Inhibin and activin subunits are differentially expressed in endometrial cells and leukocytes during the menstrual cycle, in early pregnancy and in women using progestin-only contraception. Mol Hum Reprod 2000; 6:1107-1117.

205. Piestrzeniewicz-Ulanska D, McGuinness DH, Yeaman GR. TGF-β Signaling in Endometrial Cancer. In: Jakowlew SB (ed.) Transforming Growth Factor-β in Cancer Therapy, Volume II: Cancer Treatment and Therapy. Totowa, NJ: Humana Press; 2008: 63-78.

206. Eritja N, Yeramian A, Chen B-J, Llobet-Navas D, Ortega E, et al. Endometrial Carcinoma: Specific Targeted Pathways. In: Hedrick Ellenson L (ed.) Molecular Genetics of Endometrial Carcinoma. Cham: Springer International Publishing; 2017: 149-207.

207. Bulun SE. Uterine fibroids. N Engl J Med 2013; 369:1344-1355.

208. Baird DD, Dunson DB, Hill MC, Cousins D, Schectman JM. High cumulative incidence of uterine leiomyoma in black and white women: ultrasound evidence. Am J Obstet Gynecol 2003; 188:100-107.

209. Dou Q, Zhao Y, Tarnuzzer RW, Rong H, Williams RS, et al. Suppression of transforming growth factor-beta (TGF beta) and TGF beta receptor messenger ribonucleic acid and protein expression in leiomyomata in women receiving gonadotropin-releasing hormone agonist therapy. J Clin Endocrinol Metab 1996; 81:3222-3230.

210. Ciarmela P, Bloise E, Gray PC, Carrarelli P, Islam MS, et al. Activin-A and myostatin response and steroid regulation in human myometrium: disruption of their signalling in uterine fibroid. J Clin Endocrinol Metab 2011; 96:755-765.

211. Shen T, Shi H, Xu Q, Song Q, Xu Y, et al. Effects of TGF-beta on uterine fibroids of women of childbearing age and uterine artery embolization. Minim Invasive Ther Allied Technol 2017:1-8.

212. Arici A, Sozen I. Transforming growth factor-beta3 is expressed at high levels in leiomyoma where it stimulates fibronectin expression and cell proliferation. Fertil Steril 2000; 73:1006-1011.

213. Islam MS, Catherino WH, Protic O, Janjusevic M, Gray PC, et al. Role of activin-A and myostatin and their signaling pathway in human myometrial and leiomyoma cell function. J Clin Endocrinol Metab 2014; 99:E775-785.

214. Norian JM, Malik M, Parker CY, Joseph D, Leppert PC, et al. Transforming growth factor beta3 regulates the versican variants in the extracellular matrix-rich uterine leiomyomas. Reprod Sci 2009; 16:1153-1164.

215. Joseph DS, Malik M, Nurudeen S, Catherino WH. Myometrial cells undergo fibrotic transformation under the influence of transforming growth factor beta-3. Fertil Steril 2010; 93:1500-1508.

216. De Falco M, Staibano S, D'Armiento FP, Mascolo M, Salvatore G, et al. Preoperative treatment of uterine leiomyomas: clinical findings and expression of transforming growth factor-beta3 and connective tissue growth factor. J Soc Gynecol Investig 2006; 13:297-303.

217. Ohara N, Morikawa A, Chen W, Wang J, DeManno DA, et al. Comparative effects of SPRM asoprisnil (J867) on proliferation, apoptosis, and the expression of growth factors in cultured uterine leiomyoma cells and normal myometrial cells. Reprod Sci 2007; 14:20-27.

218. Garcia L, Isaacson K. Adenomyosis: review of the literature. J Minim Invasive Gynecol 2011; 18:428-437.

219. Maheshwari A, Gurunath S, Fatima F, Bhattacharya S. Adenomyosis and subfertility: a systematic review of prevalence, diagnosis, treatment and fertility outcomes. Hum Reprod Update 2012; 18:374-392.

220. Sunkara SK, Khan KS. Adenomyosis and female fertility: a critical review of the evidence. J Obstet Gynaecol 2012; 32:113-116.

221. Liu X, Shen M, Qi Q, Zhang H, Guo SW. Corroborating evidence for platelet-induced epithelial-mesenchymal transition and fibroblast-to-myofibroblast transdifferentiation in the development of adenomyosis. Hum Reprod 2016; 31:734-749.

222. Carrarelli P, Yen CF, Arcuri F, Funghi L, Tosti C, et al. Myostatin, follistatin and activin type II receptors are highly expressed in adenomyosis. Fertil Steril 2015; 104:744-752 e741.

223. Siegel RL, Miller KD, Jemal A. Cancer Statistics, 2017. CA Cancer J Clin 2017; 67:7-30.

224. Cancer Genome Atlas Research N, Kandoth C, Schultz N, Cherniack AD, Akbani R, et al. Integrated genomic characterization of endometrial carcinoma. Nature 2013; 497:67-73.

225. Gao J, Aksoy BA, Dogrusoz U, Dresdner G, Gross B, et al. Integrative analysis of complex cancer genomics and clinical profiles using the cBioPortal. Sci Signal 2013; 6:pl1.

226. Cerami E, Gao J, Dogrusoz U, Gross BE, Sumer SO, et al. The cBio cancer genomics portal: an open platform for exploring multidimensional cancer genomics data. Cancer Discov 2012; 2:401-404.

227. Piestrzeniewicz-Ulanska D, Brys M, Semczuk A, Jakowicki JA, Krajewska WM. Expression of TGF-beta type I and II receptors in normal and cancerous human endometrium. Cancer Lett 2002; 186:231-239.

228. Parekh TV, Gama P, Wen X, Demopoulos R, Munger JS, et al. Transforming growth factor beta signaling is disabled early in human endometrial carcinogenesis concomitant with loss of growth inhibition. Cancer Res 2002; 62:2778-2790.

229. Piestrzeniewicz-Ulanska D, Brys M, Semczuk A, Rechberger T, Jakowicki JA, et al. TGF-beta signaling is disrupted in endometrioid-type endometrial carcinomas. Gynecol Oncol 2004; 95:173-180.

230. Dowdy SC, Mariani A, Reinholz MM, Keeney GL, Spelsberg TC, et al. Overexpression of the TGF-beta antagonist Smad7 in endometrial cancer. Gynecol Oncol 2005; 96:368-373.

231. Chandra A, Copen CE, Stephen EH. Infertility and impaired fecundity in the United States, 1982-2010: data from the National Survey of Family Growth. Natl Health Stat Report 2013:1-18, 11 p following 19.

232. Memon MA, Anway MD, Covert TR, Uzumcu M, Skinner MK. Transforming growth factor beta (TGFbeta1, TGFbeta2 and TGFbeta3) null-mutant phenotypes in embryonic gonadal development. Mol Cell Endocrinol 2008; 294:70-80.

233. Mu Z, Yang Z, Yu D, Zhao Z, Munger JS. TGFbeta1 and TGFbeta3 are partially redundant effectors in brain vascular morphogenesis. Mech Dev 2008; 125:508-516.

234. Shull MM, Ormsby I, Kier AB, Pawlowski S, Diebold RJ, et al. Targeted disruption of the mouse transforming growth factor-beta 1 gene results in multifocal inflammatory disease. Nature 1992; 359:693-699.

235. Sanford LP, Ormsby I, Gittenberger-de Groot AC, Sariola H, Friedman R, et al. TGFbeta2 knockout mice have multiple developmental defects that are non-overlapping with other TGFbeta knockout phenotypes. Development 1997; 124:2659-2670.

236. Kaartinen V, Voncken JW, Shuler C, Warburton D, Bu D, et al. Abnormal lung development and cleft palate in mice lacking TGF-beta 3 indicates defects of epithelial-mesenchymal interaction. Nat Genet 1995; 11:415-421.

237. Proetzel G, Pawlowski SA, Wiles MV, Yin M, Boivin GP, et al. Transforming growth factor-beta 3 is required for secondary palate fusion. Nat Genet 1995; 11:409-414.

238. Larsson J, Goumans MJ, Sjostrand LJ, van Rooijen MA, Ward D, et al. Abnormal angiogenesis but intact hematopoietic potential in TGF-beta type I receptor-deficient mice. EMBO J 2001; 20:1663-1673.

239. Oshima M, Oshima H, Taketo MM. TGF-beta receptor type II deficiency results in defects of yolk sac hematopoiesis and vasculogenesis. Dev Biol 1996; 179:297-302.

240. Nagashima T, Kim J, Li Q, Lydon JP, DeMayo FJ, et al. Connective tissue growth factor is required for normal follicle development and ovulation. Mol Endocrinol 2011; 25:1740-1759.

241. Rajanahally S, Agno JE, Nalam RL, Weinstein MB, Loveland KL, et al. Genetic evidence that SMAD2 is not required for gonadal tumor development in inhibin-deficient mice. Reprod Biol Endocrinol 2010; 8:69.

242. Gao Y, Bayless KJ, Li Q. TGFBR1 is required for mouse myometrial development. Mol Endocrinol 2014; 28:380-394.

243. Tong D, Lu X, Wang HX, Plante I, Lui E, et al. A dominant loss-of-function GJA1 (Cx43) mutant impairs parturition in the mouse. Biol Reprod 2009; 80:1099-1106.

244. Brody JR, Cunha GR. Histologic, morphometric, and immunocytochemical analysis of myometrial development in rats and mice: II. Effects of DES on development. Am J Anat 1989; 186:21-42.

245. King KE, Iyemere VP, Weissberg PL, Shanahan CM. Kruppel-like factor 4 (KLF4/GKLF) is a target of bone morphogenetic proteins and transforming growth factor beta 1 in the regulation of vascular smooth muscle cell phenotype. J Biol Chem 2003; 278:11661-11669.

246. Kennard S, Liu H, Lilly B. Transforming growth factor-beta (TGF- 1) down-regulates Notch3 in fibroblasts to promote smooth muscle gene expression. J Biol Chem 2008; 283:1324-1333.

247. Hu J, Zhang X, Nothnick WB, Spencer TE. Matrix metalloproteinases and their tissue inhibitors in the developing neonatal mouse uterus. Biol Reprod 2004; 71:1598-1604.

248. Sage EH. Regulation of interactions between cells and extracellular matrix: a command performance on several stages. J Clin Invest 2001; 107:781-783.

249. Hynes RO. The extracellular matrix: not just pretty fibrils. Science 2009; 326:1216-1219.

250. Zode GS, Sethi A, Brun-Zinkernagel AM, Chang IF, Clark AF, et al. Transforming growth factor-beta2 increases extracellular matrix proteins in optic

nerve head cells via activation of the Smad signaling pathway. Mol Vis 2011; 17:1745-1758.

251. Busnadiego O, Gonzalez-Santamaria J, Lagares D, Guinea-Viniegra J, Pichol-Thievend C, et al. LOXL4 is induced by transforming growth factor beta1 through Smad and JunB/Fra2 and contributes to vascular matrix remodeling. Mol Cell Biol 2013; 33:2388-2401.

252. Hedin U, Roy J, Tran PK, Lundmark K, Rahman A. Control of smooth muscle cell proliferation--the role of the basement membrane. Thromb Haemost 1999; 82 Suppl 1:23-26.

253. Thyberg J, Hedin U, Sjolund M, Palmberg L, Bottger BA. Regulation of differentiated properties and proliferation of arterial smooth muscle cells. Arteriosclerosis 1990; 10:966-990.

254. Seki T, Naito I, Oohashi T, Sado Y, Ninomiya Y. Differential expression of type IV collagen isoforms, alpha 5(IV) and alpha 6(IV) chains, in basement membranes surrounding smooth muscle cells. Histochem Cell Biol 1998; 110:359-366.

255. Livak KJ, Schmittgen TD. Analysis of relative gene expression data using real-time quantitative PCR and the 2(-Delta Delta C(T)) Method. Methods 2001; 25:402-408.

256. Dixelius J, Jakobsson L, Genersch E, Bohman S, Ekblom P, et al. Laminin-1 promotes angiogenesis in synergy with fibroblast growth factor by distinct

regulation of the gene and protein expression profile in endothelial cells. J Biol Chem 2004; 279:23766-23772.

257. Nagaraja AK, Andreu-Vieyra C, Franco HL, Ma L, Chen R, et al. Deletion of Dicer in somatic cells of the female reproductive tract causes sterility. Mol Endocrinol 2008; 22:2336-2352.

258. Frank KM, Zhou T, Moreno-Vinasco L, Hollett B, Garcia JG, et al. Host response signature to Staphylococcus aureus alpha-hemolysin implicates pulmonary Th17 response. Infect Immun 2012; 80:3161-3169.

259. Shynlova OP, Oldenhof AD, Liu M, Langille L, Lye SJ. Regulation of c-fos expression by static stretch in rat myometrial smooth muscle cells. Am J Obstet Gynecol 2002; 186:1358-1365.

260. Daikoku T, Tranguch S, Friedman DB, Das SK, Smith DF, et al. Proteomic analysis identifies immunophilin FK506 binding protein 4 (FKBP52) as a downstream target of Hoxa10 in the periimplantation mouse uterus. Mol Endocrinol 2005; 19:683-697.

261. Chen L, Belton RJ, Jr., Nowak RA. Basigin-mediated gene expression changes in mouse uterine stromal cells during implantation. Endocrinology 2009; 150:966-976.

262. Lee M, Rodansky ES, Smith JK, Rodgers GM. ADAMTS13 promotes angiogenesis and modulates VEGF-induced angiogenesis. Microvasc Res 2012; 84:109-115.

263. Filant J, Zhou H, Spencer TE. Progesterone inhibits uterine gland development in the neonatal mouse uterus. Biol Reprod 2012; 86:146, 141-149.

264. Sohni A, Mulas F, Ferrazzi F, Luttun A, Bellazzi R, et al. TGFbeta1-induced Baf60c regulates both smooth muscle cell commitment and quiescence. PLoS One 2012; 7:e47629.

265. Deaton RA, Su C, Valencia TG, Grant SR. Transforming growth factor-beta1-induced expression of smooth muscle marker genes involves activation of PKN and p38 MAPK. J Biol Chem 2005; 280:31172-31181.

266. Elberg G, Chen L, Elberg D, Chan MD, Logan CJ, et al. MKL1 mediates TGF-beta1-induced alpha-smooth muscle actin expression in human renal epithelial cells. Am J Physiol Renal Physiol 2008; 294:F1116-1128.

267. Wang Z, Wang DZ, Pipes GC, Olson EN. Myocardin is a master regulator of smooth muscle gene expression. Proc Natl Acad Sci U S A 2003; 100:7129-7134.

268. Schedin P, Keely PJ. Mammary gland ECM remodeling, stiffness, and mechanosignaling in normal development and tumor progression. Cold Spring Harb Perspect Biol 2011; 3:a003228.

269. Lu P, Takai K, Weaver VM, Werb Z. Extracellular matrix degradation and remodeling in development and disease. Cold Spring Harb Perspect Biol 2011; 3:a005058.

270. Luo X, Ding L, Xu J, Chegini N. Gene expression profiling of leiomyoma and myometrial smooth muscle cells in response to transforming growth factor-beta. Endocrinology 2005; 146:1097-1118.

271. Ma C, Chegini N. Regulation of matrix metalloproteinases (MMPs) and their tissue inhibitors in human myometrial smooth muscle cells by TGF-beta1. Mol Hum Reprod 1999; 5:950-954.

272. Schwenke M, Knofler M, Velicky P, Weimar CH, Kruse M, et al. Control of human endometrial stromal cell motility by PDGF-BB, HB-EGF and trophoblast-secreted factors. PLoS One 2013; 8:e54336.

273. Hughes AD, Clunn GF, Refson J, Demoliou-Mason C. Platelet-derived growth factor (PDGF): actions and mechanisms in vascular smooth muscle. Gen Pharmacol 1996; 27:1079-1089.

274. Edson MA, Nagaraja AK, Matzuk MM. The mammalian ovary from genesis to revelation. Endocr Rev 2009; 30:624-712.

275. Green AR, Styles JA, Parrott EL, Gray D, Edwards RE, et al. Neonatal tamoxifen treatment of mice leads to adenomyosis but not uterine cancer. Exp Toxicol Pathol 2005; 56:255-263.

276. Grainger DJ, Metcalfe JC, Grace AA, Mosedale DE. Transforming growth factor-beta dynamically regulates vascular smooth muscle differentiation in vivo. J Cell Sci 1998; 111 ( Pt 19):2977-2988.

277. Darby I, Skalli O, Gabbiani G. Alpha-smooth muscle actinis transiently expressed by myofibroblasts during experimental wound-healing. Lab Invest 1990; 63:21-29.

278. Qian J, Kumar A, Szucsik JC, Lessard JL. Tissue and developmental specific expression of murine smooth muscle gamma-actin fusion genes in transgenic mice. Dev Dyn 1996; 207:135-144.

279. Zhang JC, Kim S, Helmke BP, Yu WW, Du KL, et al. Analysis of SM22alpha-deficient mice reveals unanticipated insights into smooth muscle cell differentiation and function. Mol Cell Biol 2001; 21:1336-1344.

280. Xiao Q, Zeng L, Zhang Z, Hu Y, Xu Q. Stem cell-derived Sca-1+ progenitors differentiate into smooth muscle cells, which is mediated by collagen IV-integrin alpha1/beta1/alphav and PDGF receptor pathways. Am J Physiol Cell Physiol 2007; 292:C342-352.

281. Suzuki S, Narita Y, Yamawaki A, Murase Y, Satake M, et al. Effects of extracellular matrix on differentiation of human bone marrow-derived mesenchymal stem cells into smooth muscle cell lineage: utility for cardiovascular tissue engineering. Cells Tissues Organs 2010; 191:269-280.

282. Thyberg J, Hultgardh-Nilsson A. Fibronectin and the basement membrane components laminin and collagen type IV influence the phenotypic properties of subcultured rat aortic smooth muscle cells differently. Cell Tissue Res 1994; 276:263-271.

283. Costello I, Biondi CA, Taylor JM, Bikoff EK, Robertson EJ. Smad4-dependent pathways control basement membrane deposition and endodermal cell migration at early stages of mouse development. BMC Dev Biol 2009; 9:54.

284. Nishinaka K, Fukuda Y. Changes in extracellular matrix materials in the uterine myometrium of rats during pregnancy and postparturition. Acta Pathol Jpn 1991; 41:122-132.

285. Battegay EJ, Raines EW, Seifert RA, Bowen-Pope DF, Ross R. TGF-beta induces bimodal proliferation of connective tissue cells via complex control of an autocrine PDGF loop. Cell 1990; 63:515-524.

286. Marx M, Perlmutter RA, Madri JA. Modulation of platelet-derived growth factor receptor expression in microvascular endothelial cells during in vitro angiogenesis. J Clin Invest 1994; 93:131-139.

287. Gaengel K, Genove G, Armulik A, Betsholtz C. Endothelial-mural cell signaling in vascular development and angiogenesis. Arterioscler Thromb Vasc Biol 2009; 29:630-638.

288. Gao Y, Duran S, Lydon JP, DeMayo FJ, Burghardt RC, et al. Constitutive activation of transforming growth factor Beta receptor 1 in the mouse uterus impairs uterine morphology and function. Biol Reprod 2015; 92:34.

289. Massague J. How cells read TGF-beta signals. Nat Rev Mol Cell Biol 2000; 1:169-178.

290. Attisano L, Wrana JL. Signal transduction by the TGF-beta superfamily. Science 2002; 296:1646-1647.

291. Derynck R, Zhang YE. Smad-dependent and Smad-independent pathways in TGF-beta family signalling. Nature 2003; 425:577-584.

292. Yan X, Liu Z, Chen Y. Regulation of TGF-beta signaling by Smad7. Acta Biochim Biophys Sin (Shanghai) 2009; 41:263-272.

293. Yan X, Chen YG. Smad7: not only a regulator, but also a cross-talk mediator of TGF-beta signalling. Biochem J 2011; 434:1-10.

294. Schmierer B, Hill CS. TGFbeta-SMAD signal transduction: molecular specificity and functional flexibility. Nat Rev Mol Cell Biol 2007; 8:970-982.

295. Alcaraz LB, Exposito JY, Chuvin N, Pommier RM, Cluzel C, et al. Tenascin-X promotes epithelial-to-mesenchymal transition by activating latent TGF-beta. J Cell Biol 2014; 205:409-428.

296. Neptune ER, Frischmeyer PA, Arking DE, Myers L, Bunton TE, et al. Dysregulation of TGF-beta activation contributes to pathogenesis in Marfan syndrome. Nat Genet 2003; 33:407-411.

297. Huang XR, Chung AC, Wang XJ, Lai KN, Lan HY. Mice overexpressing latent TGF-beta1 are protected against renal fibrosis in obstructive kidney disease. Am J Physiol Renal Physiol 2008; 295:F118-127.

298. Massague J. TGFbeta in Cancer. Cell 2008; 134:215-230.

299. Soyal SM, Mukherjee A, Lee KYS, Li J, Li HG, et al. Cre-mediated recombination in cell lineages that express the progesterone receptor. Genesis 2005; 41:58-66.

300. Bartholin L, Cyprian FS, Vincent D, Garcia CN, Martel S, et al. Generation of mice with conditionally activated transforming growth factor beta signaling through the TbetaRI/ALK5 receptor. Genesis 2008; 46:724-731.

301. Charng MJ, Frenkel PA, Lin Q, Yamada M, Schwartz RJ, et al. A constitutive mutation of ALK5 disrupts cardiac looping and morphogenesis in mice. Dev Biol 1998; 199:72-79.

302. Soriano P. Generalized lacZ expression with the ROSA26 Cre reporter strain. Nat Genet 1999; 21:70-71.

303. Large MJ, Wetendorf M, Lanz RB, Hartig SM, Creighton CJ, et al. The epidermal growth factor receptor critically regulates endometrial function during early pregnancy. PLoS Genet 2014; 10:e1004451.

304. Vincent DF, Kaniewski B, Powers SE, Havenar-Daughton C, Marie JC, et al. A rapid strategy to detect the recombined allele in LSL-TbetaRICA transgenic mice. Genesis 2010; 48:559-562.

305. Truett GE, Heeger P, Mynatt RL, Truett AA, Walker JA, et al. Preparation of PCR-quality mouse genomic DNA with hot sodium hydroxide and tris (HotSHOT). Biotechniques 2000; 29:52, 54.

306. Monga M, Ku CY, Dodge K, Sanborn BM. Oxytocin-stimulated responses in a pregnant human immortalized myometrial cell line. Biol Reprod 1996; 55:427-432.

307. Burghardt RC, Barhoumi R, Stickney M, Monga M, Ku CY, et al. Correlation between connexin43 expression, cell-cell communication, and oxytocin-induced

Ca2+ responses in an immortalized human myometrial cell line. Biol Reprod 1996; 55:433-438.

308. Kim PY, Zhong M, Kim YS, Sanborn BM, Allen KG. Long chain polyunsaturated fatty acids alter oxytocin signaling and receptor density in cultured pregnant human myometrial smooth muscle cells. PLoS One 2012; 7:e41708.

309. Popova AP, Bozyk PD, Goldsmith AM, Linn MJ, Lei J, et al. Autocrine production of TGF-beta1 promotes myofibroblastic differentiation of neonatal lung mesenchymal stem cells. Am J Physiol Lung Cell Mol Physiol 2010; 298:L735-743.

310. Lamouille S, Connolly E, Smyth JW, Akhurst RJ, Derynck R. TGF-beta-induced activation of mTOR complex 2 drives epithelial-mesenchymal transition and cell invasion. J Cell Sci 2012; 125:1259-1273.

311. Spandidos A, Wang X, Wang H, Seed B. PrimerBank: a resource of human and mouse PCR primer pairs for gene expression detection and quantification. Nucleic Acids Res 2010; 38:D792-799.

312. Ismail PM, Li J, DeMayo FJ, O'Malley BW, Lydon JP. A novel LacZ reporter mouse reveals complex regulation of the progesterone receptor promoter during mammary gland development. Mol Endocrinol 2002; 16:2475-2489.

313. Lee K, Jeong J, Kwak I, Yu CT, Lanske B, et al. Indian hedgehog is a major mediator of progesterone signaling in the mouse uterus. Nat Genet 2006; 38:1204-1209.

314. Filant J, DeMayo FJ, Pru JK, Lydon JP, Spencer TE. Fibroblast growth factor receptor two (FGFR2) regulates uterine epithelial integrity and fertility in mice. Biol Reprod 2014; 90:7.

315. Gray CA, Bartol FF, Tarleton BJ, Wiley AA, Johnson GA, et al. Developmental biology of uterine glands. Biol Reprod 2001; 65:1311-1323.

316. Plapinger L. Morphological effects of diethylstilbestrol on neonatal mouse uterus and vagina. Cancer Res 1981; 41:4667-4677.

317. Hayashi K, Yoshioka S, Reardon SN, Rucker EB, 3rd, Spencer TE, et al. WNTs in the neonatal mouse uterus: potential regulation of endometrial gland development. Biol Reprod 2011; 84:308-319.

318. Margadant C, Sonnenberg A. Integrin-TGF-beta crosstalk in fibrosis, cancer and wound healing. EMBO Rep 2010; 11:97-105.

319. Branton MH, Kopp JB. TGF-beta and fibrosis. Microbes Infect 1999; 1:1349-1365.

320. Lipson KE, Wong C, Teng Y, Spong S. CTGF is a central mediator of tissue remodeling and fibrosis and its inhibition can reverse the process of fibrosis. Fibrogenesis Tissue Repair 2012; 5:S24.

321. Cutroneo KR. TGF-beta-induced fibrosis and SMAD signaling: oligo decoys as natural therapeutics for inhibition of tissue fibrosis and scarring. Wound Repair Regen 2007; 15 Suppl 1:S54-60.

322. Pangas SA, Li X, Robertson EJ, Matzuk MM. Premature luteinization and cumulus cell defects in ovarian-specific Smad4 knockout mice. Mol Endocrinol 2006; 20:1406-1422.

323. Pangas SA, Jorgez CJ, Tran M, Agno J, Li X, et al. Intraovarian activins are required for female fertility. Mol Endocrinol 2007; 21:2458-2471.

324. Li X, Tripurani SK, James R, Pangas SA. Minimal fertility defects in mice deficient in oocyte-expressed Smad4. Biol Reprod 2012; 86:1-6.

325. Massague J. TGFbeta signalling in context. Nat Rev Mol Cell Biol 2012; 13:616-630.

326. Estrada KD, Wang W, Retting KN, Chien CT, Elkhoury FF, et al. Smad7 regulates terminal maturation of chondrocytes in the growth plate. Dev Biol 2013; 382:375-384.

327. Sonnylal S, Denton CP, Zheng B, Keene DR, He R, et al. Postnatal induction of transforming growth factor beta signaling in fibroblasts of mice recapitulates clinical, histologic, and biochemical features of scleroderma. Arthritis Rheum 2007; 56:334-344.

328. Hall BE, Zheng C, Swaim WD, Cho A, Nagineni CN, et al. Conditional overexpression of TGF-beta1 disrupts mouse salivary gland development and function. Lab Invest 2010; 90:543-555.

329. Verdi J, Tan A, Shoae-Hassani A, Seifalian AM. Endometrial stem cells in regenerative medicine. J Biol Eng 2014; 8:20.

330. Mao X, Debenedittis P, Sun Y, Chen J, Yuan K, et al. Vascular smooth muscle cell Smad4 gene is important for mouse vascular development. Arterioscler Thromb Vasc Biol 2012; 32:2171-2177.

331. Kurpinski K, Lam H, Chu J, Wang A, Kim A, et al. Transforming growth factor-beta and notch signaling mediate stem cell differentiation into smooth muscle cells. Stem Cells 2010; 28:734-742.

332. Morelli SS, Yi P, Goldsmith LT. Endometrial stem cells and reproduction. Obstet Gynecol Int 2012; 2012:851367.

333. Harris WT, Kelly DR, Zhou Y, Wang D, MacEwen M, et al. Myofibroblast differentiation and enhanced TGF-B signaling in cystic fibrosis lung disease. PLoS One 2013; 8:e70196.

334. Hinz B. Formation and function of the myofibroblast during tissue repair. J Invest Dermatol 2007; 127:526-537.

335. Hu B, Phan SH. Myofibroblasts. Curr Opin Rheumatol 2013; 25:71-77.

336. Velasquez LS, Sutherland LB, Liu Z, Grinnell F, Kamm KE, et al. Activation of MRTF-A-dependent gene expression with a small molecule promotes myofibroblast differentiation and wound healing. Proc Natl Acad Sci U S A 2013; 110:16850-16855.

337. Oliver C, Montes MJ, Galindo JA, Ruiz C, Olivares EG. Human decidual stromal cells express alpha-smooth muscle actin and show ultrastructural similarities with myofibroblasts. Hum Reprod 1999; 14:1599-1605.

338. Scharenberg MA, Pippenger BE, Sack R, Zingg D, Ferralli J, et al. TGF-beta-induced differentiation into myofibroblasts involves specific regulation of two MKL1 isoforms. J Cell Sci 2014; 127:1079-1091.

339. Sone M, Oyama K, Mohri Y, Hayashi R, Clevers H, et al. LGR4 expressed in uterine epithelium is necessary for uterine gland development and contributes to decidualization in mice. FASEB J 2013; 27:4917-4928.

340. Hong JH, Song C, Shin Y, Kim H, Cho SP, et al. Estrogen induction of smooth muscle differentiation of human prostatic stromal cells is mediated by transforming growth factor-beta. J Urol 2004; 171:1965-1969.

341. Gantus MA, Alves LM, Stipursky J, Souza EC, Teodoro AJ, et al. Estradiol modulates TGF-beta1 expression and its signaling pathway in thyroid stromal cells. Mol Cell Endocrinol 2011; 337:71-79.

342. Kipp JL, Kilen SM, Bristol-Gould S, Woodruff TK, Mayo KE. Neonatal exposure to estrogens suppresses activin expression and signaling in the mouse ovary. Endocrinology 2007; 148:1968-1976.

343. Wira CR, Rossoll RM. Oestradiol regulation of antigen presentation by uterine stromal cells: role of transforming growth factor-beta production by epithelial cells in mediating antigen-presenting cell function. Immunology 2003; 109:398-406.

344. Akhmetshina A, Palumbo K, Dees C, Bergmann C, Venalis P, et al. Activation of canonical Wnt signalling is required for TGF-beta-mediated fibrosis. Nat Commun 2012; 3:735.

345. Setiawan VW, Yang HP, Pike MC, McCann SE, Yu H, et al. Type I and II endometrial cancers: have they different risk factors? J Clin Oncol 2013; 31:2607-2618.

346. Gao Y, Lin P, Lydon JP, Li Q. Conditional abrogation of Transforming Growth Factor Beta Receptor 1 in PTEN-inactivated endometrium promotes endometrial cancer progression in mice. J Pathol 2017; 10.1002/path.4930.

347. Engelman JA. Targeting PI3K signalling in cancer: opportunities, challenges and limitations. Nat Rev Cancer 2009; 9:550-562.

348. Podsypanina K, Ellenson LH, Nemes A, Gu J, Tamura M, et al. Mutation of Pten/Mmac1 in mice causes neoplasia in multiple organ systems. Proc Natl Acad Sci U S A 1999; 96:1563-1568.

349. Daikoku T, Hirota Y, Tranguch S, Joshi AR, DeMayo FJ, et al. Conditional loss of uterine Pten unfailingly and rapidly induces endometrial cancer in mice. Cancer Res 2008; 68:5619-5627.

350. Nguyen DX, Bos PD, Massague J. Metastasis: from dissemination to organ-specific colonization. Nat Rev Cancer 2009; 9:274-284.

351. Pecorelli S. Revised FIGO staging for carcinoma of the vulva, cervix, and endometrium. Int J Gynaecol Obstet 2009; 105:103-104.

352. Larson DM, Connor GP, Broste SK, Krawisz BR, Johnson KK. Prognostic significance of gross myometrial invasion with endometrial cancer. Obstet Gynecol 1996; 88:394-398.

353. Sohaib SA, Houghton SL, Meroni R, Rockall AG, Blake P, et al. Recurrent endometrial cancer: patterns of recurrent disease and assessment of prognosis. Clin Radiol 2007; 62:28-34; discussion 35-26.

354. Kurra V, Krajewski KM, Jagannathan J, Giardino A, Berlin S, et al. Typical and atypical metastatic sites of recurrent endometrial carcinoma. Cancer Imaging 2013; 13:113-122.

355. Bogenrieder T, Herlyn M. Axis of evil: molecular mechanisms of cancer metastasis. Oncogene 2003; 22:6524-6536.

356. Sarvaiya PJ, Guo D, Ulasov I, Gabikian P, Lesniak MS. Chemokines in tumor progression and metastasis. Oncotarget 2013; 4:2171-2185.

357. Galdiero MR, Bonavita E, Barajon I, Garlanda C, Mantovani A, et al. Tumor associated macrophages and neutrophils in cancer. Immunobiology 2013; 218:1402-1410.

358. Lindberg ME, Stodden GR, King ML, MacLean JA, 2nd, Mann JL, et al. Loss of CDH1 and Pten accelerates cellular invasiveness and angiogenesis in the mouse uterus. Biol Reprod 2013; 89:8.

359. Gordon KJ, Blobe GC. Role of transforming growth factor-beta superfamily signaling pathways in human disease. Biochim Biophys Acta 2008; 1782:197-228.

360. Anzai Y, Gong Y, Holinka CF, Murphy LJ, Murphy LC, et al. Effects of transforming growth factors and regulation of their mRNA levels in two human

endometrial adenocarcinoma cell lines. J Steroid Biochem Mol Biol 1992; 42:449-455.

361. Van Themsche C, Mathieu I, Parent S, Asselin E. Transforming growth factor-beta3 increases the invasiveness of endometrial carcinoma cells through phosphatidylinositol 3-kinase-dependent up-regulation of X-linked inhibitor of apoptosis and protein kinase c-dependent induction of matrix metalloproteinase-9. J Biol Chem 2007; 282:4794-4802.

362. Lei X, Wang L, Yang J, Sun LZ. TGFbeta signaling supports survival and metastasis of endometrial cancer cells. Cancer Manag Res 2009; 2009:15-24.

363. Lesche R, Groszer M, Gao J, Wang Y, Messing A, et al. Cre/loxP-mediated inactivation of the murine Pten tumor suppressor gene. Genesis 2002; 32:148-149.

364. Gao Y, Vincent DF, Davis AJ, Sansom OJ, Bartholin L, et al. Constitutively active transforming growth factor beta receptor 1 in the mouse ovary promotes tumorigenesis. Oncotarget 2016; 7:40904-40918.

365. Horm TM, Schroeder JA. MUC1 and metastatic cancer: expression, function and therapeutic targeting. Cell Adh Migr 2013; 7:187-198.

366. Lazennec G, Richmond A. Chemokines and chemokine receptors: new insights into cancer-related inflammation. Trends Mol Med 2010; 16:133-144.

367. Hembruff SL, Jokar I, Yang L, Cheng N. Loss of transforming growth factor-beta signaling in mammary fibroblasts enhances CCL2 secretion to promote

mammary tumor progression through macrophage-dependent and -independent mechanisms. Neoplasia 2010; 12:425-433.

368. Yang L, Huang J, Ren X, Gorska AE, Chytil A, et al. Abrogation of TGF beta signaling in mammary carcinomas recruits Gr-1+CD11b+ myeloid cells that promote metastasis. Cancer Cell 2008; 13:23-35.

369. Novitskiy SV, Pickup MW, Gorska AE, Owens P, Chytil A, et al. TGF-beta receptor II loss promotes mammary carcinoma progression by Th17 dependent mechanisms. Cancer Discov 2011; 1:430-441.

370. Yan HH, Jiang J, Pang Y, Achyut BR, Lizardo M, et al. CCL9 Induced by TGFbeta Signaling in Myeloid Cells Enhances Tumor Cell Survival in the Premetastatic Organ. Cancer Res 2015; 75:5283-5298.

371. Sica A, Invernizzi P, Mantovani A. Macrophage plasticity and polarization in liver homeostasis and pathology. Hepatology 2014; 59:2034-2042.

372. Komohara Y, Niino D, Saito Y, Ohnishi K, Horlad H, et al. Clinical significance of CD163(+) tumor-associated macrophages in patients with adult T-cell leukemia/lymphoma. Cancer Sci 2013; 104:945-951.

373. Austyn JM, Gordon S. F4/80, a monoclonal antibody directed specifically against the mouse macrophage. Eur J Immunol 1981; 11:805-815.

374. de Caestecker MP, Piek E, Roberts AB. Role of transforming growth factor-beta signaling in cancer. J Natl Cancer Inst 2000; 92:1388-1402.

375. Gold LI, Parekh TV. Loss of growth regulation by transforming growth factor-beta (TGF-beta) in human cancers: studies on endometrial carcinoma. Semin Reprod Endocrinol 1999; 17:73-92.

376. Tashiro H, Blazes MS, Wu R, Cho KR, Bose S, et al. Mutations in PTEN are frequent in endometrial carcinoma but rare in other common gynecological malignancies. Cancer Res 1997; 57:3935-3940.

377. Kim TH, Yoo JY, Kim HI, Gilbert J, Ku BJ, et al. Mig-6 suppresses endometrial cancer associated with Pten deficiency and ERK activation. Cancer Res 2014; 74:7371-7382.

378. Kim TH, Franco HL, Jung SY, Qin J, Broaddus RR, et al. The synergistic effect of Mig-6 and Pten ablation on endometrial cancer development and progression. Oncogene 2010; 29:3770-3780.

379. Xu X, Ehdaie B, Ohara N, Yoshino T, Deng CX. Synergistic action of Smad4 and Pten in suppressing pancreatic ductal adenocarcinoma formation in mice. Oncogene 2010; 29:674-686.

380. Bian Y, Hall B, Sun ZJ, Molinolo A, Chen W, et al. Loss of TGF-beta signaling and PTEN promotes head and neck squamous cell carcinoma through cellular senescence evasion and cancer-related inflammation. Oncogene 2012; 31:3322-3332.

381. Lecanda J, Parekh TV, Gama P, Lin K, Liarski V, et al. Transforming growth factor-beta, estrogen, and progesterone converge on the regulation of p27Kip1 in the normal and malignant endometrium. Cancer Res 2007; 67:1007-1018.

382. Bierie B, Chung CH, Parker JS, Stover DG, Cheng N, et al. Abrogation of TGF-beta signaling enhances chemokine production and correlates with prognosis in human breast cancer. J Clin Invest 2009; 119:1571-1582.

383. Itatani Y, Kawada K, Fujishita T, Kakizaki F, Hirai H, et al. Loss of SMAD4 from colorectal cancer cells promotes CCL15 expression to recruit CCR1+ myeloid cells and facilitate liver metastasis. Gastroenterology 2013; 145:1064-1075 e1011.

384. Kitamura T, Kometani K, Hashida H, Matsunaga A, Miyoshi H, et al. SMAD4-deficient intestinal tumors recruit CCR1+ myeloid cells that promote invasion. Nat Genet 2007; 39:467-475.

385. Gao Y, Guan Z, Chen J, Xie H, Yang Z, et al. CXCL5/CXCR2 axis promotes bladder cancer cell migration and invasion by activating PI3K/AKT-induced upregulation of MMP2/MMP9. Int J Oncol 2015; 47:690-700.

386. Zhou SL, Dai Z, Zhou ZJ, Wang XY, Yang GH, et al. Overexpression of CXCL5 mediates neutrophil infiltration and indicates poor prognosis for hepatocellular carcinoma. Hepatology 2012; 56:2242-2254.

387. Wong YF, Cheung TH, Lo KW, Yim SF, Siu NS, et al. Identification of molecular markers and signaling pathway in endometrial cancer in Hong Kong Chinese women by genome-wide gene expression profiling. Oncogene 2007; 26:1971-1982.

388. Pena CG, Nakada Y, Saatcioglu HD, Aloisio GM, Cuevas I, et al. LKB1 loss promotes endometrial cancer progression via CCL2-dependent macrophage recruitment. J Clin Invest 2015; 125:4063-4076.

389. Stodden GR, Lindberg ME, King ML, Paquet M, MacLean JA, et al. Loss of Cdh1 and Trp53 in the uterus induces chronic inflammation with modification of tumor microenvironment. Oncogene 2015; 34:2471-2482.

390. Park SO, Lee YJ, Seki T, Hong KH, Fliess N, et al. ALK5- and TGFBR2-independent role of ALK1 in the pathogenesis of hereditary hemorrhagic telangiectasia type 2. Blood 2008; 111:633-642.

391. Zeng N, Yang KT, Bayan JA, He L, Aggarwal R, et al. PTEN controls beta-cell regeneration in aged mice by regulating cell cycle inhibitor p16ink4a. Aging Cell 2013; 12:1000-1011.

392. Li L, Huang LP, Vergis AL, Ye H, Bajwa A, et al. IL-17 produced by neutrophils regulates IFN-gamma-mediated neutrophil migration in mouse kidney ischemia-reperfusion injury. J Clin Invest 2010; 120:331-342.

393. Duchene J, Lecomte F, Ahmed S, Cayla C, Pesquero J, et al. A novel inflammatory pathway involved in leukocyte recruitment: role for the kinin B1 receptor and the chemokine CXCL5. J Immunol 2007; 179:4849-4856.

394. Saur D, Seidler B, Schneider G, Algul H, Beck R, et al. CXCR4 expression increases liver and lung metastasis in a mouse model of pancreatic cancer. Gastroenterology 2005; 129:1237-1250.

## APPENDIX A

## FIGURES

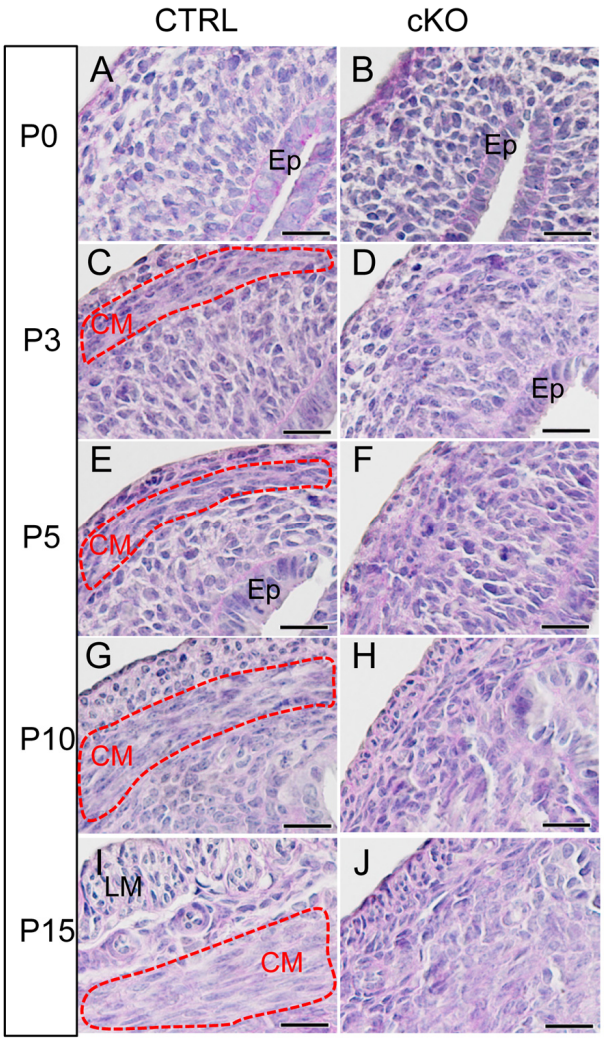


**A-1.** Histological analysis of postnatal myometrial defects in *Tgfbr1* cKO mice. (A-J) PAS-hematoxylin staining of uterine sections at P0 (A and B), P3 (C and D), P5 (E and F), P10 (G and H), and P15 (I and J) from control and *Tgfbr1* cKO mice. Representative images are shown for each time point (n = 3). Red dotted lines indicate the circular smooth muscle layers in the control mice. Note the formation of circular myometrium in the controls during P3-P15, and the disorganized smooth muscle in the *Tgfbr1* cKO mice. CM, circular smooth muscle layer; Ep, epithelium. Scale bar = 20 μm.

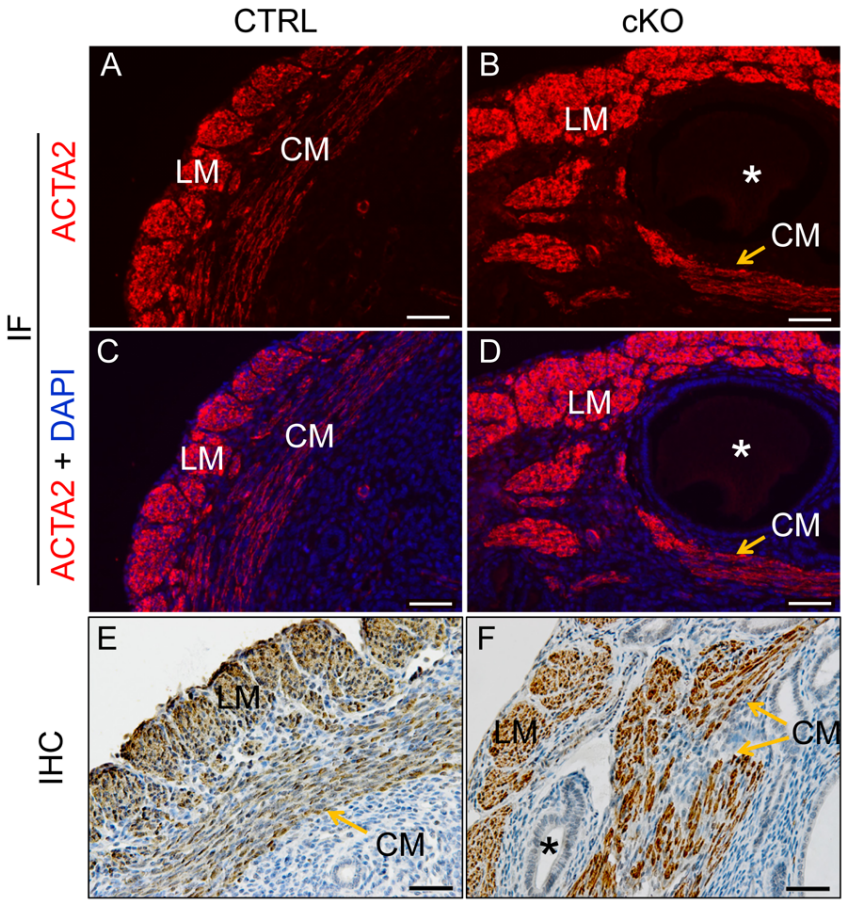


**A-2.** Uterine adenomyosis in *Tgfbr1* cKO mice. (A-D) Immunofluorescence of ACTA2 (Red) in the uteri of a 3-month old control (A and C) and *Tgfbr1* cKO mice (B and D). CM, circular smooth muscle layer; LM, longitudinal smooth muscle layer. (E and F) Immunohistochemical staining of CNN1 (brown staining) in the uteri of 3-month old control (E) and *Tgfbr1* cKO mice (F). The sections were counter stained with hematoxylin. Representative images are shown for each group (n = 3). Note the disrupted myometrium and presence of uterine glands within the muscle layers (denoted by *) in the *Tgfbr1* cKO mice compared with controls in which highly organized myometrium was visualized. Scale bar = 50 μm.

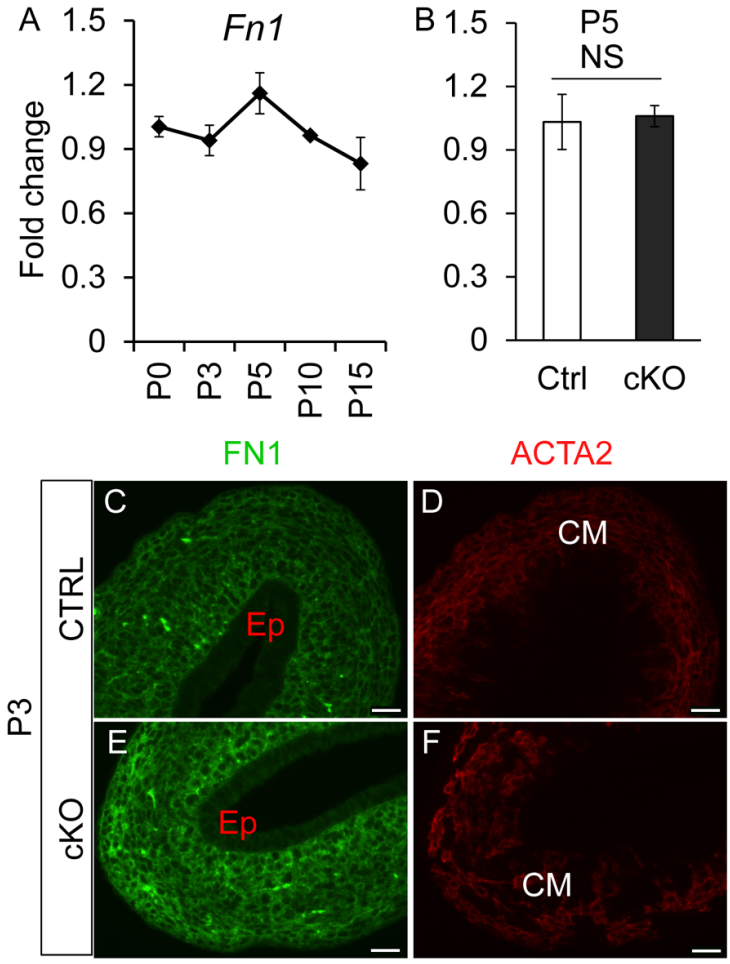


**A-3.** Expression and localization of FN1 in the uteri of control and *Tgfbr1* cKO mice. (A) Transcript levels of *Fn1* in wild type uterus during postnatal uterine development at P0 ($n$ = 5), P3 ($n$ = 4), P5 ($n$ = 3), P10 ($n$ = 4), and P15 ($n$ = 4). (B) Relative levels of mRNA for *Fn1* in the uterus of control and *Tgfbr1* cKO mice at P5 ($n$ = 5 per group). Data are mean ± SEM. NS, no significance. (C-F) Immunofluorescence of FN1 (green) and ACTA2 (red) in the uteri of control (C and D) and *Tgfbr1* cKO (E and F) mice. CM, circular smooth muscle layer; Ep, epithelium. Scale bar = 20 μm.

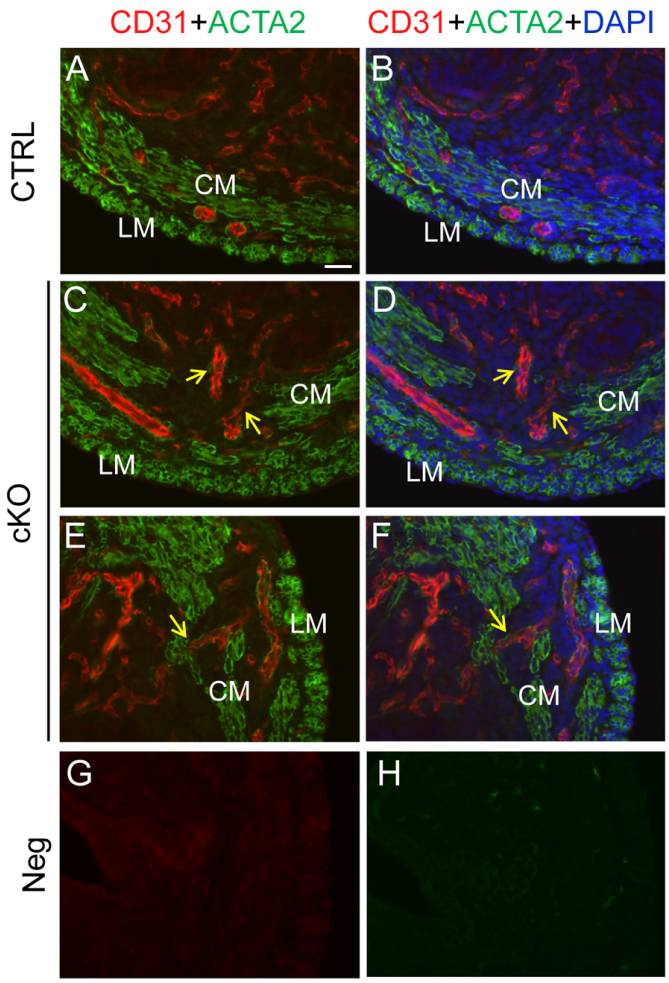


**A-4.** Abnormal distribution of vasculature in *Tgfbr1* cKO uterus at P15. (A and B) Double immunofluorescence of CD31 (Red) and ACTA2 (Green) without (A) or with DAPI (Blue; B). Note that vessels were well organized and mostly distributed between circular and longitudinal muscle layers and within the endometrium on the cross section. (C-F) Double immunofluorescence of CD31 (Red) and ACTA2 (Green) without (C and E) or with DAPI (Blue; D and F). Arrows indicate uterine vessels. Note the presence of vessels inside the disrupted myometrial layers of the *Tgfbr1* cKO uteri. (G and H) Representative negative controls where primary antibodies were replaced with rabbit (G) or mouse (H) IgG. Note no specific staining was detected in the absence of primary antibodies. CM, circular smooth muscle layer; LM, longitudinal smooth muscle layer. Scale bar (20 μm) is representatively depicted in (A).

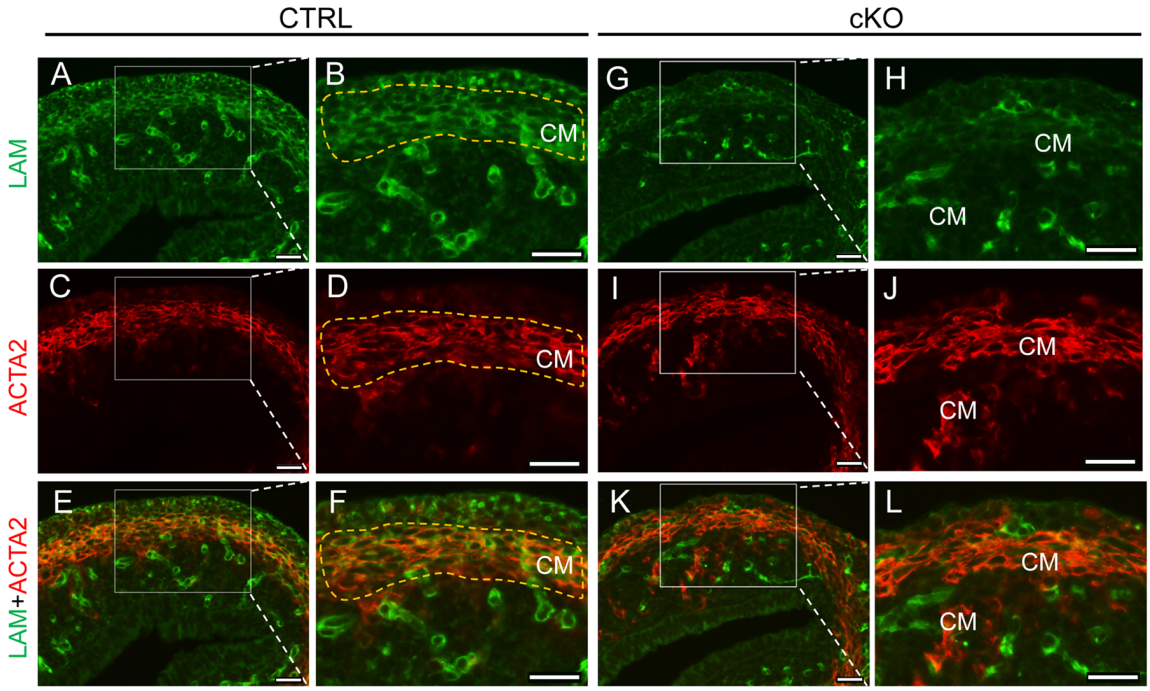


**A-5.** Impaired laminin production by myometrial cells during early uterine development. (A-F) Subcellular localization of laminin (Green; A and B), ACTA2 (Red; C and D), and laminin and ACTA2 (E and F) in the uteri of control mice at P5. (G-L) Subcellular localization of laminin (Green; G and H), ACTA2 (Red; I and J), and laminin and ACTA2 (K and L) in the uteri of *Tgfbr1* cKO mice at P5. Note the lack of typical laminin immunofluorescence signals in the smooth muscle cells of *Tgfbr1* cKO mice (G-L) compared with controls (A-F). Representative images are shown for each group (n = 3). The yellow dotted lines indicate the circular smooth muscle layers developed at P5. CM, circular smooth muscle layer; LAM, laminin. Scale bar = 20 μm.

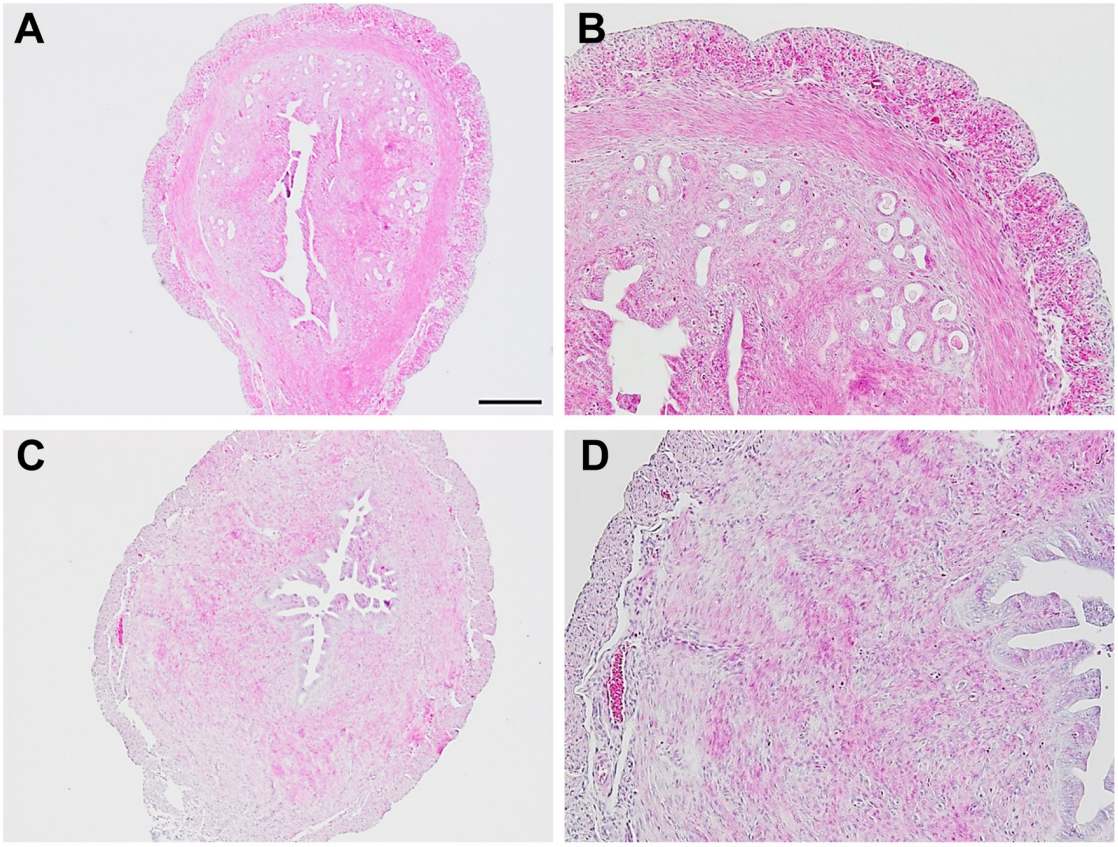


**A-6.** Histology of uterine samples from control and TGFBR1 *Pgr*-Cre CA mice. Uteri from control and TGFBR1$^{CA\ Lox/Lox}$; *Pgr*-Cre mice were stained with hematoxylin and eosin and representative images are shown. Scale bar = 250 μm (A and C) and 100 μm (B and D).

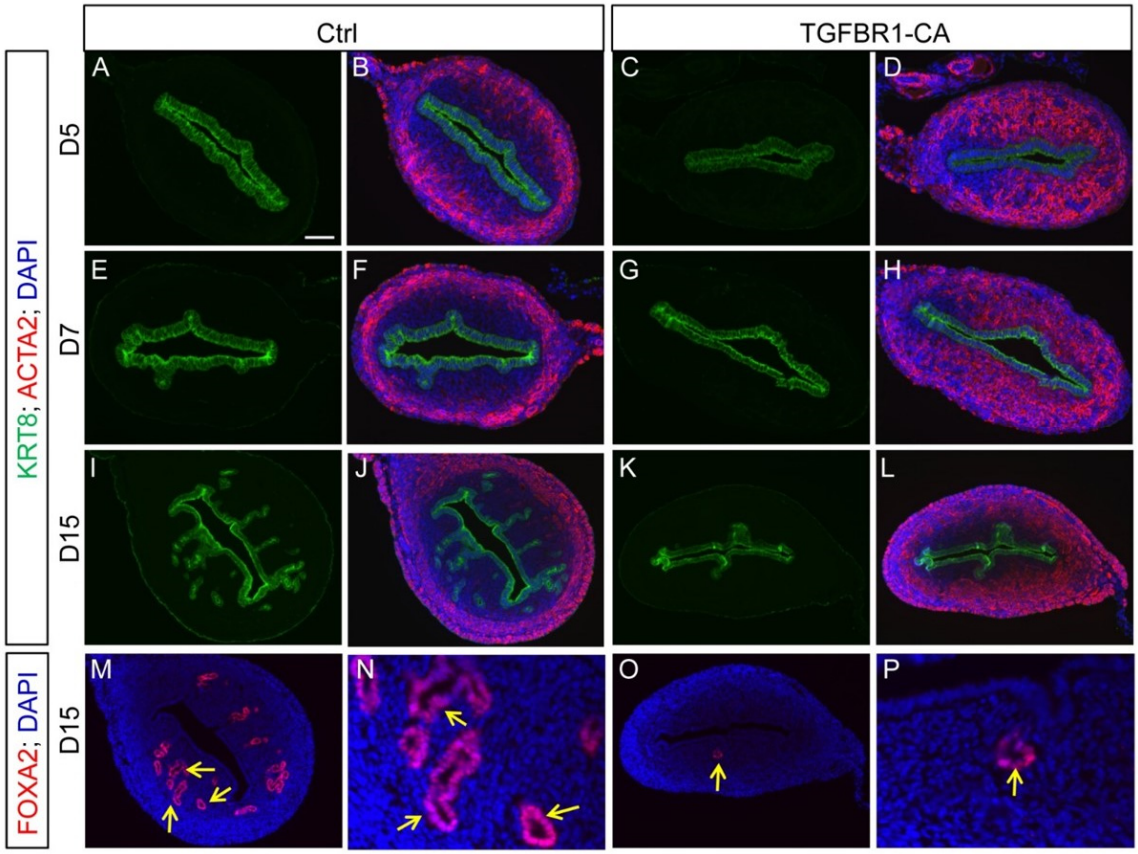


**A-7.** Immunofluorescence analysis of endometrial glandular and stromal alterations during early postnatal uterine development. (A-L) Immunolocalization of cytokeratin 8 (KRT8; green) or KRT8 and smooth muscle actin (ACTA2; red) in the uteri of control (Ctrl) and TGFBR1 *Pgr*-Cre CA mice at postnatal day 5 (PD5; A-D), PD7 (E-H), PD15 (I-L). Note the distinct staining pattern of ACTA2 between Ctrl and TGFBR1 *Pgr*-Cre CA mice, and a reduction of uterine glands marked by KRT8 in the TGFBR1 *Pgr*-Cre CA mice versus Ctrl. (M-P) Immunofluorescence staining of forkhead box A2 (FOXA2; red) in the uteri of Ctrl and TGFBR1 *Pgr*-Cre CA mice at PD15. Yellow arrows (M-P) indicate the localization of FOXA2. DAPI (blue) was used to counterstain the nuclei. Scale bar is representatively shown in (A) and equals 50 μm (A-H), 100 μm (I-M, and O), and 25 μm (N and P).

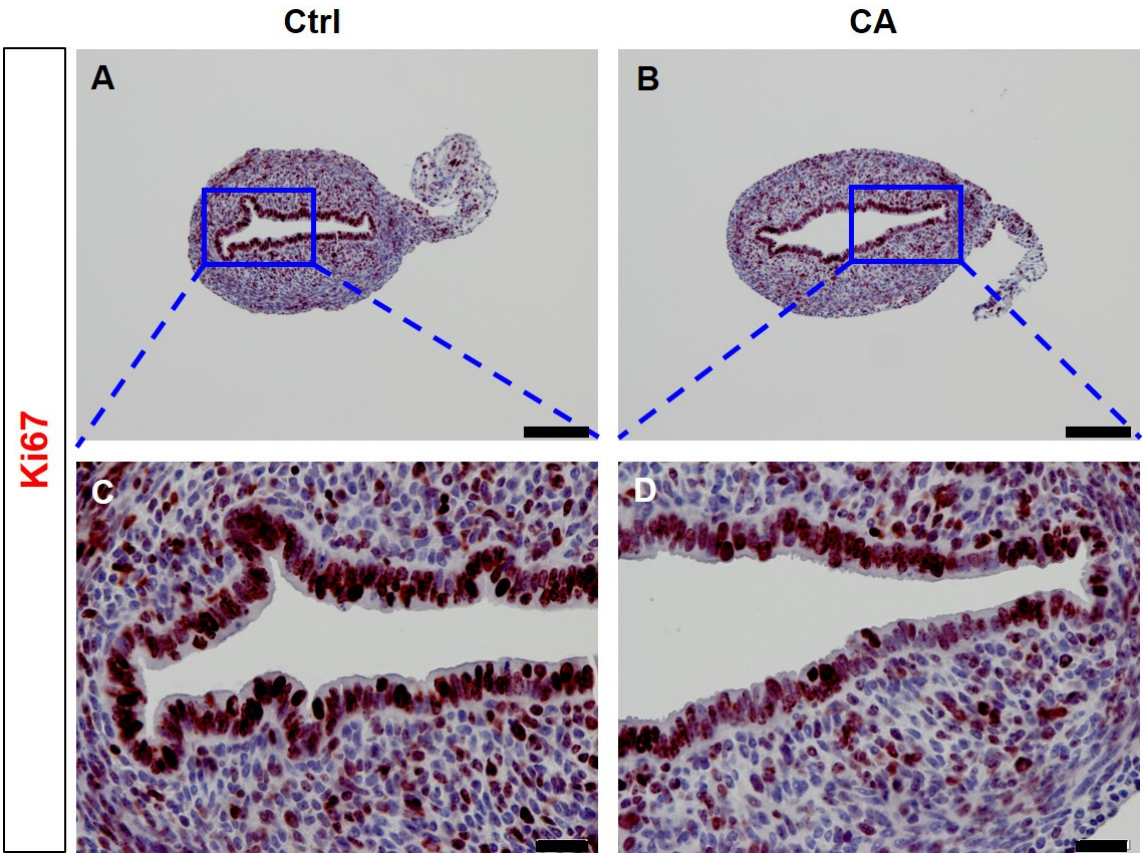


**A-8.** Immunohistochemistry analysis of luminal epithelial cell proliferation at postnatal day 7. (A-D) Immunohistochemistry of ki67 in the uteri of control (Ctrl) and TGFBR1 *Pgr*-Cre CA (CA) mice at postnatal day 7 (D7). Panels (C and D) represent higher magnification images for corresponding panels (A and B). Note the extensive luminal epithelial cell proliferation in both Ctrl and TGFBR1 *Pgr*-Cre CA mice. Scale bar equals 100 µm (A and B), and 20 µm (C and D).

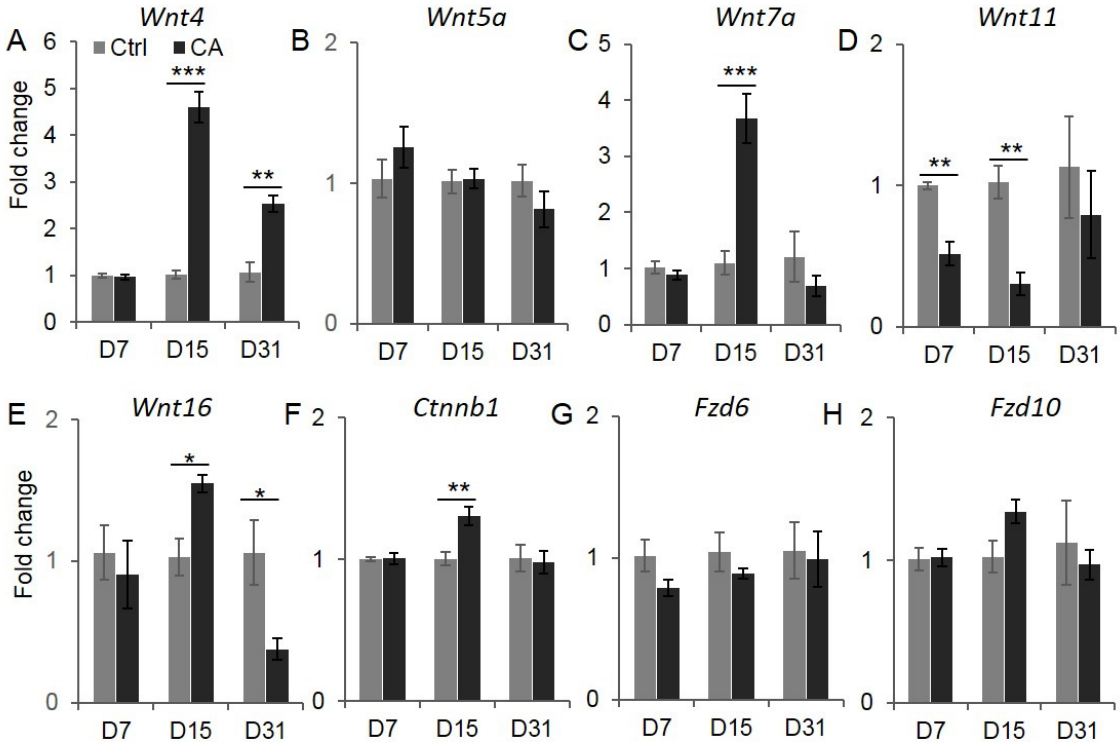


**A-9.** Expression analysis of genes encoding WNT signaling pathway components in TGFBR1 *Pgr*-Cre CA mice. Transcript levels of *Wnt4* (A), *Wnt5a* (B), *Wnt7a*(C), *Wnt11*(D), *Wnt16*(E), catenin beta 1 (*Ctnnb1*) (F), frizzled homolog 6 (*Fzd6*) (G), and Fzd10(H) in the uteri of control and TGFBR1 *Pgr*-Cre CA mice at postnatal day 7 (D7) (n = 4), D15 (n = 5 for control group, n = 4 for TGFBR1 *Pgr*-Cre CA group), D31 (n = 4). Quantitative PCR was performed using ΔΔCT method. *Rpl19* was used as an internal control. Data are means ± S.E.M. **P*<0.05.

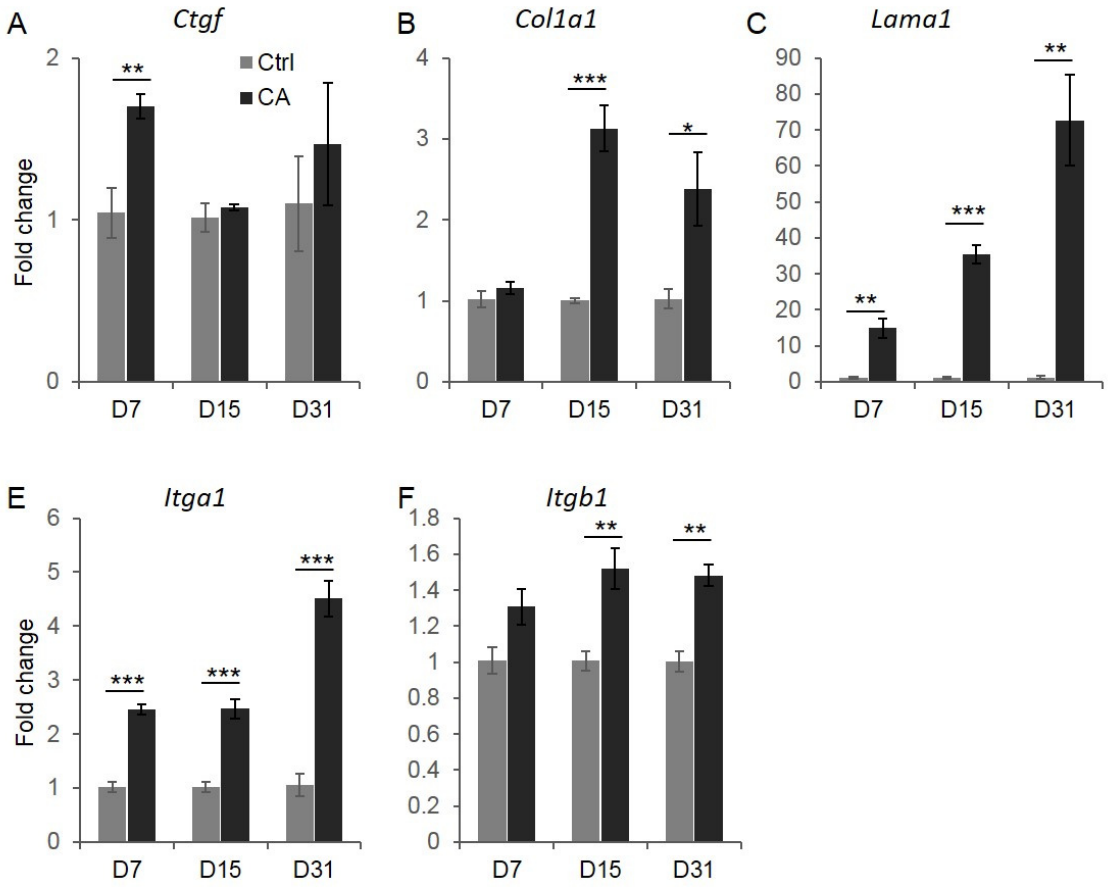


**A-10.** Up-regulation of pro-fibrotic genes in TGFBR1 *Pgr*-Cre CA uteri. Transcript levels of *Ctgf* (A), *Col1a1* (B), *Lama1*(C), *Itga1*(D), and *Itgb1*(E) in the uteri of control and TGFBR1 *Pgr*-Cre CA mice at postnatal day 7 (D7) (n = 4), D15 (n = 5 for control group, n = 4 for TGFBR1 *Pgr*-Cre CA group), D31 (n = 4). Quantitative PCR was performed using ΔΔCT method. *Rpl19* was used as an internal control. Data are means ± S.E.M. **P*<0.05.

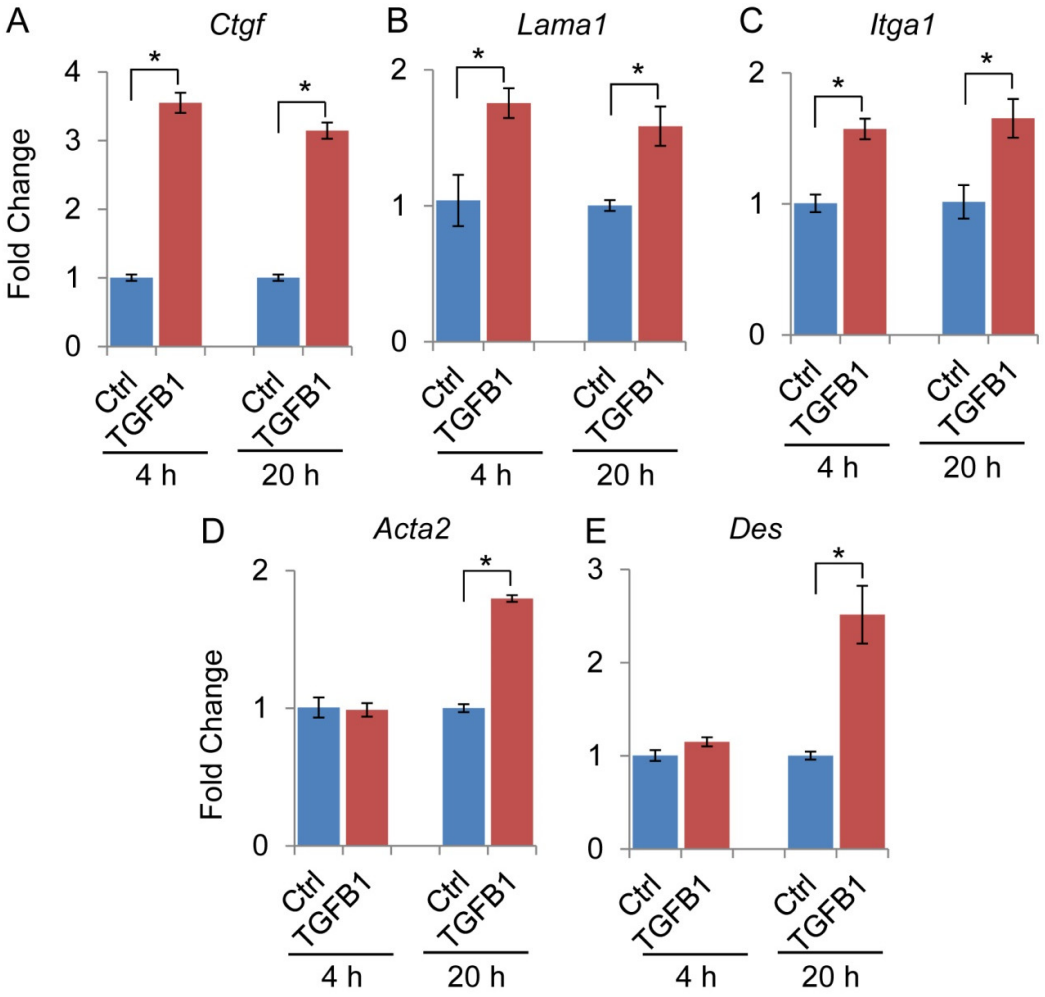


**A-11.** TGFB ligand induces the expression of genes associated with extracellular matrix deposition/function and smooth muscle cell property in uterine stromal cells. (A-E) TGFB1 (5ng/ml) induced mRNA expression of *Ctgf*; (A), *Lama1* (B), *Itga1* (C), *Acta2* (D) and *Des* (E) in uterine stromal cells. Uterine stromal cells were isolated and cultured overnight, serum starved, and treated with TGFB1. Cells were collected after 4h and 20 h of treatment and processed for quantitative PCR analysis using ΔΔCT method. Ribosomal protein L19 (Rpl19) was used as an internal control. Data represent results from three independent experiments. Data are means ± S.E.M. *P<0.05.

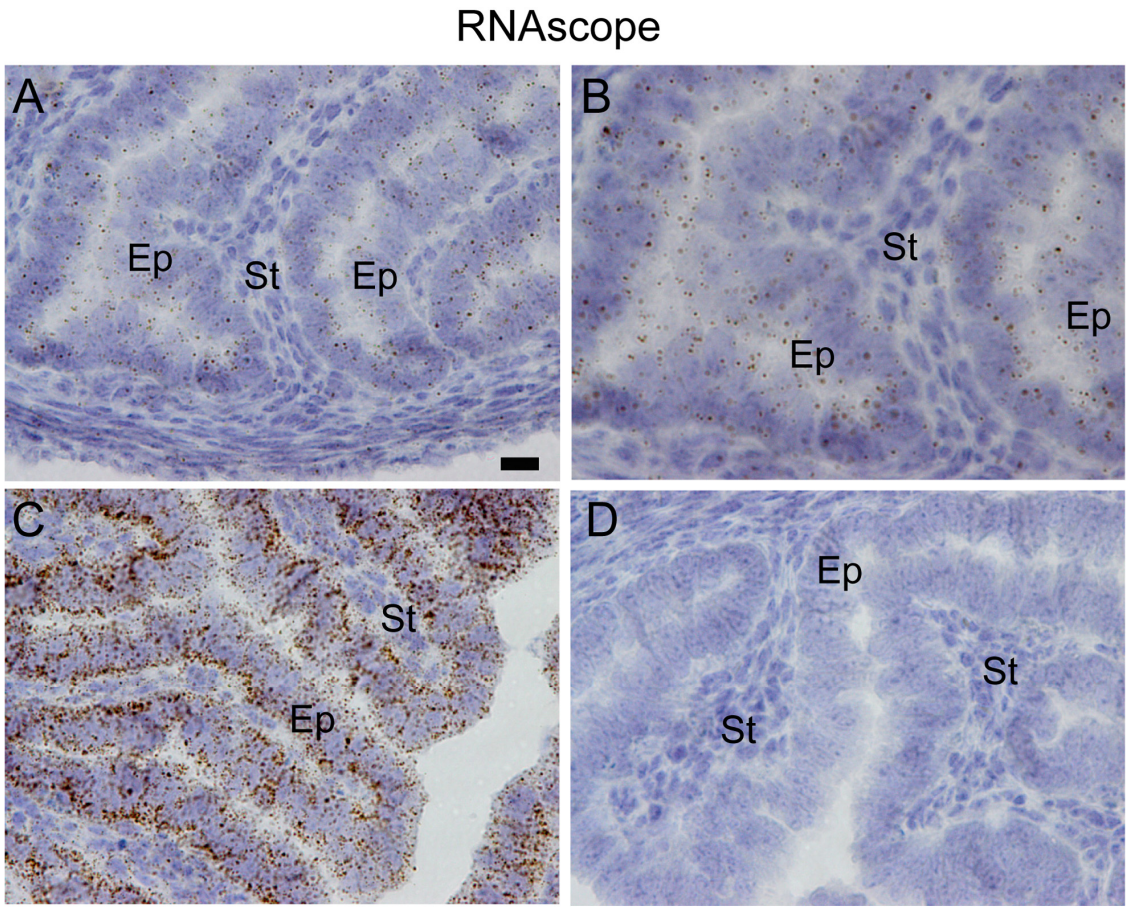


**A-12.** Localization of *Tgfbr1* mRNA expression in *Pten*$^{d/d}$ uteri. (A-D) RNAscope analysis of *Tgfbr1* mRNA localization (A, B) along with positive (C) and negative (D) controls. Panel (B) is a higher magnification image for panel (A). Scale bar is representatively shown in (A) and equals 10 µm (B) and 15 µm (A, C, D). Ep, epithelium; St, stroma.

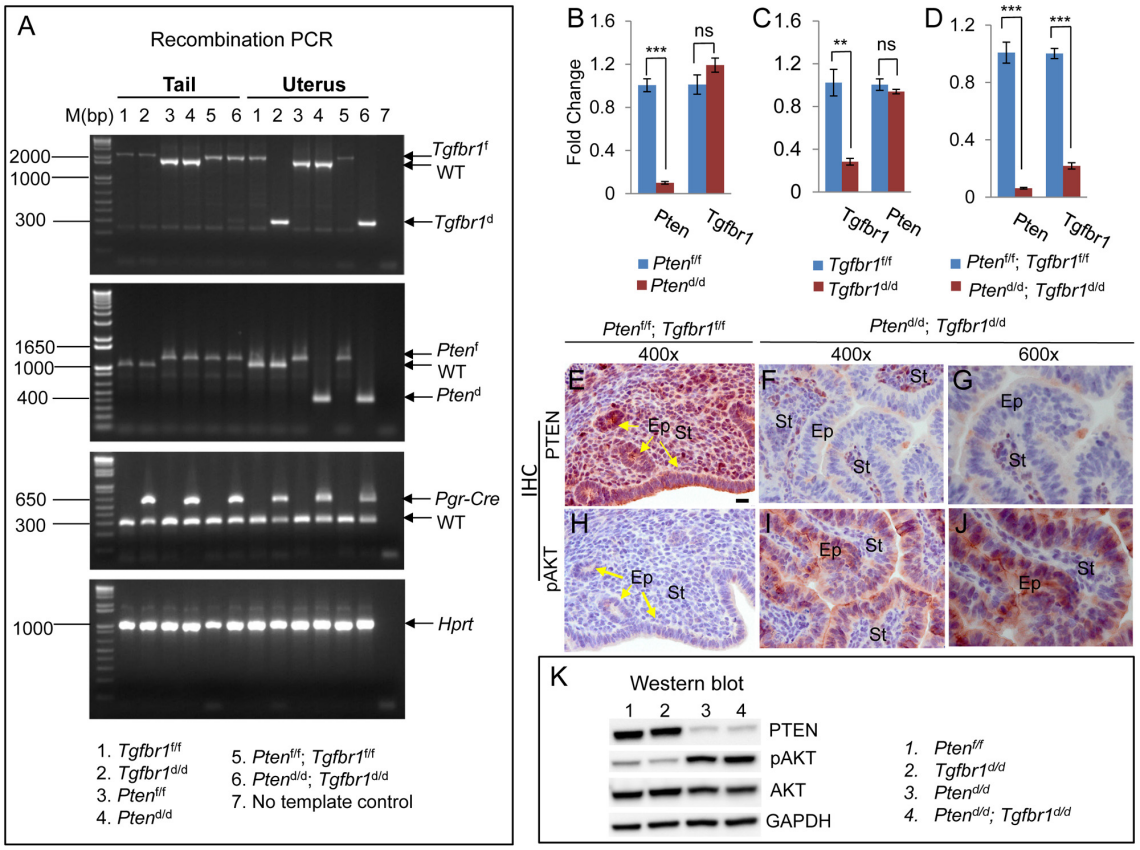


**A-13.** Validation of *Tgfbr1*, *Pten*, and *Tgfbr1/Pten* conditional knockout mice. (A) Analysis of recombination of *Pten/Tgfbr1* conditional alleles using tails and uteri from 9-week-old control, *Pten*$^{d/d}$, *Tgfbr1*$^{d/d}$, and *Pten*$^{d/d}$; *Tgfbr1*$^{d/d}$ mice. (B-D) Reduction of *Pten* and/or *Tgfbr1* mRNA levels in the uteri of 2-week-old *Pten*$^{d/d}$, *Tgfbr1*$^{d/d}$, and *Pten*$^{d/d}$; *Tgfbr1*$^{d/d}$ mice compared with corresponding controls. Quantitative real-time PCR was performed using ΔΔCT method. *Rpl19* was used as internal control. Data are mean ± s.e.m. n = 4. **P < 0.01 and ***P < 0.001. Ns, P ≥ 0.05. (E-K) Reduced expression of PTEN and increased expression of pAKT in *Pten*$^{d/d}$; *Tgfbr1*$^{d/d}$ uteri. Note the reduced signal intensity of PTEN staining, but increased expression of immunoreactive pAKT in the uteri of 2-week-old *Pten*$^{d/d}$; *Tgfbr1*$^{d/d}$ mice using immunohistochemical analysis (E-J). The immunoreactive signals were developed using NovaRED. Immunohistochemistry was performed using independent samples from 3 mice per genotype. Ep, epithelia; St, stroma. Scale bar is representatively depicted in (E) and equals 15 µm (E, F, H, I) and 10 µm (G, J). Results were further verified by western blot using uterine protein lysates (n = 4; K).

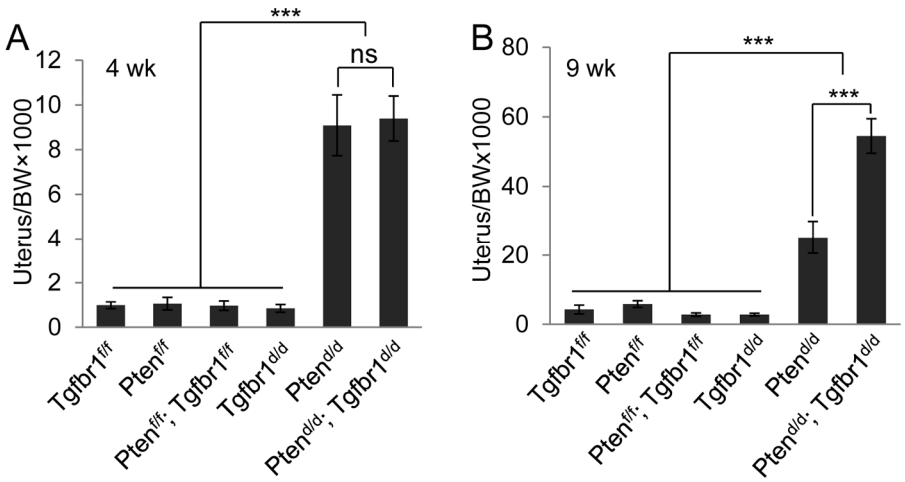


**A-14**. Gross analysis of endometrial cancer development. (A, B) Ratios of the uterus/body weight (BW) in *Tgfbr1*$^{f/f}$, *Pten*$^{f/f}$, *Pten*$^{f/f}$; *Tgfbr1*$^{f/f}$, *Tgfbr1*$^{d/d}$, *Pten*$^{d/d}$, and *Pten*$^{d/d}$; *Tgfbr1*$^{d/d}$ mice at 4 and 9 weeks of age. Note the significantly increased uterus/body weight ratio of *Pten*$^{d/d}$; *Tgfbr1*$^{d/d}$ mice compared with that of *Pten*$^{d/d}$ mice at 9 weeks of age. $n$ = 4-7 for (A) and $n$ = 5 for (B). Data are mean ± s.e.m. $^{***}P < 0.001$. Ns, $P \geq 0.05$.

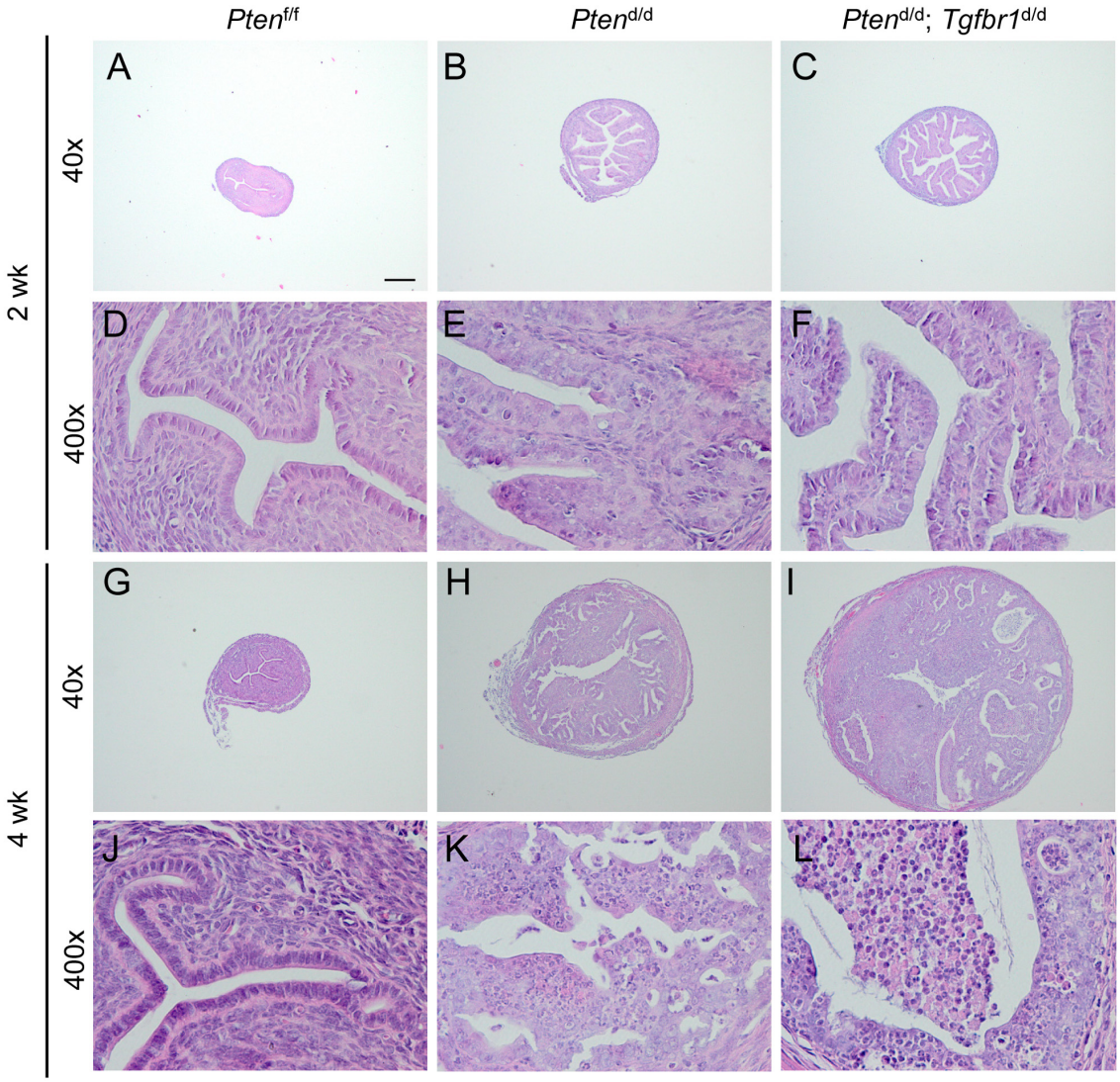


**A-15.** Histological analysis of endometrial cancer development. (A-L) H & E staining of the uteri from *Pten*$^{d/d}$ and *Pten*$^{d/d}$; *Tgfbr1*$^{d/d}$ mice at 2 and 4 weeks of age. *Pten*$^{f/f}$ and *Pten*$^{f/f}$; *Tgfbr1*$^{f/f}$ mice (not shown) were included as controls. Panels (D-F) and (J-L) represent higher power images for panels (A-C) and (G-I), respectively. H & E staining was performed using at least 3 independent samples per genotype. Scale bar is representatively depicted in (A) and equals 200 µm (A-C, G-I) and 20 µm (D-F, J-L).

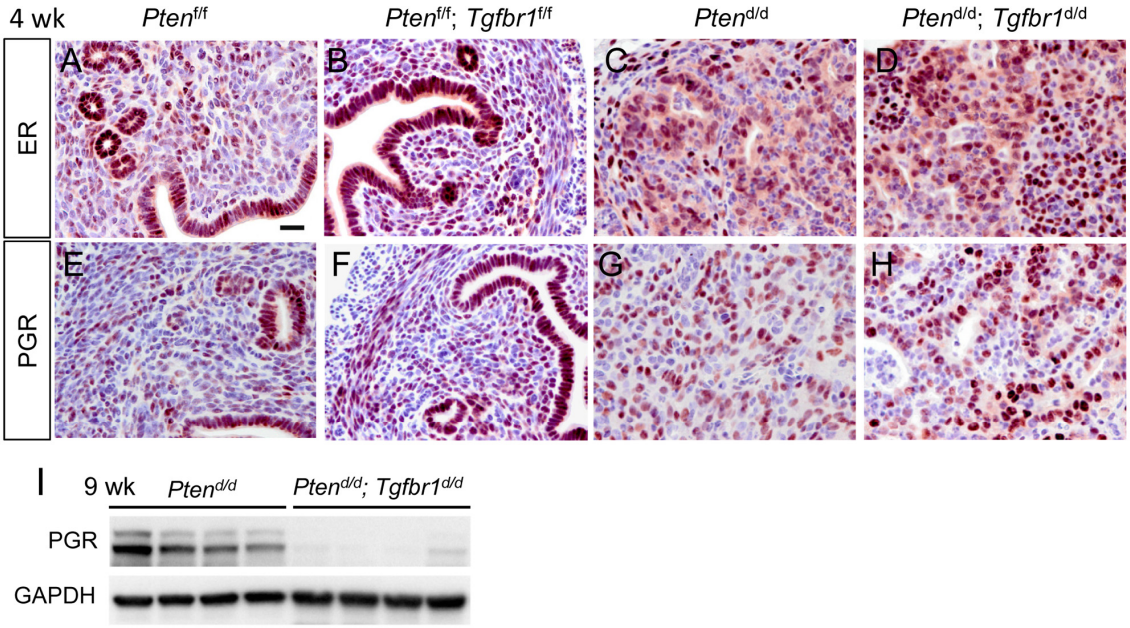


**A-16**. Expression of ER and PGR in mouse uteri with conditional deletion of *Pten* and/or *Tgfbr1*. (A-H) Immunostaining of ER and PGR in the uteri of 4-week-old *Pten*$^{f/f}$, *Pten*$^{f/f}$; *Tgfbr1*$^{f/f}$, *Pten*$^{d/d}$, and *Pten*$^{d/d}$; *Tgfbr1*$^{d/d}$ mice. Immunoreactive signals were developed using NovaRED. The sections were counterstained with hematoxylin. Results represent experiments using 3 independent samples per genotype. Scale bar is representatively depicted in (A) and equals 20 μm (A-H). (I) Western blot analysis of PGR protein expression in the uteri of *Pten*$^{d/d}$ and *Pten*$^{d/d}$; *Tgfbr1*$^{d/d}$ mice at 9 weeks of age.

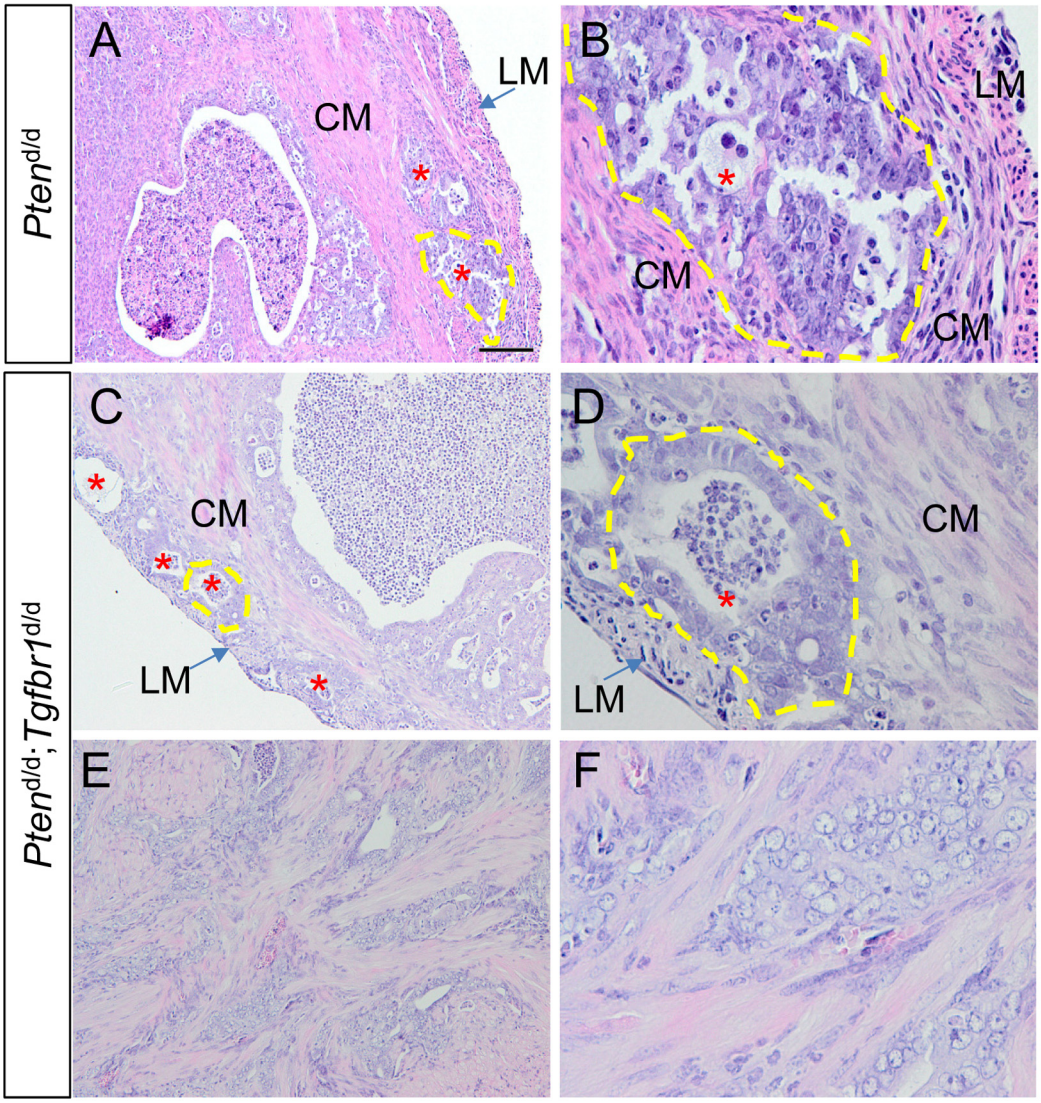


**A-17.** Histological analysis of tumor development and myometrial invasion. (A-F) H & E staining of uterine sections from *Pten*$^{d/d}$ and *Pten*$^{d/d}$; *Tgfbr1*$^{d/d}$ mice at ~2 months of age. Note myometrial invasion was detected in both *Pten*$^{d/d}$ and *Pten*$^{d/d}$; *Tgfbr1*$^{d/d}$ mice although the latter tended to be more severe, culminating in myometrial disruption and unrecognizable myometrial layers (see Figure 19). Desmoplastic stroma and haphazard glandular pattern were also observed in *Pten*$^{d/d}$; *Tgfbr1*$^{d/d}$ uteri (E, F). H & E staining was performed using independent samples from *Pten*$^{d/d}$ (n = 12) and *Pten*$^{d/d}$; *Tgfbr1*$^{d/d}$ (n = 13) mice. CM, circular muscle layer; LM, longitudinal muscle layer. Asterisks indicate epithelial invasion. Dotted yellow line marks the epithelial lesions within the myometrium. Scale bar is representatively depicted in (A) and equals 100 µm (A, C, E) and 25 µm (B, D, F).

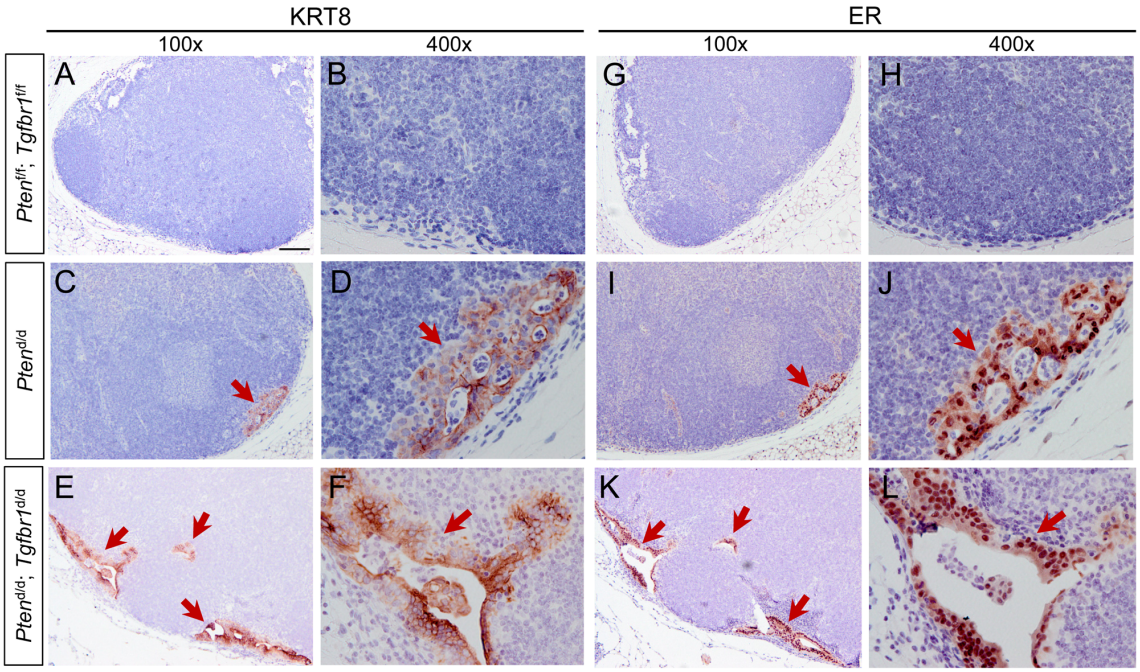


**A-18.** Identification of endometrial cancer metastasis in lymph nodes. (A-L) Immunohistochemical staining of KRT8 and ER using iliac lymph node tissues from control, *Pten*$^{d/d}$, and *Pten*$^{d/d}$; *Tgfbr1*$^{d/d}$ mice. Note that no KRT8 and ER expression was detected in control lymph nodes (A, B, G, H). However, metastases positive for KRT8 and ER were found in the lymph nodes of both *Pten*$^{d/d}$ (C, D, I, J) and *Pten*$^{d/d}$; *Tgfbr1*$^{d/d}$ mice (E, F, K, L). Immunohistochemistry was performed using 9-16 week old *Pten*$^{d/d}$ and *Pten*$^{d/d}$; *Tgfbr1*$^{d/d}$ mice ($n$ = 4). Signals were developed using NovaRED. The sections were counterstained with hematoxylin. Arrows indicate metastases. Panels (B, D, F, H, J, L) represent higher power images for corresponding panels (A, C, E, G, I, K). Scale bar is representatively depicted in (A) and equals 100 µm (A, C, E, G, I, K) and 25 µm (B, D, F, H, J, L).

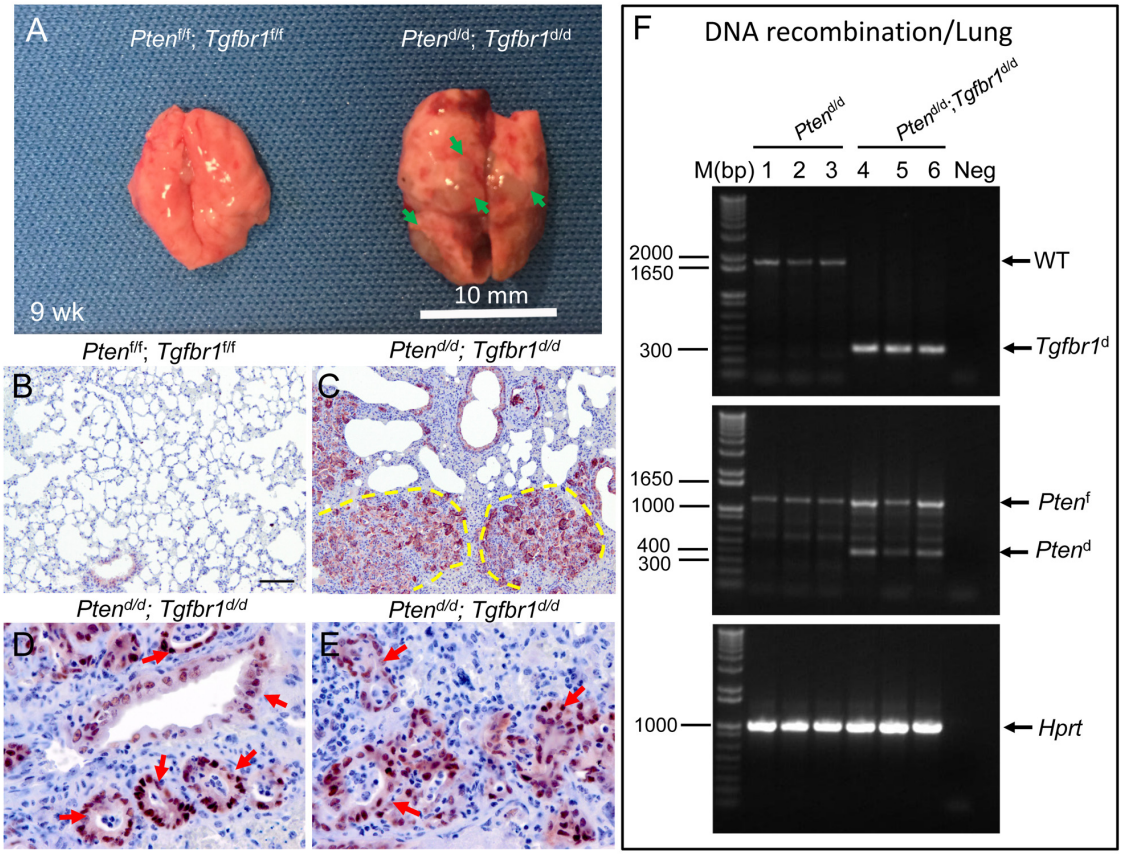


**A-19**. Lung metastasis in *Pten*$^{d/d}$; *Tgfbr1*$^{d/d}$ mice. (A) Gross analysis of lung metastases in 9-week-old *Pten*$^{d/d}$; *Tgfbr1*$^{d/d}$ mice. Note the lungs of *Pten*$^{d/d}$; *Tgfbr1*$^{d/d}$ mice were occupied with tumor foci/nodules (arrows). (B, C) Immunohistochemical analysis of KRT8 staining using lungs from 9-week-old control and *Pten*$^{d/d}$; *Tgfbr1*$^{d/d}$ mice. Dotted yellow line indicates metastatic lesions in the lungs of *Pten*$^{d/d}$; *Tgfbr1*$^{d/d}$ mice. (D, E) Immunohistochemical analysis of ER staining using lungs from 9-week-old *Pten*$^{d/d}$; *Tgfbr1*$^{d/d}$ mice. Images represent different microscopic fields of a lung sample from the same mouse. Arrows indicate endometrial gland-like structures within the metastatic sites of the lungs. Immunoreactive signals were developed using NovaRED. The sections were counterstained with hematoxylin. Scale bar is representatively depicted in (B) and equals 100 µm (B, C) and 25 µm (D, E). (F) Analysis of recombination of *Pten/Tgfbr1* conditional alleles using lungs from *Pten*$^{d/d}$ and *Pten*$^{d/d}$; *Tgfbr1*$^{d/d}$ mice at 9 weeks of age. Neg, no-template control. Note the recombined *Pten/Tgfbr1* conditional alleles were only detected in the lung metastases of *Pten*$^{d/d}$; *Tgfbr1*$^{d/d}$ mice but not in the lung tissues of *Pten*$^{d/d}$ mice, supporting that the epithelial lesions in the lungs of *Pten*$^{d/d}$; *Tgfbr1*$^{d/d}$ mice were derived from the primary uterine tumors.

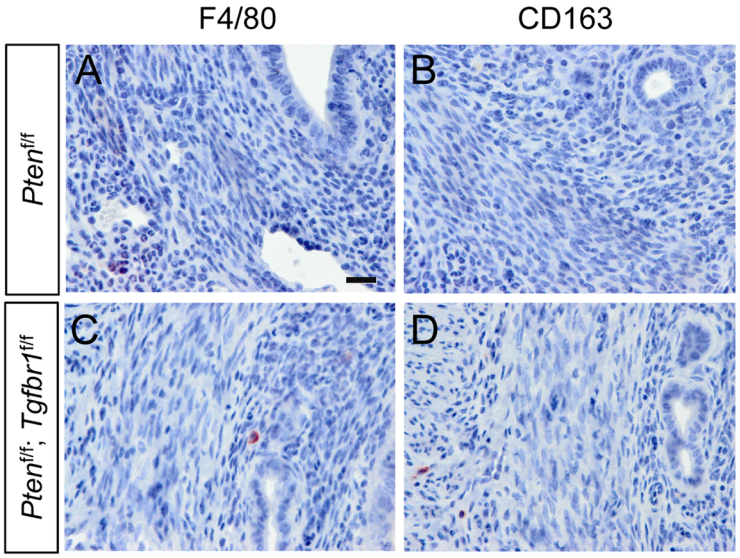


**A-20**. Expression of F4/80 and CD163 in control uteri. (A-D) Immunostaining of F4/80 and CD163 using uteri from *Pten*$^{f/f}$ and *Pten*$^{f/f}$; *Tgfbr1*$^{f/f}$ mice at 9 weeks of age. Immunoreactive signals were developed using NovaRED. The sections were counterstained with hematoxylin. Uterine samples from 5 mice per genotype were examined. Scale bar is representatively depicted in (A) and equals 20 μm (A-D).

## APPENDIX B

## TABLES

**B-1.** Primers for conventional PCR and quantitative real-time PCR

| Target | Sequence (5′-3′) | | Source |
|---|---|---|---|
| *Tgfbr1*$^{flox}$ | Forward | ACTCACATGTTGGCTCTCACTGTC | [179] |
| | Reverse | AGTCATAGAGCATGTGTTAGAGTC | |
| *Pten*$^{flox}$ | Forward | CAAGCACTCTGCGAACTGAG | The Jackson |
| | Reverse | AAGTTTTTGAAGGCAAGATGC | Laboratory |
| *Pgr-Cre* | Forward | TATACCGATCTCCCTGGACG | [147] |
| | Reverse | ATGTTTAGCTGGCCCAAATG | |
| | Reverse | CCCAAAGAGACACCAGGAAG | |
| *Tgfbr1*$^{d}$ | Forward | ATTTCTTCTGCTATAATCCTGCAG | [390] |
| | Reverse | AGTCATAGAGCATGTGTTAGAGTC | |
| *Pten*$^{d}$ | Forward | ACTCAAGGCAGGGATGAGC | [363] |
| | Reverse | AATCTAGGGCCTCTTGTGCC | |
| | Reverse | GCTTGATATCGAATTCCTGCAGC | |
| *Hprt* | Forward | GGACCTCTCGAAGTGTTGGATAC | [179] |
| | Reverse | CTTGCGCTCATCTTAGGCTT | |
| *Tgfbr1* | Forward | TGCCATAACCGCACTGTCA | [179] |
| | Reverse | AATGAAAGGGCGATCTAGTGATG | |
| *Pten* | Forward | TGAAGACCATAACCCACCACA | [391] |
| | Reverse | TCATTACACCAGTCCGTCCCT | |
| *Cxcl1* | Forward | TGGCTGGGATTCACCTCAAGAACA | [392] |
| | Reverse | TGTGGCTATGACTTCGGTTTGGGT | |
| *Cxcl5* | Forward | GCATTTCTGTTGCTGTTCACGCTG | [393] |
| | Reverse | CCTCCTTCTGGTTTTTCAGTTTAGC | |
| *Cxcl12* | Forward | CCAGAGCCAACGTCAAGCAT | [394] |
| | Reverse | CAGCCGTGCAACAATCTGAA | |
| *Cxcr2* | Forward | ATGCCCTCTATTCTGCCAGAT | PrimerBank ID |
| | Reverse | GTGCTCCGGTTGTATAAGATGAC | 6753456a1 |
| *Ccl2* | Forward | TTAAAAACCTGGATCGGAACCAA | PrimerBank ID |
| | Reverse | GCATTAGCTTCAGATTTACGGGT | 6755430a1 |
| *Ccl9* | Forward | CCCTCTCCTTCCTCATTCTTACA | PrimerBank ID |
| | Reverse | AGTCTTGAAAGCCCATGTGAAA | 6755434a1 |
| *Rpl19* | Forward | ATGAGTATGCTCAGGCTACAGA | [242] |
| | Reverse | GCATTGGCGATTTCATTGGTC | |

**B-2**. Primary antibodies for immunostaining and western blot

| Name | Manufacturer | Catalog no. | Host | IHC/IF | Western |
|---|---|---|---|---|---|
| PTEN | Cell Signaling | 9559 | Rabbit | 1:400 | 1:1000 |
| Phospho-AKT | Cell Signaling | 4060 | Rabbit | 1:50 | 1:2000 |
| AKT | Cell Signaling | 4691 | Rabbit | | 1:1000 |
| GAPDH | Cell Signaling | 2118 | Rabbit | | 1:1000 |
| KRT8 | DSHB | TROMA-1 | Rat | 1:200 | |
| ECAD | Cell Signaling | 3195 | Rabbit | 1:400 | |
| ER | Santa Cruz | sc-542 | Rabbit | 1:1000 | |
| PGR | Thermo Scientific | RB-9017 | Rabbit | 1:200 | 1:1000 |
| CNN1 | Millipore | 04-589 | Rabbit | 1:500 | |
| CD163 | Abcam | ab182422 | Rabbit | 1:1000 | 1:1000 |
| F4/80 | AbD Serotec | MCA497GA | Rat | 1:200 | |
| CXCL5 | Bioss | bs-2549R | Rabbit | 1:800 | |
| MUC1 | Novus Biologicals | NB120-15481 | Rabbit | 1:200 | |

**B-3**. Visible metastasis at advanced tumor stage in *Pten*$^{d/d}$; *Tgfbr1*$^{d/d}$ versus *Pten*$^{d/d}$ mice

| Organ/tissue | *Pten*$^{d/d}$ (n = 7; 25-36 wks) | *Pten*$^{d/d}$; *Tgfbr1*$^{d/d}$ (n = 16; 7-16 wks) |
|---|---|---|
| Lung | 0 | 15 |
| Liver | 0 | 1 |
| Spleen | 0 | 0 |
| Kidney | 0 | 0 |
| Heart | 0 | 0 |
| Peritoneum | 0 | 2 |
| Bladder | 0 | 0 |